Rapid and Cost-effective Virus Detection Methods using Molecular Sensors and Nano-devices

by

Lina Stella Franco

A Dissertation Presented in Partial Fulfillment
of the Requirements for the Degree
Doctor of Philosophy

Approved May 2016 by the
Graduate Supervisory Committee:

Vladimiro Mujica, Co-Chair
Joseph N. Blattman, Co-Chair
Antonio A. Garcia
Petra Fromme
Mark Hayes

ARIZONA STATE UNIVERSITY

August 2016

ABSTRACT

Accurate virus detection is important for diagnosis in a timely manner to facilitate rapid interventions and treatments. RNA viruses affect an extensive amount of the world's population, particularly in tropical countries where emerging infectious agents often arise. Current diagnostic methods have three main problems: they are time consuming, typically not field-portable, and expensive. My research goal is to develop rapid, field-portable and cost sensitive diagnostic methods for RNA viruses. Herein, two different approaches to detect RNA viruses were proposed: Conjugated gold nanoparticles for detection of viral particles or virus-specific antibodies by monitoring changes in their optical properties, and Tentacle Probes coupled with qPCR for detection and differentiation of closely-related viral strains. The first approach was divided into two projects: the study and characterization of the gold nanoparticle-antibody system for detection of virus particles using dynamic light scattering (DLS) and UV-Vis spectrophotometry, and development of a detection method for antibodies using static light scattering (SLS) and antigen-conjugated gold nanoparticles. Bovine serum albumin (BSA) conjugated gold nanoparticles could successfully detect BSA-specific antibodies in vitro, and protein E from Dengue Virus serotype 2 conjugated gold nanoparticles could detect Dengue-specific antibodies, both in vitro and in serum samples. This method is more accurate than currently used detection methods such as dot blots. The second approach uses Tentacle Probes, which are modified molecular beacons, to detect with high specificity two different strains of Lymphocytic Choriomeningitis Virus (LCMV), Armstrong and Clone-13, which differ in only one nucleotide at the target sequence. We successfully designed and use Tentacle Probes for detection of both strains of LCMV, in

vitro and in serum from infected mice. Moreover, detection of as little as 10% of Clone-13 strain was possible when diluted in 90% Armstrong strain. This approach enables the detection of different strains of virus even within a mixed quasispecies and may be important for improving intervention strategies for reducing disease. The detection methods provide rapid detection of viruses, including viral strains within mixed populations, and should enhance our ability in providing early responses to emerging infectious diseases due to RNA viruses including Zika or Dengue virus.

DEDICATION

This thesis is dedicated to my family, especially to the two most important persons in my life so far. Without them I would not have been here.

To my mother who is my inspiration, my strength, everyday companion, infinitely patient and most supportive person that I will ever know.

And to my father, who has the kindest words and infinite love, even in the most difficult moments.

ACKNOWLEDGMENTS

I would like to acknowledge everyone who has helped me in any way during my entire graduate study by supporting me, giving constructive criticism and advice, specially my friends.

I would like to thank my advisors: Dr. Joseph Blattman, Dr. Antonio Garcia and Dr. Vladimiro Mujica, who guided me, taught me really valuable lessons and encouraged me to continue in this journey.

I would also like to thank my committee members, Dr. Mark Hayes and Dr. Petra Fromme, and collaborator, Dr. Michael Caplan, for the scientific discussions and constant advice.

I would like to thank some fellow undergrad, graduate students and post-docs with whom I enjoyed working closely: Dr. Susan Holechek, Vanessa Guzman, Lizbeth Nieves, Kavita Manhas, Kristen Morrow, Charles Miller, Abhinav Markus, Dr. Jose Martín-García and Dr. Xiaodong Qi.

Finally, I would like to acknowledge COLCIENCIAS, who funded the initial years of my graduate studies through the Francisco Jose de Caldas Fellowship for International Doctorates.

TABLE OF CONTENTS

Page

CHAPTER Page

LIST OF TABLES

LIST OF FIGURES

Figure Page

Figure Page

Chapter 1

1. INTRODUCTION

1.1 RNA Viruses

Viruses that have genetic content single stranded RNA (ssRNA) or double stranded RNA (dsRNA) are called RNA viruses. Viruses with ssRNA are classified depending if they have a positive sense ssRNA, a negative sense ssRNA, or ambisense viruses, which encode proteins in both directions (Strauss & Strauss, 2007). Arenaviridae, Coronaviridae, Flaviviridae, Orthomyxoviridae, among other families, are part of the ssRNA virus families and include viruses that cause diseases like Yellow Fever, Dengue, Zika and Influenza (Guzman et al., 2010; Strauss & Strauss, 2007). Negative sense ssRNA virus' genome has a replicase (RNA-dependent RNA polymerase), which is needed for their genome replication, and other proteins, like capsid proteins and non-structural proteins. Positive sense ssRNA viruses have a similar genome structure, but it uses more host proteins to replicate (Strauss & Strauss, 2007).

RNA viruses have a higher rate of mutation than DNA viruses since they lack proofreading RNA polymerases. Despite this, there are some sequences that are conserved because they are needed for survival (i.e. RNA polymerase). The high mutation rate is mainly because of two reasons: high replication rate that lead to high number of viral particles, and fast viral generation time (Moya, Elena, Bracho, Miralles, & Barrio, 2000). This genetic variability can lead to the formation of quasispecies of a virus, which become important at the time of diagnosis or choosing the correct treatment (Domingo, Sheldon, & Perales, 2012; Lauring & Andino, 2010).

One of the most representative families of viruses among RNA viruses is the Flaviviridae family, which includes Yellow Fever Virus, Zika virus, Dengue virus, West Nile virus and Hepatitis C virus (Guzman et al., 2010; Hoen, Keller, Verma, Buckeridge, & Brownstein, 2012; T. F. Tsai & Halstead, 2001). Most of these viruses cause vector-dependent viral diseases, are epidemic in many tropical countries and are emerging or re-emerging viruses (Figure 1.1). Early virus detection is important to prevent viral outbreaks, especially in developing countries where a lack of control and surveillance mechanisms prevails (Guzman et al., 2010; Jelinek, 2009). Some of the viruses of the Flaviviridae family cause hemorrhagic fevers as well as viruses from the Arenaviridae, Filoviridae, Rhabdoviridae, and Bunyaviridae. Viral hemorrhagic fevers can be lethal even in the primary infection, like in the case of Ebola, or in the secondary infection, like in the case of Dengue (T. F. Tsai & Halstead, 2001).

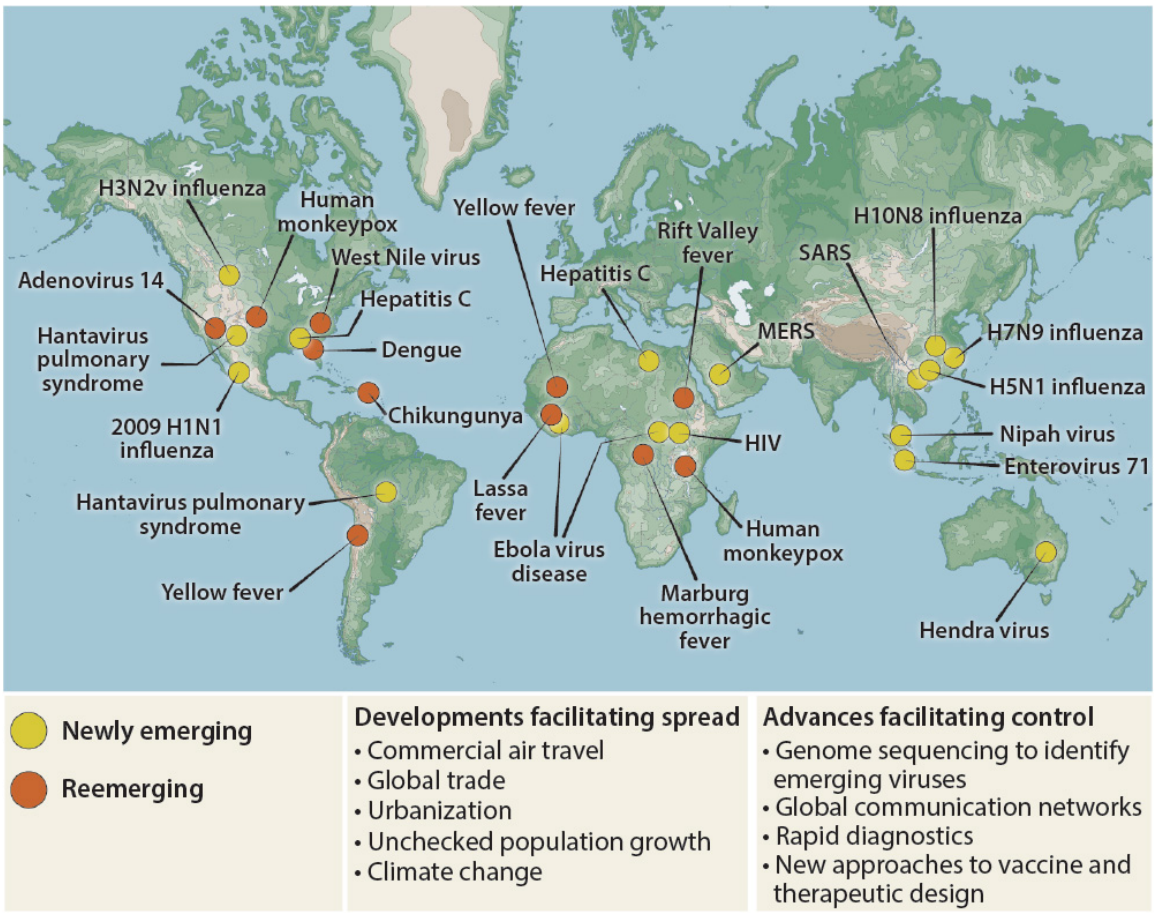

Figure 1.1. Current Emerging and Re-Emerging Viruses in the World.
Taken from (Marston et al., 2014).

Lymphocytic choriomeningitis virus (LCMV) is part of the Arenaviridae family, is an emerging virus and is used in the following studies as a model virus for RNA viruses. The capsid and spike structure are similar to the ones present in other viruses such as Dengue virus, and its antigenic variance is evidenced in the different LCMV strains (Ahmed, Salmo, Butler, Chiller, & Oldstone, 1984; Zhou, Ramachandran, Mann, & Popkin, 2012). The LCMV wild type Armstrong strain differs with the Clone-13 strain in only three point mutations. One of these point mutations is translated in an amino acid difference in one of the receptor proteins (GP1), which causes that the infection to be

either acute (Armstrong) or chronic (Clone-13) (Ahmed et al., 1984). In the studies discussed in this dissertation, LCMV was used as a model virus for RNA viruses due to its well described biology and structure, as well as its immune response in mice.

1.2 Detection Methods for Viruses

Detection methods for viruses can be classified as directly, indirectly, immune-detection and fluorescence-based technologies (Cella, Blackstock, Yates, Mulchandani, & Chen, 2013). Direct detection involves techniques were direct visualization is possible, like Electron Microscopy (EM), although this technique is primarily used to study viral biology and structure. Indirect detection are the most common techniques used that include amplification of nucleic acids and cell culture growth. The latter is still the "gold standard" technique for detection of viruses and discovery of new ones (Ahmed et al., 1984). However, this technique is time consuming and lacks the specificity and sensibility of molecular techniques and need a priori knowledge of the identity of the virus (Ahmed et al., 1984; Cella et al., 2013; Korns Johnson & Homann, 2012). Immunology-based techniques are the most common indirect technique and rely mainly in the detection of antibodies against the virus, or detection of virus particles (Cella et al., 2013; Driskell, Jones, Tompkins, & Tripp, 2011; Fukushi, Tani, Yoshikawa, Saijo, & Morikawa, 2012; Korns Johnson & Homann, 2012; Wong, Krupin, Sekaran, Mahamd Adikan, & Berini, 2014). The main problem with this type of technique in the possible cross-reaction detection between closely related viruses.

Lastly, fluorescent-based techniques are molecular methods that monitor the fluorescence of probes that are complementary to the target or fluorescent dyes that bind

to dsDNA (Cella et al., 2013; Satterfield, Bartosiewicz, West, & Caplan, 2010; Satterfield, West, & Caplan, 2007). Although molecular methods such as PCR are highly sensitive, they require skilled lab technicians, careful storage of reagents, and cannot detect infective viruses (McCausland & Crotty, 2008). Thus, these methods are not the most appropriate to use in developing countries where fast and cost-effective detection is desired.

1.3 Molecular Sensing: Fundamental Principles and Biomedical Applications

Molecular sensing refers to any device that can detect and/or record a chemical or physical change in a property and has sensitivity and specificity at a molecular level (Zhang & Hoshino, 2014). Many of these modern molecular sensors are based in observations in nature and the one of the main applications is disease diagnosis. They have a variety of capture and recognition mechanisms including antibodies and other proteins, nucleotides, and polymers (Zhang & Hoshino, 2014). This recognition of a particular change is translated into a signal that can be electrical signal, optical or mechanical. Optical signals are going to be main signal used during the following chapters.

1.4 Nanophotonic Detection Devices

Nanophotonic devices refer to the devices that study the change in optical properties at a nanoscale. Many times these devices use metallic colloids to amplify any change (chemical or physical) at small distances (i.e. surface of a gold nanoparticle) because of the plasmon resonance of the metallic nanoparticles (Compton & Osterloh, 2007; Doak, Gupta, Manivannan, Ghosh, & Kahol, 2010; Haiss, Thanh, Aveyard, &

Fernig, 2007; Thanh & Rosenzweig, 2002; D.-H. Tsai et al., 2011). Other applications include optical integrated circuits, photonic crystals, antennas for light and metamaterials (Koenderink, Alù, & Polman, 2015). Nowadays, this type of device is combined with other technologies and therefore expand the applications of both technologies. One example is the enhancement of single-molecule fluorescence with nanophotonics. Single-molecule fluorescence is limited in some environments by the small concentrations of a single-molecule at the time of the measurements. Nanophotonic structures can amplify the excitation intensity play a critical role as an antenna and overcome the concentration barrier from single-molecule detection (Acuna, Grohmann, & Tinnefeld, 2014). Therefore, nanophotonic structures can be complementary to other current optical devices to improve any size dependent disadvantage and could have significant applications to the development of biosensors and therapeutical systems.

1.5 Light Scattering Detection Devices

As nanophotonic devices are being applied to multiple fields, it is important to highlight one of its applications: light scattering devices. Although other light scattering detection devices do not necessarily use nanophotonic structures (i.e. gold nanoparticles), the devices discussed in here are going to be associated to the use of gold nanoparticles.

Light scattering devices coupled with gold nanoparticles are being applied broadly because of the scattering and amplifying properties of the gold nanoparticles, as discussed before. Static light scattering and dynamic light scattering are two of the most common techniques for detection of light scattering. These techniques give good results when samples have a high concentration of the solute in order to be detectable. Another technique is Raman scattering that is used with low concentrations, like single-molecule

experiments, gold nanoparticles enhance the signal (Fan, Zheng, & Singh, 2014). New applications of these light scattering and nanophotonics have led to new experimental developments such as optical trapping, optical tweezers and nanospasers, all of them enhanced by the plasmonic excitations with light (Fan et al., 2014). One example of an applied biosensor is the use of light scattering spectroscopy for early detection of cancer with minimal invasion, allowing real-time diagnosis (Perelman, 2006). Thus, light scattering devices are applied in biosensors widely and this opens new possibilities of applications of biosensors with the advantage of nanoparticles enhancing the signal.

1.6 Kinetic Considerations: Detection, Stability and Aggregation Phenomena

Aggregation in gold nanoparticles in solution is known to have an important role in the efficiency of electronic, magnetic or optical devices that use the gold nanoparticles (Mohammad, Abdelrahman, El-Deab, Okajima, & Ohsaka, 2008; Yang, Matsubara, Nogami, & Shi, 2007). The aggregation in solution is influenced by cationic and oligocationic species and causes a red-shifted displacement in the plasmon absorbance (Yang et al., 2007). Aggregation is also influenced by the pH of the medium. There has been evidence of linear aggregation when gold nanoparticles are in ethanol, but no evidence of aggregation when the nanoparticles are citrate-stabilized (Mohammad et al., 2008). This means that gold nanoparticles will aggregate when the conjugate is not bound and/or the conjugation is not stable (Chen, Wang, Ge, & Zhao, 2009; Raoof et al., 2012).

Kinetics influence the detection of optical change that is being monitored. Kim *et al*. (Kim, Lee, Joo, & Lee, 2008) described a model based on Brownian movements to predict aggregation in gold nanoparticles and it gave some insight into the optimization of colorimetric sensors using gold nanoparticles. In the case of UV-Vis

spectrophotometry, aggregation can be observed in the red-shifted plasmon peak and in the region of 640-680 nm (Thanh & Rosenzweig, 2002; Thobhani et al., 2010; Yang et al., 2007).

The following studies intend to give an insight of new detection methods and a better understanding of the viral detection methods by approaching current problems with diagnostic methods: cost-effectiveness, fast diagnosis, field-portable and specificity of the method. The two approaches discussed cover different areas of application of the diagnostic methods, and the use of each approach depend on the need of the researcher/clinician. The first approach, a nano-device coupled with static light scattering successfully detect antibodies in a serum sample. The second approach, a molecular fluorescent-based method coupled with qPCR, is highly specific even in the presence of multiple strains in a sample. Herein, factors affecting both approaches are studied and discussed to optimize each method and obtain better detection results.

Chapter 2

2. OPTIMAL CONDITIONS AND PROTOCOLS FOR PREPARATION OF GOLD NANOPARTICLES

2.1 Introduction

Gold nanoparticles (AuNPs) are highly sensitive to chemistry surface changes and have already been employed as sensors for biomedical applications and for cancer therapy (Daniel & Astruc, 2004; Raoof et al., 2012; Thobhani et al., 2010). Changes at the surface of nanoparticles can be monitored using any of a number of their optical properties including surface plasmon resonance, optical absorption or scattering, fluorescence, among others (Compton & Osterloh, 2007; Daniel & Astruc, 2004; Doak, Gupta, Manivannan, Ghosh, & Kahol, 2010; van Dijk, 2007). AuNPs have previously been used for virus detection of H5N1 (Pham, Hoang, Phan, Conrad, & Chu, 2012), Influenza (Driskell, Jones, Tompkins, & Tripp, 2011) and Dengue using RNA isolated from mosquitoes (Carter, Balaraman, Kucharski, Fraser, & Fraser Jr, 2013). These are examples in which the optical properties of AuNPs have been coupled with different analytical techniques.

While over the past several decades, approaches for synthesizing, preparing, and detecting gold nanoparticles for homogeneous assays have been described, important challenges remain when translating their use from successful applications of gold nanoparticles in heterogeneous assays to reliable and sensitive homogeneous assays (Du, Li, & Cheng, 2008; Linares, Kubota, Michaelis, & Thalhammer, 2012). The motivation for the development of homogeneous assays is to increase assay speed and improve

sensitivity of detection by utilizing instrumentation suitable for liquid phase measurement.

There are three main steps for the preparation and detection of antibodies with conjugated gold nanoparticles: conjugation of the nanoparticles, centrifugation and incubation with sample. Chemically, the conjugation step to the protein usually takes place either through covalent S-S bonds (directional) or non-covalent bonding (Kumar, Aaron, & Sokolov, 2008; Raj & Sreenivasan, 2010; Tsai et al., 2011). The amount of protein needed to cover the surface of the gold nanoparticles is often determined empirically by titration of the protein. However, the titration is not always efficient to cover the majority of the gold nanoparticles and can result in increased non-specific binding of analyte and less efficiency (Brewer, Glomm, Johnson, Knag, & Franzen, 2005). The centrifugation step is critical to remove free protein in solution to avoid unspecific binding of free protein to conjugate with their target (La Belle, Faichild, Demirok, & Verma, 2013). Speed and times in this step vary depending on the size of the gold nanoparticles, and can be performed one or more times, but the resuspension step of the nanoparticles is not well described in literature. Lastly, incubation of the gold nanoparticles with the sample has been described at varying temperatures, but has not been accurately assessed for variance.

For researchers and method developers inexperienced in gold nanoparticle assays, there are a number of commercial web sites that describe specific steps and numerous research articles reporting findings for homogeneous immunoassays. However, the lack of detailed descriptions of gold nanoparticle preparation steps can lead to confusion regarding optimal preparation. Subsequently, low sensitivity or spurious results can

occur. Even for researchers with experience using gold nanoparticle in heterogeneous assays, translating the format to homogeneous assays can pose new challenges since steps to bind antibodies and proteins to gold surfaces requires careful attention to preparative steps in order to maintain sensitivity due to the presence of free antibody and protein.

Hence, a detailed procedure is proposed for the preparation of gold nanoparticles that includes the three main steps: conjugation of the protein, centrifugation and incubation with the target. As a proof of concept, the procedure was tested with the conjugation of Bovine Serum Albumin (BSA) to 60 nm gold nanoparticles and posterior recognition of the anti-BSA antibody. The procedure was optimized to obtain the best results for the detection of the target using static light scattering and UV-vis spectrophotometry.

2.2 Proposed Procedure for the Conjugation of Gold Nanoparticles

Conjugation:

An aliquot of 1 ml containing 2.6 x 10^{10} particles/ml of 60 nm gold colloids is combined with 50 or 100 microliters of freshly prepared pH = 5 acetate buffer (appropriate for BSA conjugation) prior to the addition of 100 microliters of from 0.5 mg/ml BSA. A frozen cold pack was placed on the tube and the mixture was gently rocked using an orbital table for 30 minutes as a practical incubation time for BSA binding.

Centrifugation:

Three centrifugation steps are conducted in order to reduce the concentration of BSA not bound to gold nanoparticles. The centrifugation conditions used were adapted

from Cytodiagnostics Inc. (www.cytodiagnostics.com) recommended conditions. To minimize aggregation of gold nanoparticles and ensure re-suspension after centrifugation all centrifugation steps should be at 4 ˚C. All centrifugation steps should be for 30 minutes at 1,125×*g*. After each step, remove as much of the supernatant as possible without touching the pellet. Resuspend the pellet with 1 ml of pH = 5 acetate buffer after the first and second centrifugation steps, and resuspend with 1 ml of phosphate buffer saline (PBS) pH = 7.0 after the final centrifugation step.

Incubation:

Incubation of the gold nanoparticle preparation with 10 or 100 µl of sample for 30 min could be at room temperature or at 37 ˚C with constant rocking.

2.3 Results

2.3.1 Conjugation of Gold Nanoparticles

The pH of the buffer used for conjugation of the protein to the gold nanoparticles is going to influence the net charge of the protein and the surface interactions with the gold nanoparticle. Usually this pH is above the isoelectric point (pI) of the protein for binding, and for BSA the most appropriate buffer was acetate buffer (pH = 5). To determine the amount of buffer necessary to add to the gold nanoparticles different amounts of acetate buffer were tested. Fifty microliters and 100 µl of acetate buffer induced aggregation of the gold nanoparticles evidenced by a color change in the solution from pink to purple or gray and the tailing seen in the 600-800 nm region in the visible light extinction spectrum compared to the spectrum of the gold nanoparticles without the buffer. Ten microliters of acetate buffer did not induced aggregation of the gold

nanoparticles, a result confirmed by visible spectroscopy (results not shown).

The amount of protein added to the solution for conjugation to the gold nanoparticles is also important because a sufficient amount of protein on the surface of the gold nanoparticles will protect the particles from aggregation in the presence of sodium chloride. Stoichiometric calculations based on surface coverage were performed to ensure that at least an average of 10 molecules of BSA were present on the surface of the gold nanoparticles. A concentration of 0.5 mg/ml of BSA was enough to have this coverage, which was confirmed visually after the centrifugation steps and final re-suspension with PBS by lack of color change.

In connection with these results, Tsai *et al.* (2011) referred that to get 90% coverage of the gold nanoparticle of the same size, at least a 2 mg/ml BSA solution was needed. For this reason, a 7 mg/ml solution of BSA in DI H_2O was used for the conjugation step to ensure the maximal saturating coverage of the gold nanoparticles. The procedure was repeated having as a result a lack in color change of the gold nanoparticles in the presence of PBS, and the visible spectrum showed no signs of aggregation compared to the spectrum of the gold nanoparticle solution before conjugation (not shown).

2.3.2 Centrifugation

After 30 min of incubation with the protein to conjugate, usually there is excess of free protein in solution, which would interfere with the assay because the interaction of free protein with antibodies will not be detected. This problem is addressed using centrifugation to remove the supernatant containing the remaining protein in solution. This step can be done one or many times. For this purpose, three steps of centrifugation

were proposed for gold nanoparticles of 60 nm of diameter, conjugated with BSA. Supernatant was collected after each centrifugation step and the UV-Vis spectrum of the supernatant was measured to monitor the amount of BSA present. Figure 2.1 shows that after the second and third step of centrifugation, the amount of BSA in the supernatant collected was minimum.

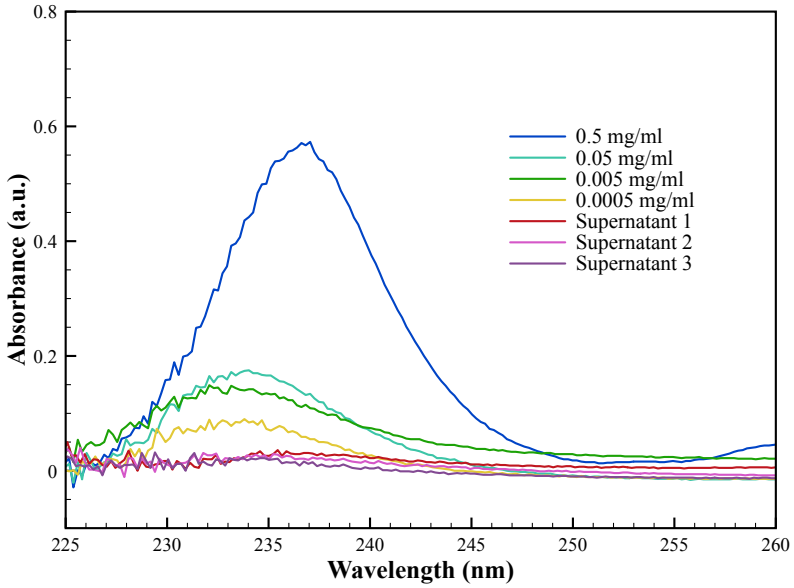

Figure 2.1. Three Centrifugation Steps are Enough to Eliminate Free Protein after Conjugation.
UV-Vis spectra of different known concentrations of BSA (0.0005-0.5 mg/ml) compared to the supernatants collected after each centrifugation step.

After the first centrifugation step of gold nanoparticles incubated with 0.5 mg/ml, the supernatant was removed carefully and the red pellet was re-suspended in 1 ml of acetate buffer. A second round of centrifugation at the same conditions was performed and a black pellet obtained could not be re-suspended. To solve this problem, 0.25 % of Tween 20 surfactant was added to the buffer used for re-suspension to help the gold nanoparticles disperse.

To determine the optimal time of each one of the three steps of centrifugation, a second round of centrifugation during 30 minutes using the surfactant and acetate buffer for each re-suspension was carried out. As a result, a black pellet was obtained after two centrifugations and it couldn't be re-suspended. Therefore, the time of centrifugation of the second step was decreased from 30 min to 15 min and the third centrifugation time was also reduced from 15 min to 10 min to favor re-suspension of the gold nanoparticles. This reduction in centrifugation time enabled the re-suspension of the gold nanoparticles after three steps of centrifugation. The buffer used to re-suspend after the third centrifugation step was PBS. These conditions were also tested and confirmed as optimal with gold nanoparticles conjugated with a solution of 7 mg/ml of BSA.

2.3.3 Incubation

To test if increasing the temperature during incubation with the antibody would result in an enhanced detection of binding, incubation at 40 ˚C during 30 min with different amounts of antibody was tried. Figure 2.2 shows static light scattering measurements of each sample with increasing concentrations of antibody. The results are similar to the results obtained at room temperature. The different intensity counts likely indicate fewer aggregates in solution because they precipitated over time. Therefore, changes in incubation temperature do not affect significantly the trend of detection when more antibody is added to the conjugated AuNPs.

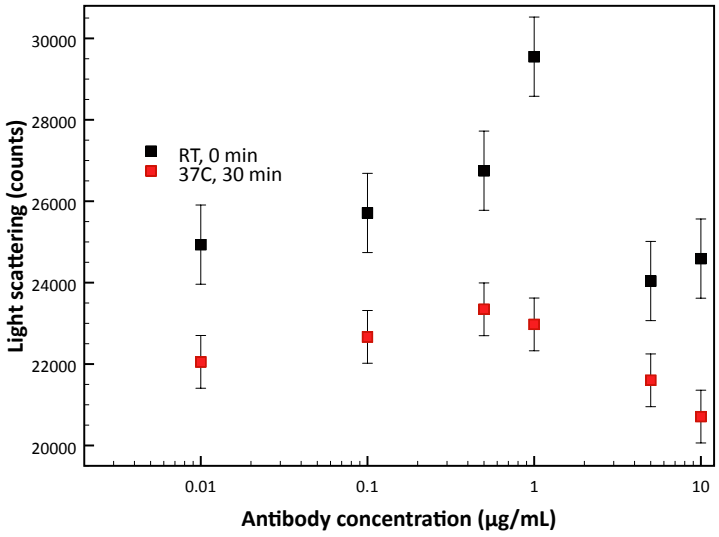

Figure 2.2. Incubation of Antibody with Conjugated Nanoparticles at Different Temperatures.
Light scattering at 532 nm measured at RT after 0 min or after 30 min at 37 ˚C of addition of 0-10 µg/ml of antibody anti-BSA (right).

2.4 Discussion

2.4.1 Binding Protein

The conventional approach to preparing gold nanoparticles for assays is to perform a titration by continually adding higher concentrations or amounts of protein so that when the mixture is "challenged" by the addition of a high concentration of sodium chloride solution (about 10% or 5 M), the amount of protein adsorbed on the surface of the gold nanoparticles can avoid aggregation and subsequent precipitation from solution. This titration test is reasonably simple to conduct and can be a cost-effective way of preparing particles with expensive proteins or monoclonal antibodies. It also would appear reasonable that adding another protein or blocking agent to cover the gold nanoparticle surface that may still be exposed leading to unintended non-specific binding, is a complementary step that mirrors traditional ELISA methods. However, as discussed

by several researchers (Brewer et al., 2005; Engleienne, 1998), this may lead to quite low surface coverage by the protein – as low as 10%. Assay sensitivity and analysis speed may be lower as a result since both are driven by the overall antibody accessible protein concentration. Moreover, for the detection of antibodies in response to a disease state, higher surface coverage can improve the probability of bridging multiple particles, given that the target is a polyclonal population of antibodies with multiple binding sites. Therefore, it is recommended that, when possible, the concentration of the protein used for conjugation would be in excess to ensure maximum coverage. However, the practical tradeoff between cost and sensitivity/speed is also complicated by the possibility of BSA, when used as a blocking agent, to get unspecific binding. It may also be useful to determine if BSA, or any other blocking agent used for other protein immunoassays, yields unwanted false positives in the case there is too little of the target protein on the surface and components or buffers present in the sample could promote protein-protein aggregation, specific and unspecific.

2.4.2 Centrifugation

Introducing a multi-step centrifugation to remove unbound protein appears to be worthwhile for homogeneous assays based on experience and reports by several researchers (Du et al., 2008; Gilger et al., 2001; Huang, 2006; La Belle et al., 2013; Raj & Sreenivasan, 2010). In some published gold nanoparticle preparations, there are membrane or dialysis alternatives to centrifugation (Aslan, Holley, Davies, Lakowicz, & Geddes, 2005) but most proteins are too large for proper removal using this method. Moreover, when the technique for supernatant removal is well honed, centrifugation can be done relatively easily and quickly.

In the experiments with 60 nm gold nanoparticles, the addition of a small amount of Tween 20 and centrifugation at 4 ˚C was determined to be very important for avoiding irreversible aggregation leading to the loss of gold nanoparticles. Also, time and centrifugation force recommendations published in articles and on commercial web sites should only be regarded as initial guidelines. Shorter times and lower centrifugal forces may provide better and more consistent results, as it was observed in the experiments described. This may be due to the variability of protein coverage and aggregation behavior for different protein binding preparations. Whatever combination of conditions used, it should be noted that the most important goal of this step is to remove as much unbound protein as possible without significant loss of gold nanoparticles in the suspension or due to pellets that cannot be fully re-suspended. Multiple and shorter centrifugation steps may be better than a single longer centrifugation, especially for large gold nanoparticles. It is important to mention that the pellet should not be allowed to sit for more than 2-3 min before re-suspension because of the tendency of the gold nanoparticles to remain aggregated, even after different attempts of resuspension.

2.5 Conclusions and Recommendations

There are a number of specific steps and some overall observations that are important to note based on the data and observations obtained during this study. The centrifugation steps are essential for minimizing the amount of non-conjugated protein left in the suspension, but care must be exercised in order to avoid conjugate particle instability. Specifically, one of the key factors is the time between each centrifugation step, as discussed before.

Secondly, the amount of protein added depends on several factors, including relative cost and quantity of protein available for assay use. A higher concentration of protein is preferred because it leads to higher gold nanoparticle surface coverage as compared to conjugation with the minimum amount of protein used in titration, which would suggest better capacity for immunoassay detection because of the probability of binding to the target. When sufficient protein is not available and hence the concentration of protein used for binding is low, it is recommended that a suitable blocking agent can effectively help maintain conjugated gold nanoparticle stability. The choice of blocking agent can also depend upon other aspects of the immunoassay, and there are other alternatives in the literature.

Another aspect that needs attention is incubation with the target protein, either antibody or antigen depending on the system, can be performed at 37-40 ˚C to increase the interactions and obtain better assay results. Before incubation with the target protein, it is preferable to let the conjugated gold nanoparticles sit overnight to avoid possible aggregates interfere with the light scattering measurement in the presence of the target.

2.6 References

Aslan, K., Holley, P., Davies, L., Lakowicz, J., & Geddes, C. (2005). Angular-Ratiometric Plasmon-Resonance Based Light Scattering for Bioaffinity Sensing. *JACS, 127*, 12115-12121.

Brewer, S., Glomm, W., Johnson, M., Knag, M., & Franzen, S. (2005). Probing BSA Binding to Citrate-Coated Gold Nanoparticles and Surfaces. *Langmuir, 21*, 9303-9307.

Carter, J. R., Balaraman, V., Kucharski, C. A., Fraser, T. S., & Fraser Jr, M. J. (2013). A novel dengue virus detection Method that couples DNAzyme and gold nanoparticle approaches. *Virology Jounal, 10*.

Compton, O. C., & Osterloh, F. E. (2007). Evolution of size and shape in the colloidal crystallization of gold nanoparticles. *Journal of American Chemical Society, 129*, 7793-7798.

Daniel, M.-C., & Astruc, D. (2004). Gold Nanoparticles: Assembly, Supramolecular Chemistry, Quantum-Size-Related Properties and Applications toward Biology, Catalysis and Nanotechnology. *Chemistry Reviews, 104*, 293-346.

Doak, J., Gupta, R., Manivannan, K., Ghosh, K., & Kahol, P. (2010). Effect of particle size distributions on absorbance spectra of gold nanoparticles. *Physica E Low Dimens Syst Nanostruct., 42*, 1605-1609.

Driskell, J. D., Jones, C. A., Tompkins, S. M., & Tripp, R. A. (2011). One-step assay for detecting influenza virus using dynamic light scattering and gold nanoparticles. *Analyst, 136*(15), 3083-3090. doi:10.1039/c1an15303j

Du, B., Li, Z., & Cheng, Y. (2008). Homogeneous immunoassay based on aggregation of antibody-functionalized gold nanoparticles coupled with light scattering detection. *Talanta, 75*, 959-964.

Engleienne, P. (1998). Use of colloidal gold surface plasmon resonance peak shift to infer affinity constants from the interactions between protein antigens and antibodies specific for single or multiple epitopes. *Analyst, 123*, 1599-1603.

Gilger, C., Grigiori, F., De Beaufort, C., Michel, G., Freilinger, J., & Hentges, F. (2001). Differential binding of IgG and IgA antibodies to antigenic determinants of bovine serum albumin. *Clin. Exp Immunol, 123*, 387-394.

Huang, S.-H. (2006). Gold nanoparticle-based immunochromatographic test for identification of *Staphylococcus aureus* from clinical specimens. *Clinica Chim. Acta, 373*, 139-143.

Kumar, S., Aaron, J., & Sokolov, K. (2008). Directional conjugation of antibodies to nanoparticles for synthesis of multiplexed optical contrast agents with both delivery and targeting moieties. *Nature Protocols, 3*, 314-320.

La Belle, J. T., Faichild, A., Demirok, U. K., & Verma, A. (2013). Method for fabrication and verification of conjugated nanoparticle-antibody tuning elements for multiplexed electrochemical biosensors. *Methods, 61*, 39-51.

Linares, E. M., Kubota, L. T., Michaelis, J., & Thalhammer, S. (2012). Enhancement of the detection limit for lateral flow immunoassays: Evaluation and comparison of bioconjugates. *J. Immunol Methods, 375*, 264-270.

Pham, V. D., Hoang, H., Phan, T. H., Conrad, U., & Chu, H. H. (2012). Production of antibody labeled gold nanoparticles for influenza virus H5N1 diagnosis kit development. *Adv. Nat. Sci.: Nanosci. Nanotechnol., 3*, 45017-45024.

Raj, V., & Sreenivasan, K. (2010). Selective detection and stimation of C-reactive protein in serum using surface-functionalized gold nano-particles. *Anal. Chim. Acta, 662*, 186-192.

Raoof, M., Corr, S. J., Kaluarachchi, W. D., Massey, K. L., Briggs, K., Zhu, C., . . . Curley, S. A. (2012). Stability of antibody-conjugated gold nanoparticles in the endolysosomal nanoenvironment: implications for noninvasive radiofrequency-based cancer therapy. *Nanomedicine, 8*(7), 1096-1105. doi:10.1016/j.nano.2012.02.001

Thobhani, S., Attree, S., Boyd, R., Kumarswami, N., Noble, J., Szymanski, M., & Porter, R. A. (2010). Bioconjugation and characterisation of gold colloid-labelled proteins. *J Immunol Methods, 356*(1-2), 60-69. doi:10.1016/j.jim.2010.02.007

Tsai, D.-H., DelRio, D. W., Keene, A. M., Tyner, K. M., MacCuspie, R. I., Cho, T. J., . . . Hackley, V. A. (2011). Adsoption and Conformation of Serum Abumin Protein on Gold Nanoparticles Investigated using Dimensional Measurements and in situ Spectroscopic Methods. *Langmuir, 27*, 2464-2477.

van Dijk, M. A. (2007). *Nonlinear-optical studies of single gold nanoparticles.* (Doctor in Philosophy), University of Leiden.

Chapter 3

3. VIRUS PARTICLE DETECTION USING NANO-SENSORS

3.1 Introduction

Effective and accurate diagnostic methods are needed in vector-dependent viral diseases, such as Yellow Fever, Dengue or Zika, which are epidemic in many tropical countries and recently extending their global reach to the US (Guzman et al., 2010; Hoen, Keller, Verma, Buckeridge, & Brownstein, 2012; Jelinek, 2009). Early virus detection is important to prevent viral outbreaks, especially in developing countries where there is a lack of control and surveillance mechanisms (Guzman et al., 2010; Jelinek, 2009). Virus detection methods employed currently, include molecular methods (McCausland & Crotty, 2008), isolation and quantification of the virus in cell culture (Ahmed, Salmo, Butler, Chiller, & Oldstone, 1984), and detection in serum of virus-specific antibodies (Korns Johnson & Homann, 2012). Although molecular methods such as PCR are highly sensitive, they require skilled lab technicians, careful storage of reagents, and cannot detect infective viruses (McCausland & Crotty, 2008). Techniques based on isolation of the virus in cell culture, such as the classical plaque assay, are accurate but require at least one week for diagnosis, are not sensitive, and need a priori knowledge of the identity of the virus (Ahmed et al., 1984; Korns Johnson & Homann, 2012). Thus, these methods are not appropriate for developing countries where fast detection is desired. Additionally, poor field conditions and limited training restrict application of many virus detection methods.

Gold nanoparticles (AuNPs) are often used as molecular sensors. The sensing capability is associated to surface changes, which can be monitored by changes in the

optical properties including surface plasmon resonance, optical absorption or scattering and fluorescence (Compton & Osterloh, 2007; Daniel & Astruc, 2004; Doak, Gupta, Manivannan, Ghosh, & Kahol, 2010; van Dijk, 2007). AuNPs have previously been used for virus detection of H5N1 (Pham, Hoang, Phan, Conrad, & Chu, 2012), Influenza (Driskell, Jones, Tompkins, & Tripp, 2011) and Dengue using RNA isolated from mosquitoes (Carter, Balaraman, Kucharski, Fraser, & Fraser Jr, 2013).

In this study, AuNPs coupled with an antibody are used for the detection of virus particles (whole virus or the specific surface protein). For this purpose, a virus model for RNA viruses, Lymphocytic Choriomeningitis Virus (LCMV), was used. Detection of a surface protein in LCMV (GP1) is using the change in optical properties of gold nanoparticles. The changes in the surface plasmon resonance intensity and maximum frequency shift of the AuNPs were monitored observing the absorbance spectrum. Dynamic light scattering (DLS) was also used to monitor size changes associated to the detection of virus samples obtained in vitro.

3.2 Materials and Methods

3.2.1 Mice and Virus

Lymphocytic Choriomeningitis Virus strain Clone13 ($LCMV_{CL13}$) was harvested on BHK cells in Gibco® Minimum Essential Media (MEM) with phenol red (Thermo Fisher Scientific, Pittsburgh, PA https://www.fishersci.com/us/en/home.html) or Phosphate Buffer Saline (PBS) with 5 % Fetal Bovine Serum (FBS) and tittered on Vero cells by plaque assay (Ahmed et al., 1984).

3.2.2 Antibody and Reagents

Anti-LCMV antibody IgG isotype 1 (Cat. N˚: BM5090; Acris Antibodies Inc., Rockville, MD, https://us.acris-antibodies.com) was dialyzed in borate buffer (pH = 8.5) and stored at 4 ˚C. The final concentration was 0.2 mg/mL, measured using Nanodrop1000 (mass ε= 14.00). Gold nanoparticle (AuNPs) Sols (Ted Pella Inc, Redding, CA, http://www.tedpella.com) of 10 nm and 40 nm diameter (citrate stabilized), and phosphate buffered saline (PBS; Thermo Fisher Scientific, Pittsburgh, PA https://www.fishersci.com/us/en/home.html) was filter sterilized, both stored at 4 ˚C.

3.2.3 Antibody Conjugation to AuNPs

Gold nanoparticles (AuNPs) of 10 nm and 40 nm were obtained from Ted Pella, Inc. To determine the minimum amount of antibody needed to conjugate to the AuNPs, 20 μL of different concentrations of antibody from 0.01-0.2 mg/mL were added to 1 mL of AuNPs and 100 μL of Borate buffer (pH=8.5). These solutions were challenged with NaCl (10%) to observe aggregation of the AuNPs (color change from pink to purple). The solution that did not aggregate had the minimum amount of antibody, or more, to protect the AuNPs from aggregation. These observations were also monitored measuring the UV-Vis spectra of the solutions looking for the formation of the characteristic plasmon peak at 525 nm and a concave curvature around 640-680 nm.

3.2.4 UV-Vis Spectrophotometry and Dynamic Light Scattering

UV-Vis spectra of samples with only AuNPs (10 nm and 40 nm), antibody conjugated AuNPs and antibody conjugated AuNPs with different concentrations of virus were measured a wavelength range of 200-900 nm with an Ocean Optics USB4000 UV-Vis Spectrometer (Ocean Optics, Inc., Dunedin, FL, http://oceanoptics.com). Dynamic light scattering measurements of the same samples were taken using a SpectroSize 300

(Molecular Dimensions, Altamonte Springs, FL, http://www.moleculardimensions.com). The laser wavelength is at 690nm at 170˚. Twenty measurements were taken over 30 sec in each measurement and each sample was measured 2-3 times.

3.3 Results

3.3.1 Titration of the Amount of Antibody Bound to the Gold Nanoparticles

The technique used in this study is based on the modifications of the surface plasmon of gold nanoparticles (Compton & Osterloh, 2007). The antibody is adsorbed on the AuNP by non-covalent forces and when it encounters a viral particle, the gold nanoparticle changes its optical properties. Using an optimal amount of antibody is crucial (Pham et al., 2012). therefore, different amounts of anti-LCMV antibody (0-4 μg) were adsorbed on the surface of 1 mL of ~10 nm AuNP Sols (~5×10^{12} AuNPs) and 1 mL of ~40 nm AuNP Sols (~9×10^{10} AuNPs), separately. Excess of antibody leaves free antibody in solution that can bind LCMV, but this interaction will not be detected in the absorption spectrum because it does not lead to detectable surface changes on AuNPs.

Nonetheless, if there is not enough antibody adsorbed to the AuNPs, the surface of the nanoparticles adsorbs salt ions with the addition of NaCl making the surface neutral, which changes the plasmon signal and the gold nanoparticles aggregate observed by a color change (Thobhani et al., 2010b). To avoid interference with this salt addition, dialysis of the anti-LCMV antibody was necessary. To determine the optimal amount of antibody, solutions of AuNPs with different concentrations of antibody were treated with 1 M NaCl and the UV-vis absorbance spectra were obtained. Figure 3.1 shows absorbance spectra from AuNPs treated at a range of anti-LCMV antibody

concentrations. Upon treatment of AuNPs with anti-LCMV antibody, the absorption increased due to changes in the surface plasmon. By increasing the amount of anti-LCMV antibody, less AuNP surface is exposed causing a concomitant change in the absorbance spectrum. The characteristic plasmon resonance peak (520-540 nm) (Daniel & Astruc, 2004; Doak et al., 2010) becomes more prominent when more antibody is added and the formation of a concave curve around 580-690 nm is observed. Figure 3.1A and 3.1B show the visible spectra of the titration for 10 nm and 40 nm particles, respectively. For 10 nm AuNPs, initial changes in the plasmon reasonance peak were observed when 0.6 µg (0.48 µg/µL) were added, but concavity in the 580-690 nm region was absent (pink). The minimum amount of antibody required to observe both changes was 0.8 µg (0.64 µg/µL; purple). Additional antibody aliquots did not improve the signal. The spectra obtained following the addition of 1 µg (blue) and 4 µg (not shown) had the same features as the spectrum obtained with the sample using 0.8 µg. Performing a similar analysis with the 40 nm AuNPs (Figure 3.1B), the minimum amount of antibody required to observe both changes was 1.6 µg (1.28 µg/µL; blue). Experiments were repeated in triplicate, obtaining the same results (data not shown). The data was supported by the color change, from pink to purple, of the solutions after the treatment with NaCl (data not shown).

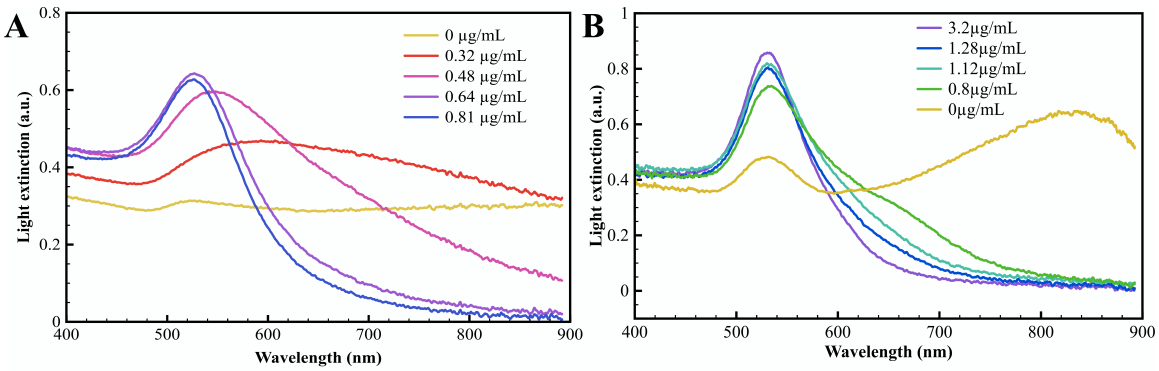

Figure 3.1. Titration Using NaCl of Gold Nanoparticles with a Range of Concentrations of Anti-LCMV Antibody.
A) For 10 nm gold nanoparticles. B) For 40 nm gold nanoparticles.

After determining the minimum amount of antibody to add to 1 ml of AuNPs for each size, the adsorption of the antibody was confirmed through UV-Vis spectroscopy and Dynamic Light Scattering (DLS). When comparing the spectra of unconjugated AuNPs and antibody conjugated AuNPs, the plasmon peak should have a shift to longer wavelengths (Pham et al., 2012; Thobhani et al., 2010a). Figure 3.2 shows a shift in the plasmon peak to the infrared wavelength when the AuNPs were conjugated with the antibody for both sizes of AuNPs, 10nm (Figure 3.2A) and 40 nm (Figure 3.2B).

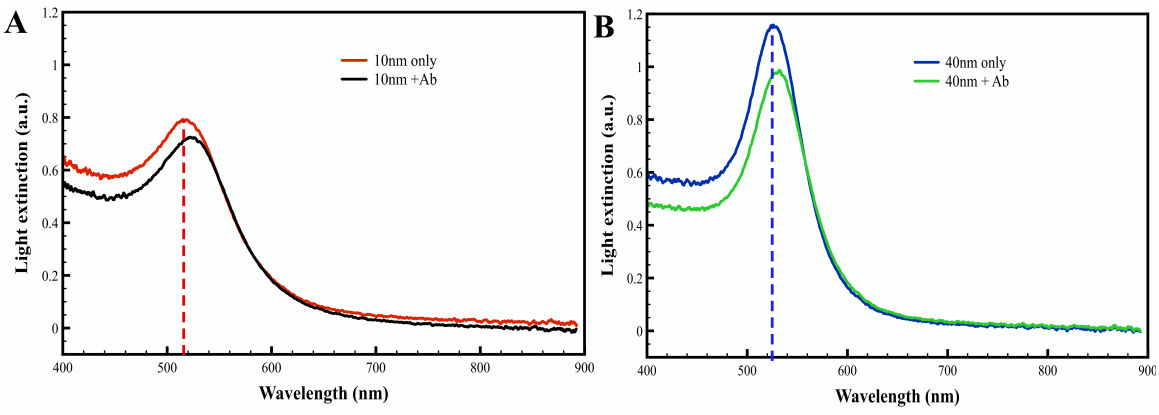

Figure 3.2. Visible Spectra of Antibody Conjugated Gold Nanoparticles.
Vis spectra of gold nanoparticles with and without antibody adsorbed in the surface of the gold nanoparticles for A) 10 nm gold nanoparticles and B) 40 nm gold nanoparticles.

DLS measurements with 40 nm unconjugated AuNPs showed an increase of the hydrodynamic radius after the conjugation of the antibody with the gold nanoparticles. Top panel of Figure 3.3 shows average radius of ~18.9 ± 0.52 nm for the gold nanoparticles, which is as expected (~20 nm). Bottom panel of Figure 3.3 shows the intensity counts of 40 nm AuNPs after the conjugation with the antibody. The average radius for conjugated AuNPs is ~21.9 ± 0.21 nm, with a high intensity count (sharp peak). The increase in diameter corresponds to the adsorption of the antibody.

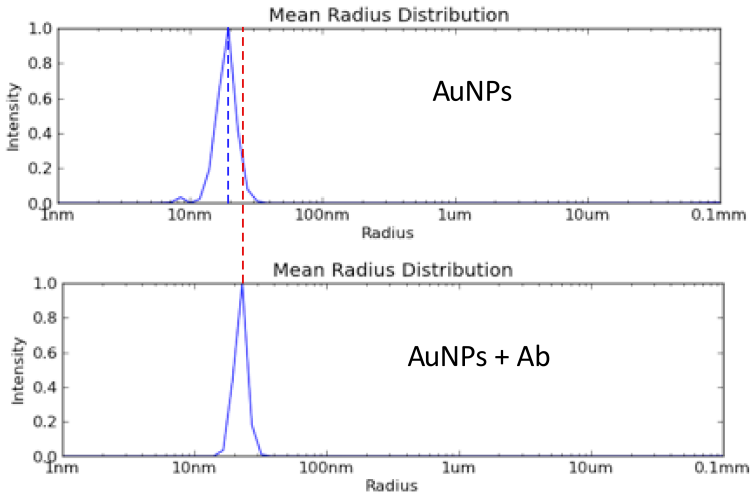

Figure 3.3. Dynamic Light Scattering of Antibody Conjugated Gold Nanoparticles. Evidence of successful conjugation or adsorption of the antibody to 40 nm gold nanoparticles observed by an increase in hydrodynamic radius of the particle. Intensity counts for gold nanoparticles without antibody (top) and with antibody conjugated (bottom) were measured.

3.3.2 Factors that Affect the Assay Measurements

Once the antibody was conjugated to the AuNPs, a standardized method would be used to monitor the changes in the optical properties of the AuNPs to determine the presence of a virus particle. To understand how the assay could be affected, three factors were tested: the medium in which the virus is harvested, pH of the medium or sample, and the blocking agent used in the conjugation of the antibody. The components of the medium in which the virus is harvested are important factors to take into account when analyzing the changes in the conjugated gold nanoparticles spectrum. These components can include pH indicator, fetal bovine serum (FBS) or amino acids (Thermo Fisher Scientific, 2016). Some amino acids and pH indicators, like phenol red, can absorb in the UV region (Sigma-Aldrich, 2016; Thermo Fisher Scientific, 2016). Figure 3.4 shows the effect of the color of the medium (MEM) due to the pH indicator red phenol. In each of

the samples that contained MEM with red phenol (yellow, red and black), there is a shift of the plasmon peak to the infrared and a shoulder around 520 nm. This effect corresponds to the absorption peak of the red phenol in its basic form (λ=557 nm) (Sigma-Aldrich, 2016). After observing the interference of the red phenol in the UV-Vis spectra of the conjugated AuNPs, the medium used for harvesting virus did not have a pH indicator, and therefore exhibited no color.

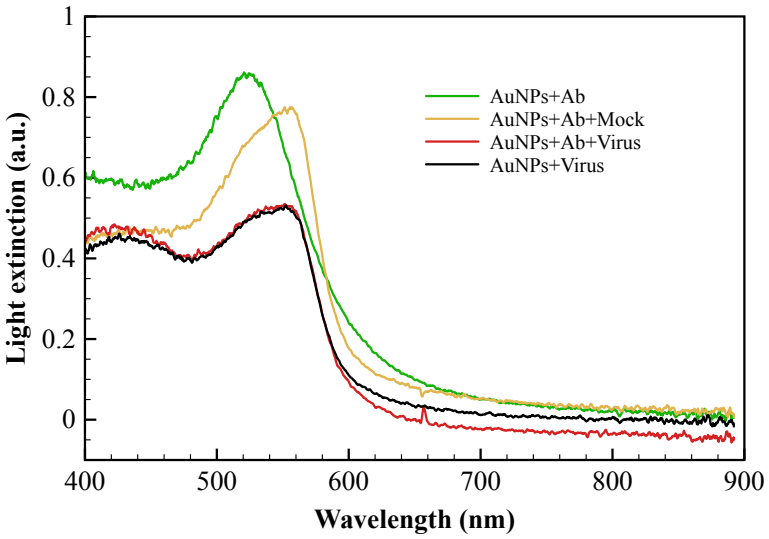

Figure 3.4. Effect of the Medium in which the Virus is Harvested.
Visible spectra of AuNPs with and without conjugated antibody in the presence of virus supernatant or mock (blank). The spectrum of antibody conjugated AuNPs was used as control.

Another factor that could influence the UV-Vis measurements is the pH of the sample because it can alter the chemistry of the gold nanoparticles surface or destabilize the protein conjugated to the gold nanoparticle (Brewer, Glomm, Johnson, Knag, & Franzen, 2005; Du, Li, & Cheng, 2008; Thobhani et al., 2010a; Tsai et al., 2011). To test the effect of pH, the conjugated gold nanoparticles were mixed in a 1:1 proportion with media (without phenol red) at different pH values. Figure 3.5 shows the UV-Vis spectra

of the conjugated gold nanoparticles at pH 6-8. It is observed that pH affects the plasmon peak intensity of the conjugated gold nanoparticles.

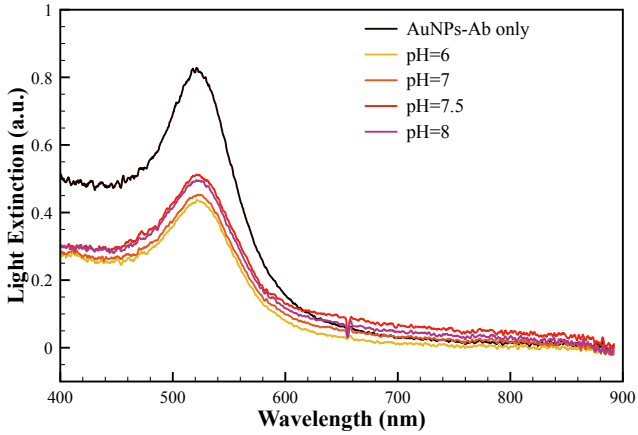

Figure 3.5. Effect of pH on the Light Extinction of Conjugated AuNPs.
Visible spectra of antibody conjugated AuNPs in the presence of medium (MEM without pH indicator) at different pHs.

To study this effect in more depth, the UV-Vis spectra of conjugated gold nanoparticles with media at different pH values were measured for 45 - 50 minutes at 5 min intervals. Figure 3.6 shows the initial (t=0 min) and final (t=45 min or t=50 min) spectra of conjugated gold nanoparticles at different pH values. At pH=6, 7.5 and 8, the light extinction of the conjugated AuNPs decreases, representing instability of the ligand (antibody) as a conjugate. At pH=6.5 and 7 the light extinction is unchanged over that period of time, suggesting stability of the interactions of the protein with the AuNPs over time.

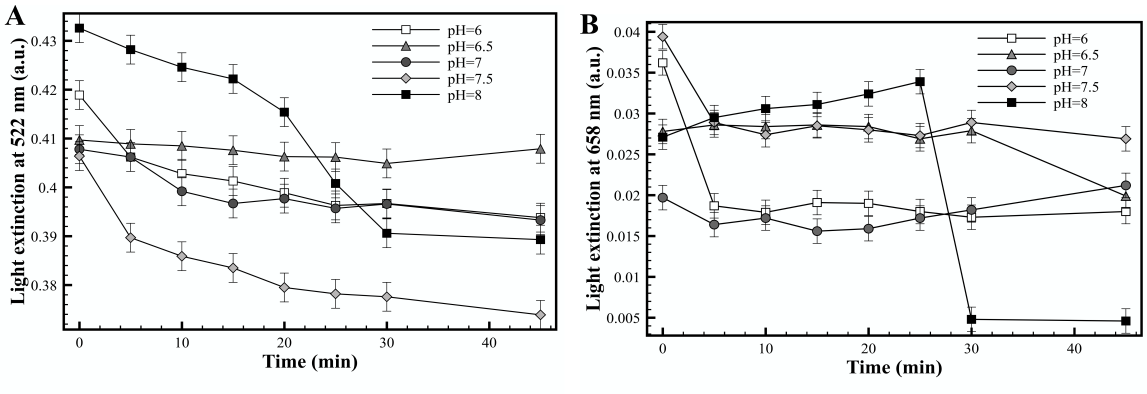

Figure 3.6. Effect Over Time of pH on the Light Extinction of Conjugated AuNPs.
Light extinction of antibody conjugated AuNPs in the presence of medium (MEM) without pH indicator at different pH values for 45 min at 5 min intervals. A) At the plasmon peak (522 nm), and B) at the aggregation region of 640-680 nm (658 nm).

Lastly, the use of a blocking agent during conjugation and its concentration, can have an effect on the interaction of the antibody and the virus. The blocking agent can block not only the empty spaces on the surface of the AuNPs, but also the sites of specific interaction between the virus particles and the antibody. For this reason, different concentrations of fetal bovine serum (FBS) and BSA were used as blocking agent during the conjugation step. Figure 3.7 shows that the minimum concentration of FBS to have the same effect as the one observed with BSA is 1%. The effect of the blocking agent is minor after a certain concentration, as expected, because it means that the empty spaces on the surfaces have adsorbed the blocking protein, and therefore increased the stability of the conjugated gold nanoparticles.

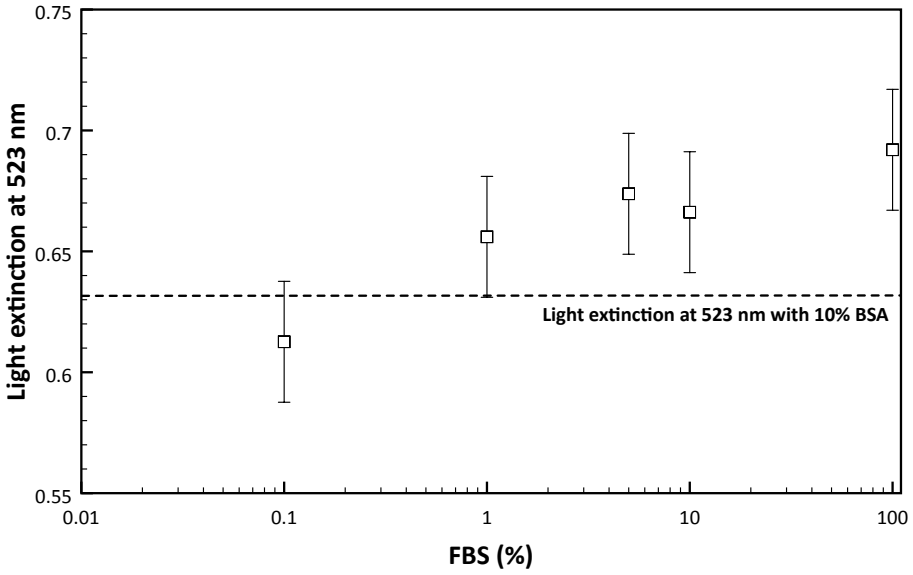

Figure 3.7. Effect of Blocking Agent on Light Extinction of Conjugated AuNPs.
Visible spectra of antibody conjugated AuNPs using different concentrations of FBS or BSA as blocking agents during the conjugation with the antibody.

3.3.3 Virus detection

After determining what were the conditions at which pH, blocking agent and medium do not affect the UV-Vis measurement, these optimized conditions were used to detect optical changes specific to the interaction between the antibody on the surface of the gold nanoparticle and the virus particle. For this purpose, conjugated gold nanoparticles were exposed to different concentrations of virus and PBS was used as a negative control. Figure 3.8A shows the UV-Vis spectra of 10 nm conjugated gold nanoparticles in the presence of different virus concentrations. Although the plasmon peak intensity changes with different viral concentrations, there is no clear trend of this change as the virus concentration increases. Figure 3.8B shows the light extinction change at 522 nm, which is the wavelength where the plasmon peak is observed for this nanoparticle size. It was observed that fluctuations exist and the readings do not indicate

a steady trend when the amount of virus particles is increased. This is observed in the three replicas of the experiment (sample 1, 2 and 3).

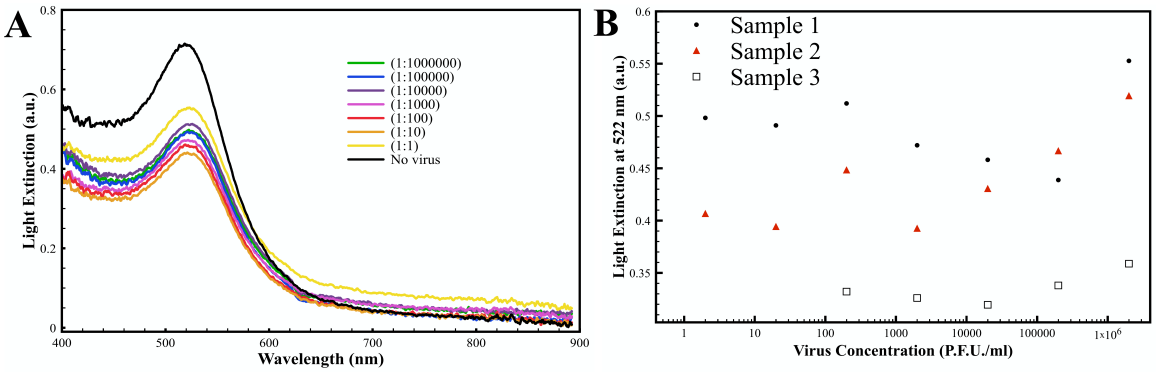

Figure 3.8. Solution of 10 nm Conjugated AuNPs in the Presence of Virus Dilutions. A) UV-Vis spectra of antibody conjugated AuNPs with dilutions of a virus sample (2×10^0-2×10^6 P.F.U.). B) Light extinction at 522 nm (plasmon peak) of antibody conjugated AuNPs in the presence of different virus dilutions (2×10^0-2×10^6 P.F.U.) in triplicate.

To determine if the size of the gold nanoparticle had any effect on the results, the same experiment performed with 10 nm conjugated gold nanoparticles was repeated with 40 nm conjugated gold nanoparticles. Figure 3.9A shows the UV-Vis spectra of 40 nm conjugated AuNPs in the presence of increasing concentrations of virus. The results are similar to the results observed with 10 nm conjugated gold nanoparticles. Looking closely at the changes in the light extinction on the plasmon peak (Figure 3.9B), the results are not reproducible between samples, except when the virus is at its highest concentration (2×10^6 P.F.U.) which for two samples generates the highest light extinction among the rest of the samples.

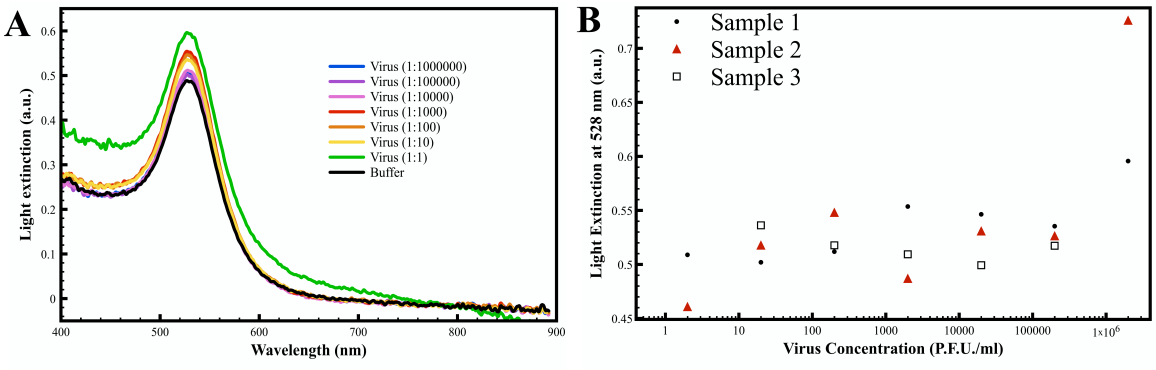

Figure 3.9. Solution of 40 nm Conjugated AuNPs in the Presence of Virus Dilutions. A) UV-Vis spectra of antibody conjugated AuNPs with dilutions of a virus sample (2×10^0-2×10^6 P.F.U.). B) Light extinction at the plasmon peak (528 nm) of antibody conjugated AuNPs in the presence of different virus dilutions (2×10^0-2×10^6 P.F.U.) in triplicate.

To confirm the recognition of the virus through an antibody conjugated AuNP, DLS measurements at the addition of virus to antibody conjugated AuNPs were performed. To confirm the size of the virus, a separate sample with only virus was measured (Figure 3.10, middle). The hydrodynamic radius of the virus sample suggested a non-homogeneous size in the virus sample because of the presence of a broad peak around 65.38 ± 3.45 nm. Nevertheless, an average diameter of 120 nm of the virus is within the expected size range for LCMV (Neuman et al., 2005). When the virus is added to antibody conjugated AuNPs (Figure 3.10, bottom), there is no increase in the radius (66.06 ± 3.59 nm) and there is no perceived peak that would represent the conjugated AuNPs by themselves.

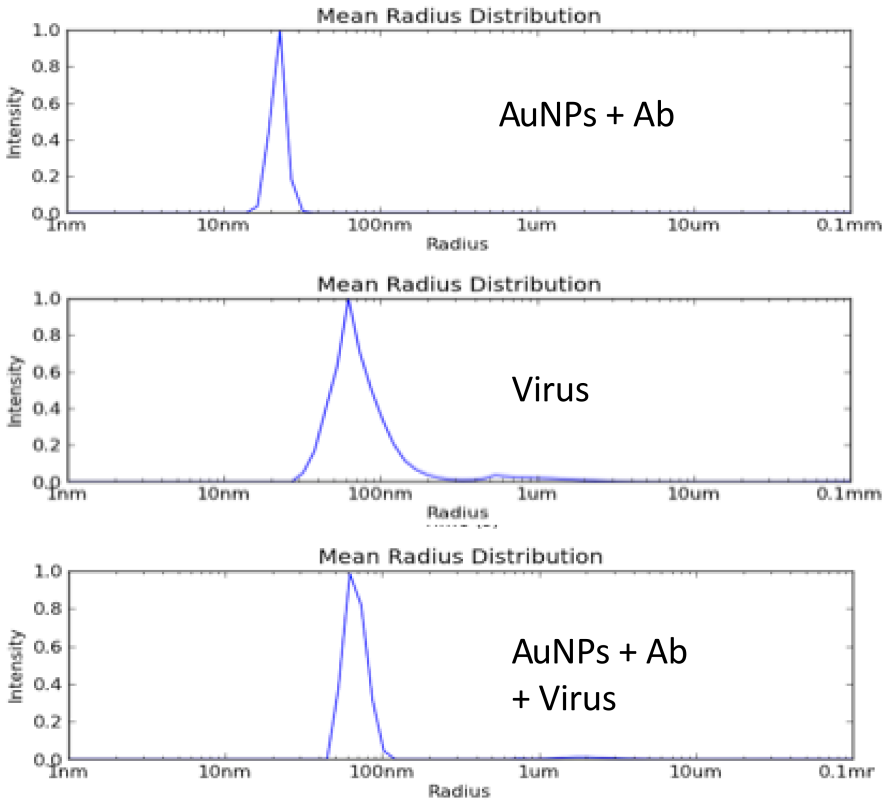

Figure 3.10. Hydrodynamic Radius of Conjugated Gold Nanoparticles and Virus. Dynamic light scattering measurements of 40 nm antibody conjugated AuNPs (top), virus (2×10^5 P.F.U./ml; middle) and the conjugated gold nanoparticles in the presence of the virus (bottom).

3.4 Discussion

AuNPs are broadly used in different fields, for example, as biosensors (Aslan, Lakowicz, & Geddes, 2004; Bogdan et al., 2012; Driskell et al., 2011; Pham et al., 2012). AuNPs are used in this study as biosensors to determine the amount of virus in different samples. Determination of the optimal amount of antibody to conjugate with AuNPs is an important step (Pham et al., 2012). The optimal amount of anti-LCMV antibody determined for 1 mL of AuNPs Sols was 0.8 µg and 1.6 µg for 10 and 40 nm AuNPs, respectively (Figure 3.1). These values were supported by the color change from pink to gray or purple when 1 M NaCl was added to these solutions. The color change is due to

aggregation of AuNPs resulting from replacement with surface-bound citrate ions by chloride ions (Thobhani et al., 2010b). Although the spectra obtained with an excess of antibody were similar to the spectrum obtained using an optimal amount of antibody, it is important to not exceed the amount of antibody that can bind the AuNPs because free antibody in solution would interfere with the sensitivity of the method and reduce the cost-benefit advantage of our technique. The absorbance spectrum with the minimum amount of antibody had two important features: the formation of a characteristic plasmon peak at 510-530 nm (Daniel & Astruc, 2004) and a rapid decrease in absorbance between 640 and 690 nm, leading to a formation of a concave curve between 580-690 nm. The latter is the feature that was analyzed throughout this study. The plasmon peak was not analyzed because there are many environmental variables that can change the intensity of the peak or cause a shift in wavelength (van Dijk, 2007). Based on this result, the stoichiometry of antibodies conjugated to each 10 nm AuNP was calculated giving ~0.57 antibodies per 10 nm AuNP. This means that not all of the AuNPs are covered with the protein (anti-GP1 antibody), which can lead to unspecific interactions with the virus particles when exposed to the virus. For this reason, other types of conjugation (i.e. covalent conjugation) or another method for non-covalent conjugation, like the method described in Chapter 2, can be used to ensure that most of the AuNPs are covered with the protein. For the 40 nm AuNPs, stoichiometry results in ~5 antibodies on average per AuNP, which suggests the assay has a nanoparticle size dependency.

After the conjugation, UV-Vis spectroscopy and DLS measurements confirmed that the AuNPs had antibody on the surface (Figure 3.2 and 3.3). The characterization of the adsorption of the antibody could be evidenced in the infrared shift and the increase on

hydrodynamic radius of the gold nanoparticle in 4 nm on average. This suggests that the position of the antibody might be tilted and not at 90˚ with respect to the AuNP (Ijeh, 2011). If the antibody would have been perpendicular to the AuNP, the hydrodynamic radius measurement would increase about 7 nm. This tilted position might be exposing one of the two epitopes present in the antibody to a greater degree. The arrangement of the antibodies on the surface of the AuNP could contribute to a decrease in sensitivity. The method used in this study to adsorb the antibodies on the surface on the AuNP does not show a preference for any position of the antibody. Hence, one of the regions interacting with some of the antibodies could be the epitopes, making difficult the recognition of its antigen. There are other methods that have improved this interaction, making it directional and preferential for the constant region of the antibody (Fc) (Kumar, Aaron, & Sokolov, 2008).

The influence of important factors such as pH, presence of other components and preparation of the AuNPs can be crucial when determining which is the best method to detect changes in the optical properties of the AuNPs due to the presence of the virus. Figure 3.5 and 3.6 showed that the most suitable pH at which the conjugated AuNPs are most stable is between 6.5 and 7. This is an advantage because clinical samples would be serum samples, which have a pH near 7. The presence of other components like red phenol was affecting the UV-Vis measurements, especially because of its absorbance peak around 524 nm. This absorption overlaps with the regions studied as seen in the blank sample (Figure 3.4). After obtaining this result, the virus was harvested in vitro in PBS + 5 % FBS, which doesn't have high amounts of components that would affect the UV-Vis measurements. Another factor that showed interference with the stability of the

conjugated AuNPs was the blocking agent used at the beginning of the study. Depending on the amount of blocking agent used, this could block epitopes of the antibody preventing interactions with the target. This suggested that the use of a blocking agent is not always needed, but it can prevent possible unspecific interactions of the virus particles and the AuNPs.

The conjugated AuNPs in the presence of virus produces fluctuations in the optical properties and do not show a steadily increasing or decreasing trend. These fluctuations may be because sample analysis to detect virus using antibody conjugated AuNPs and UV-vis spectrophotometry possibly has low sensitivity compared to the plaque assay, a classical technique to determine plaque forming units (PFU) (Ahmed et al., 1984). Another disadvantage of UV-vis spectrophotometry is the need for large amounts of sample (~500 μL). One of the reasons there is no clear trend when adding the virus is the region of wavelengths that is being studied. Although the changes in the plasmon peak did not show a conclusive trend, the region of 640-690 nm did show signs of aggregation (increased light extinction) when the highest concentration of virus is exposed to the conjugated AuNPs. Compared to the plasmon peak, this region may be more appropriate to analyze the antibody-antigen interaction.

On the other hand, DLS measurements of the hydrodynamic radius when the conjugated AuNPs were exposed to the virus show no changes comparing to the hydrodynamic radius of the conjugated AuNPs. This suggests that the virus might be surrounding ("hugging") the AuNPs and the light scattered is not showing a linear binding (AuNP-antibody-virus), but is only showing the virus. Another possibility is that the antibody that is conjugated by electrostatic interactions to the gold nanoparticle has

changed conformation due to new interactions with the gold nanoparticle. This change has been observed in other proteins when conjugation has been by non-covalent interactions (Singh, Nagappan Nair, & Aradhyam, 2013; Tsai et al., 2011). If this is the case, then the recognition of virus particles cannot take place because epitopes recognize the target protein mainly by conformation. To further test this hypothesis, it is recommended to perform an ELISA assay with conjugated gold nanoparticles and confirm that the interaction antigen (virus protein)-antibody is still present. If there is a change in conformation, it is suggested to use another type of conjugation and avoid direct interaction with the AuNP.

3.5 References

Ahmed, R., Salmo, A., Butler, L. D., Chiller, J. M., & Oldstone, M. B. A. (1984). Selection of Genetic Variants of Lymphocytic Choriomeningitis Virus in Spleens of Persistently Infected Mice: Role in Suppression of Cytotoxic T Lymphocyte Response and Viral Response. *Journal of Experimental Medicine, 60*, 521-540.

Aslan, K., Lakowicz, J. R., & Geddes, C. D. (2004). Nanogold-plasmon-resonance-based glucose sensing. *Anal Biochem, 330*(1), 145-155. doi:10.1016/j.ab.2004.03.032

Bogdan, N., Rodriguez, E. M., Sanz-Rodriguez, F., de la Cruz, M. C., Juarranz, A., Jaque, D., . . . Capobianco, J. A. (2012). Bio-functionalization of ligand-free upconverting lanthanide doped nanoparticles for bio-imaging and cell targeting. *Nanoscale, 4*(12), 3647-3650. doi:10.1039/c2nr30982c

Brewer, S., Glomm, W., Johnson, M., Knag, M., & Franzen, S. (2005). Probing BSA Binding to Citrate-Coated Gold Nanoparticles and Surfaces. *Langmuir, 21*, 9303-9307.

Carter, J. R., Balaraman, V., Kucharski, C. A., Fraser, T. S., & Fraser Jr, M. J. (2013). A novel dengue virus detection Method that couples DNAzyme and gold nanoparticle approaches. *Virology Jounal, 10*.

Compton, O. C., & Osterloh, F. E. (2007). Evolution of size and shape in the colloidal crystallization of gold nanoparticles. *Journal of American Chemical Society, 129*, 7793-7798.

Daniel, M.-C., & Astruc, D. (2004). Gold Nanoparticles: Assembly, Supramolecular Chemistry, Quantum-Size-Related Properties and Applications toward Biology, Catalysis and Nanotechnology. *Chemistry Reviews, 104*, 293-346.

Doak, J., Gupta, R. K., Manivannan, K., Ghosh, K., & Kahol, P. K. (2010). Effect of particle size distributions on absorbance spectra of gold nanoparticles. *Physica E: Low-dimensional Systems and Nanostructures, 42*(5), 1605-1609. doi:10.1016/j.physe.2010.01.004

Driskell, J. D., Jones, C. A., Tompkins, S. M., & Tripp, R. A. (2011). One-step assay for detecting influenza virus using dynamic light scattering and gold nanoparticles. *Analyst, 136*(15), 3083-3090. doi:10.1039/c1an15303j

Du, B., Li, Z., & Cheng, Y. (2008). Homogeneous immunoassay based on aggregation of antibody-functionalized gold nanoparticles coupled with light scattering detection. *Talanta, 75*, 959-964.

Guzman, M. G., Halstead, S. B., Artsob, H., Buchy, P., Farrar, J., Gubler, D. J., . . . Peeling, R. W. (2010). Dengue: A continuing global threat *Nat Rev Microbiol, 8*(12 Suppl), S7-16.

Hoen, A. G., Keller, M., Verma, A. D., Buckeridge, D. L., & Brownstein, J. S. (2012). Electronic Event–based Surveillance for Monitoring Dengue, Latin America. *Emerging Infectious Diseases, 18*(7), 1147-1150. doi:10.3201/eid1808.120055

Ijeh, M. (2011). *Covalent gold nanoparticle-antibody conjugates for sensitivity improvement in LFIA*. (Doctor in Philosophy), Hamburg University, Hamburg, Germany.

Jelinek, T. (2009). Trends in the Epidemiology of Dengue Fever an their Relevance for Importation to Europe. *Eurosurveillance, 14*(25), 1-3.

Korns Johnson, D., & Homann, D. (2012). Accelerated and improved quantification of lymphocytic choriomeningitis virus (LCMV) titers by flow cytometry. *PLoS One, 7*(5), e37337. doi:10.1371/journal.pone.0037337

Kumar, S., Aaron, J., & Sokolov, K. (2008). Directional conjugation of antibodies to nanoparticles for synthesis of multiplexed optical contrast agents with both delivery and targeting moieties. *Nat Protoc, 3*(2), 314-320. doi:10.1038/nprot.2008.1

McCausland, M. M., & Crotty, S. (2008). Quantitative PCR technique for detecting lymphocytic choriomeningitis virus in vivo. *J Virol Methods, 147*(1), 167-176. doi:10.1016/j.jviromet.2007.08.025

Neuman, B. W., Adair, B. D., Burns, J. W., Milligan, R. A., Buchmeier, M. J., & Yeager, M. (2005). Complementarity in the supramolecular design of arenaviruses and retroviruses revealed by electron cryomicroscopy and image analysis. *J Virol, 79*(6), 3822-3830. doi:10.1128/JVI.79.6.3822-3830.2005

Pham, V. D., Hoang, H., Phan, T. H., Conrad, U., & Chu, H. H. (2012). Production of antibody labeled gold nanoparticles for influenza virus H5N1 diagnosis kit development. *Adv. Nat. Sci.: Nanosci. Nanotechnol., 3*, 45017-45024.

Sigma-Aldrich, C. (2016). Phenol Red, ACS reagent. Retrieved from http://www.sigmaaldrich.com/catalog/product/sial/114529?lang=en&region=US

Singh, V., Nagappan Nair, S. P., & Aradhyam, G. K. (2013). Chemistry of conjugation to gold nanoparticles affects G-protein activity differently. *J Nanobiotechnology, 11*, 7.

Thermo Fisher Scientific, I. (2016). Medium Essential Medium (MEM). Retrieved from https://www.thermofisher.com/us/en/home/life-science/cell-culture/mammalian-cell-culture/classical-media/mem.html

Thobhani, S., Attree, S., Boyd, R., Kumarswami, N., Noble, J., Szymanski, M., & Porter, R. A. (2010a). Bioconjugation and characterisation of gold colloid-labelled proteins. *J Immunol Methods, 356*(1-2), 60-69. doi:10.1016/j.jim.2010.02.007

Thobhani, S., Attree, S., Boyd, R., Kumarswami, N., Noble, J., Szymanski, M., & Porter, R. A. (2010b). Bioconjugation and characterization of gold colloid-labelled proteins. *Journal of Immunological Methods, 356*, 60-69.

Tsai, D.-H., DelRio, D. W., Keene, A. M., Tyner, K. M., MacCuspie, R. I., Cho, T. J., . . . Hackley, V. A. (2011). Adsoption and Conformation of Serum Abumin Protein on Gold Nanoparticles Investigated using Dimensional Measurements and in situ Spectroscopic Methods. *Langmuir, 27*, 2464-2477.

van Dijk, M. A. (2007). *Nonlinear-optical studies of single gold nanoparticles.* (Doctor in Philosophy), University of Leiden.

Chapter 4

4. ANTIBODY DETECTION USING ANTIGEN CONJUGATED GOLD NANOPARTICLES

4.1 Introduction

The development of a rapid and accurate means for identifying the cause of a systemic infection has been a subject of intense interest due to the need for proper course of treatment in order to improve patient outcomes. For tropical regions of the world, there is a growing need for accurate diagnoses due to the toll in human and economic terms due to endemic diseases caused by mosquitoes. Of particular focus in developing countries in the tropical zone where Dengue Fever is endemic, is the ability to ascertain whether a patient has contracted Dengue Fever and which serotype (DEN-1, 2, 3, 4 and a probable newest serotype DEN-5) is the probable cause of the illness. While symptomatic diagnostics play an important role in all febrile disease management, some Dengue Fever serotypes are believed to be directly linked to severe courses of infection such as Dengue Shock syndrome and Dengue Hemorrhoragic Fever, making early serotype identification a potentially valuable tool. Moreover, confirmation of whether the patient has had a prior serotype infection (which has also been linked to severe Dengue infection courses) can also help to determine whether more aggressive steps should be taken to keep the patient hydrated and under hospital care ((WHO), 2009; Da Silva, 2014; Mustafa, Rasotgi, Jain, & Gupta, 2015; Tüiskunen-Bäck & Lundkvist, 2013).

Microscopy techniques using gold and other metallic nanoparticles are popular as biosensors for detecting the presence of specific biomarkers on tissue and cell samples, due to the significant contrast visualizing them when conjugated to antibodies and other

ligands (Driskell, Jones, Tompkins, & Tripp, 2011; Engleienne, 1998; S.-H. Huang, 2006; X. Huang, Jain, & El-Sayed, 2007). Accompanying these applications, there has been much attention paid over the past 25 years to the use of gold nanoparticles in solution for molecular detection as a homogeneous phase assay, primarily for antibody and nucleic acid based tests (Ghosh & Pai, 2007; X. Huang et al., 2007).

In order to meet the need for a rapid diagnostic that can be implemented in the field and closely based on patient exposure and/or immune response at an early stage of patient reported symptoms, a hybrid approach that combines gold nanoparticle conjugates used in low-cost paper diagnostics based on lateral flow immunoassay technology with high sensitivity in conjunction with a quantitative means for detecting a positive response is the subject of this feasibility study. In order to establish a relatively low cost diagnostic tool, the hybrid technology described in this chapter builds upon the employment of an optical caustic light scattering technology that employs no lenses and does not need filters (García, Nuñez, Lastra, & Mujica, 2013). Moreover, the use of battery powered LEDs and the deployment of a smartphone to analyze the scattered light are also helpful in reducing cost as well as in improving access to the device for low and middle income countries.

To commence a process of verifying the capabilities of the new hybrid technology platform in a simulated low resource setting, the first approach was to determine if an existing Dengue molecular reagent for gold nanoparticle conjugation in paper assays could detect Dengue antibodies with human patient samples using this new hybrid technology platform. This direct approach with clinically relevant samples is a faster way to determine key parameters such as: (1) size of gold nanoparticle that should be used; (2)

stability of the gold nanoparticle conjugates when subjected to transportation and varying temperature conditions; (3) whether very small amounts of human serum samples can yield reasonable signals; (4) determine the need for additional dilution or blocking steps when working with human serum; and (5) whether room or body temperature and incubation time generate differences in measurement. These key variables in the use of antigen conjugated gold nanoparticles and the effect of both particle size and stability are addressed during this study. Results obtained for the development of two specific homogeneous assays for detection of anti-BSA and anti-Protein E antibodies using conjugated gold nanoparticles of 60 nm nominal diameter are described. Specifically, the study discuss effects the addition of electrolytes to increase sensitivity using the anti-BSA homogeneous assay confirmed by ELISA results, and results with the use of multiple detection methods, light extinction, light scattering and optical caustic sensor, with confirmation of microplate results of the surface-bound protein and antibody system. Since the plasmonic response of gold nanoparticles is relatively well-understood and there are simple online simulators based on Mie Theory, numerical simulations were used to provide additional verification of the consistency.

Thus, the overall objective of this feasibility study is solely to gain experience in practical aspects of developing a rapid and hybrid quantitative homogeneous assay for detection of antibodies in serum. This case in specific studies the determination of Dengue infection by monitoring patient antibody response to Dengue antigens while simulating a low resource setting in order to expand testing in a variety of locales and with a wider variation in infrastructure than is normally the case in high income country clinics and hospitals.

4.2 Materials and Methods

4.2.1 Buffers and Protein Solutions

Phosphate Buffered Saline (PBS) with 0.2% sodium azide, acetate buffer (pH = 5), and sodium chloride (5 M) were prepared. Bovine Serum Albumin (Boston Bioproducts, Ashford, MA https://bostonbioproducts.com) was dissolved in freshly prepared pH = 5 acetate buffer (Fisher Scientific, Pittsburgh, PA https://www.fishersci.com/us/en/home.html) to create a stock solution of 10 mg/ml BSA. Recombinant DENV-2 Envelope Protein 32 kDa produced in *E. coli* (Reagent Proteins, San Diego, CA http://www.reagentproteins.com) was purchased with a concentration of 0.96 mg/ml. The solution was diluted in acetate buffer to prepare BSA binding titration experiments.

Polyclonal anti-BSA antibody from rabbit (Rockland Immunochemicals, Lemerick, PA https://www.rockland-inc.com/) was diluted with PBS containing azide to create a stock solution of 0.1mg/ml. The stock solution was diluted with PBS containing azide to obtain different solutions (10, 5, 1, 0.1 and 0.01 μg/ml) in order to prepare samples for ELISA and gold nanoparticle assays. Polyclonal anti-Envelope protein antibody from goat (1 mg/ml) was diluted with PBS containing azide to obtain different solutions (10, 5, 1, 0.1 and 0.01 μg/ml) for the gold nanoparticle assays. Lyophilized human serum (Rockland Immunochemicals, Lemerick, PA https://www.rockland-inc.com/) was reconstituted in PBS containing azide.

4.2.2 Attachment of the Antigen to Gold Nanoparticles

In a 1.5 ml Eppendorf tube, an aliquot of 1 ml containing 9 x 10^{10} particles per ml of 40 nm and 2.6 x 10^{10} particles/ml of 60 nm gold colloids (Ted Pella Inc, Redding, CA, http://www.tedpella.com) were combined with 10 microliters of freshly prepared pH = 5 acetate buffer prior to the addition of 100 microliters of from 0.1 - 10 mg/ml bovine serum albumin depending upon whether coverage at the titration point or at 90 % of expected surface saturation was the objective. A frozen cold pack was placed on the tube and the mixture was gently rocked using an orbital table for 30 minutes as a practical incubation time for BSA binding.

After 30 minutes of incubation, 2.5 µl of a 10% solution of Tween 20 (Sigma-Aldrich Corp., St. Louis, MO http://www.sigmaaldrich.com) was added to the mixture, and the mixture was rocked again for 5 minutes. For each particle size, three centrifugation steps were conducted in order to reduce the concentration of BSA not bound to gold nanoparticles. The centrifugation conditions used were adapted from Cytodiagnostics Inc. (www.cytodiagnostics.com) recommended conditions. A Beckman Coultor Microfuge 18 was placed in a 4 ˚C environmental room in order to minimize aggregation of gold nanoparticles and ensure re-suspension after centrifugation.

For 60 nm gold colloids, the first centrifugation was for 30 minutes at 3500×*g*. Immediately after centrifugation, as much of the supernatant as possible was carefully removed from the pellet. Once this was accomplished, 1 ml of pH = 5 acetate buffer was added to re-suspend the pellet. 2.5 µl of 10% Tween 20 was then added to the suspension and the mixture was gently rocked for 5 minutes. Afterwards, the suspension was centrifuged again for 15 minutes at 3500×*g*. The same procedure was used following the

second centrifugation as the first. For the 3rd centrifugation, time was shortened to 10 minutes. After the third and final centrifugation, the pellet was resuspended in 1 ml PBS buffer with azide in preparation for the gold nanoparticle immunoassays.

In the case of protein E, after the third centrifugation step, 500 µl of a solution of BSA 0.2 mg/ml in DI H_2O were used as blocking agent. After rocking for 5 min on ice, 500 µl of PBS were added.

4.2.3 Detection of Antibodies by ELISA

Wells of polystyrene microtiter plates were coated for 2 h at room temperature with different BSA solutions: 5 µg/ml BSA/0.25% of Tween 20, 5 µg/ml BSA/0.5 M NaCl, 10, 5, 1 and 0 µg/ml in either 0.1 M sodium carbonate-bicarbonate buffer (pH = 9.6) or in acetate buffer (pH = 5).

Plates were washed twice with PBS/0.05% Tween 20 and aspirating the contents. Residual binding sites were saturated by incubation with blocking buffer (5% non-fat dry milk in PBS/0.05% Tween) for 1 hr at 4 ˚C, followed by two washes of diH_2O. 50 µl of each antibody solution (10, 5, 1, 0.1 or 0.01 µg/mL) diluted 1/40 in blocking buffer were added to each well and incubated for 1 hr at 37 °C. Unbound antibody was removed by washing 3 times with PBS/0.05% Tween 20, and 50 µl of goat anti-rabbit IgG peroxidase conjugate (Alpha Diagnostic International Inc, San Antonio, TX http://www.4adi.com) diluted 1/1000 in blocking buffer was added to each well. Plates were incubated for 1 hr at 37 °C and washed 3 times with diH_2O. Bound peroxidase was determined adding 100 µl SigmaFast OPD (Sigma-Aldrich Corp., St. Louis, MO http://www.sigmaaldrich.com) substrate. Optical density was read at 490 nm and compared to the negative control (uncoated wells).

4.2.4 Testing of Human Serum Samples

All human serum samples were obtained voluntarily from Hemolab S.A. and the Lab of Arbovirology of the Universidad Autonoma de Yucatán collected for previous studies. Two 6 ml bottles of conjugated gold nanoparticle reagent GNP-60-E were created according to the protocol above except that while one GNP reagent (GNP-60-E-3) was centrifuged 3 times to remove unbound Envelope Protein, a second reagent (GNP-60-E-1) was centrifuged only once. Both reagents were stored for 16 hours at 4 ˚C then transported at room temperature for 19 hours, until refrigerated at 4 ˚C at the Universidad Autónoma de Yucatán (UADY). Both GNP-60-E reagents arrived un-aggregated at UADY based on both Nanodrop spectrometer (Bio Rad Laboratory, Hercules, CA) visible spectra taken at the Universidad Autónoma del Yucatán (UADY) before using the reagents and by visual observation of the gold nanoparticle suspension.

For each test, in a 1.5 ml Eppendorf tube, 900 microliters of PBS was combined with 10 microliters of the gold nanoparticle conjugate followed by the addition of 5 or 10 microliters of the human serum or PBS negative control samples.

For the testing at 37 ˚C, GNP-60-E-3 was used and 10 microliters of undiluted human serum was added. Incubation was performed for 30 minutes at 37 ˚C without agitation. Afterwards, each test sample was placed in an oblate spheroid chamber and capped, followed by imaging with the smartphone sensor.

For the first trial at 22 ˚C, GNP-60-E-3 was used and 5 microliters of undiluted human serum was added. Incubation was performed for 15 minutes at 22 ˚C without agitation. Afterwards, each test sample was placed in an oblate spheroid chamber and capped, followed by imaging.

For the second trial at 22 ˚C, GNP-60-E-1 was used and 2 microliters of 1:10 diluted human serum was added. Incubation was performed for 15 minutes at 22 ˚C without agitation. Afterwards, each test sample was placed in an oblate spheroid chamber and capped, followed by imaging.

4.2.5 Smartphone Optical Caustic Light Scattering Sensor

A previously described smartphone-enabled optical caustic light scattering sensor was used to capture images of samples in an oblate spheroid chamber [1]. A 532 nm green Photodiode (Industrial Fiber Optics, Tempe, AZ) illuminated the sample chamber at a 90˚ angle from a Nokia Lumia 920 (Nokia, Espoo, Finland) smartphone camera lens. Images were collected at 0.5 second exposure using the Lumia camera app. At this exposure level, and with the intensity of light used, the green channel of the RGB images saturate. However, excess light due to scattering can be imaged in the center of the sample chamber by splitting the color channels using ImageJ (NIH, Bethesda, MD). ImageJ software was used to collect the intensity of the red and blue channels for each image. Integrated density measurements from ImageJ was collected for a constant image area and used to quantify the amount of scattering observed for gold nanoparticles in water, conjugated gold nanoparticles with a serum sample, or Phosphate Buffered Saline (PBS) control.

4.2.6 UV/VIS Spectroscopy and Light Scattering

An Ocean Optics Fiber Optic Spectrometer (Ocean Optics, Dunedin, FL, http://oceanoptics.com) was used for UV/VIS spectra acquisition using a USB4000 spectrometer and SpectraSuite Software for control and data acquisition. A quartz cuvette of 1 cm path length was used to acquire samples. Two different light sources

were used for measurements. For UV detection and standard VIS spectroscopy, a Deuterium Halogen light source was employed. For higher resolution visible spectroscopy, a 12 W 350 mA (Titanium) LED source was used. Since the cuvette has all four windows clear for measurement, a InPhotonics 532 nm laser with an Ocean Optics controller was in a 90 degree configuration from the fiber optic collector to measure counts of scattered light.

Spectra for UV/VIS data collection was generally collected between 10-100 milliseconds integration time and 20-100 spectra were averaged for each sample, depending upon the light source. No special temperature stabilization was made for the optical systems, so the drift in spectral recordings was negligible. For the light scattering experiments, readings over 1 second of integration and only 2 spectra were used for averaging.

4.2.7 Mie Theory-Based Numerical Simulations

All Mie theory calculations for light extinction and light scattering were made with the Mie theory calculator from nanoComposix website (http://nanocomposix.com/pages/tools).

4.3 Results

4.3.1 Detection of Gold Nanoparticles

Before interpreting visible light extinction spectra and static light scattering data in order to test the antibody immunoassays, a series of tests were done to compare results using citrate stabilized gold nanoparticles of different sizes with predicted behavior based on the Online Mie Theory Calculator.

These calculations were obtained using both the Raleigh approximation of the Mie theory for light scattering of smaller particles, and the Guinier approximation for larger particles (Mie, 1908; Ringe, Sharma, Henry, Marks, & VanDuyne, 2013; Sorensen, 2013). Using the Mie theory calculator the light extinction of the different systems used in this study could be predicted. Calculations assumed the concentrations provided by the manufacturer were correct and the total surface area of gold nanoparticles was used to generate graphs that were compared to the experimental results. Figure 4.1 shows that for visible light extinction, there is relatively good agreement between the raw data collected by the spectrometer and the online Mie Theory calculator values. There are three main similarities that are relevant to subsequent use of light extinction to interpret immunoassay test results. First, the extinction maxima shift to higher wavelengths and increases in intensity in both theoretical calculations and experimental results. Second, the lower wavelength extinction values are roughly grouped into 5 different levels. Lastly, the three largest sized nanoparticles do not have extinction curves that approach zero at 750 nm.

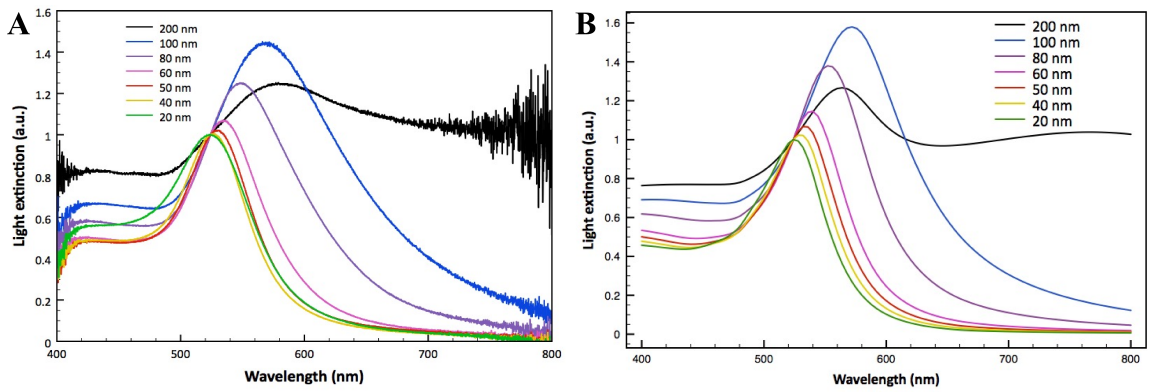

Figure 4.1. Predicted and Experimental Light Extinction from Gold Nanoparticles of Different Sizes.
Extinction measurement of gold nanoparticles with equal gold concentration, but size varying as shown: 20, 40, 50, 60, 80, 100, 200 nm. A). measured using a visible light spectrometer, and B). from calculations from the Nanocomposix web site http://nanocomposix.com/pages/tools

A basis of comparison for static light scattering between the theoretical calculations and the 532 nm green laser 90 degree scattering used experimentally is not straight-forward, due to the manner used in collecting scattering and recording counts. In order to interpret the theoretical predictions, it is also useful to introduce limits based on scattering regimes that predominate in particles ranging from 20 – 200 nm in diameter. Figure 4.2 is a graphical representation of calculations, correlations, and theoretical model limits. The main graph shows the relative scattering intensity versus particle diameter in a double log plot in order to ascertain trends more easily. Superimposed on the individual calculator predictions are curves showing functional curve fits for the limits of Rayleigh scattering dependence (for $kR \ll 1$) and the Guinier regime (for $kR \sim 1$), where k is the wave vector magnitude and R is a typical dimension of the scatterer. The inset shows the Online Mie Scattering extinction (contribution of scattering to the absorbance measured) due to scattering at 532 nm versus the experimentally measured

scattering counts. As expected, there is a reasonably strong correlation between these and the relationship is linear because the limit of small particles (< 20 nm) is zero for both scales and the upper limit of all extinction due to scattering is not approached at this wavelength for the maximum particle size used. For the purpose of comparison and interpretation, the correlation shown in the inset is useful for predicting the expected increase in static light scattering measured with small aggregates.

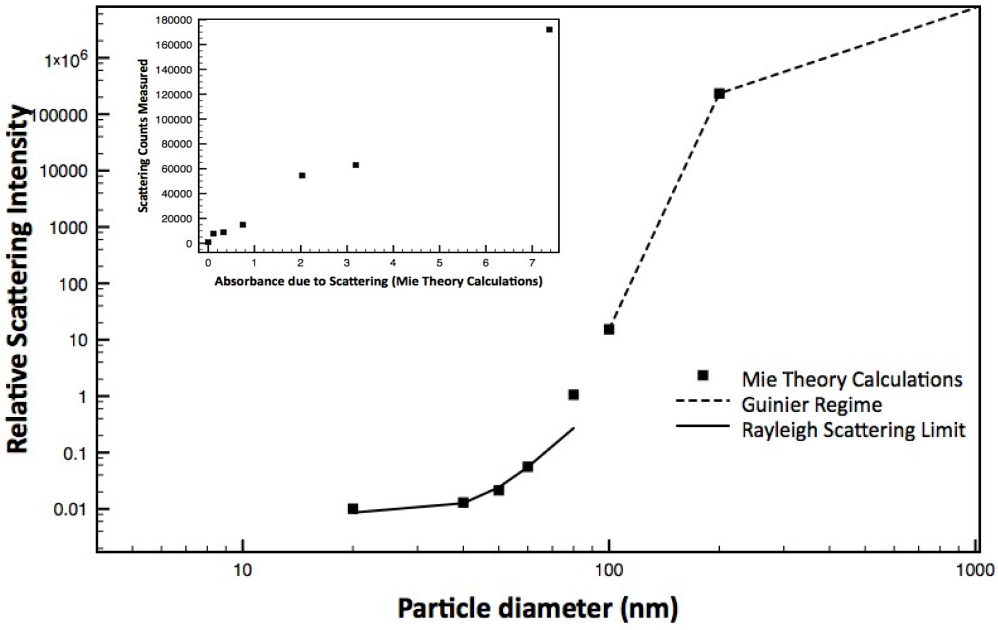

Figure 4.2. Relative Scattering Intensity of Gold Nanoparticles of Different Sizes.
Mie Scattering calculations from the Nanocomposix web site for 20-200 nm gold nanoparticles are shown along with the Rayleigh Scattering limit (kR<<1) and the Guinier regime (kR~1) for comparison. The inset shows the same Mie calculations in terms of the fractional contribution to light extinction measured as "absorbance" on the horizontal axis versus the 532 nm scattering at 90 degrees count peak heights.

4.3.2 Anti-BSA Assays

The next step to optimize was the detection step, which includes the addition of electrolytes before incubation with the sample and the incubation temperature with the

sample. To determine the sensitivity of the BSA conjugated gold nanoparticles and the optimal conditions to detect anti-BSA antibody, different concentrations of anti-BSA antibody (0.01-10 μg/ml) with different concentrations of BSA (10, 5, 1 μg/ml, 5 μg/ml/0.25% Tween 20 and 5 μg/ml/0.5 M NaCl) were tested using an enzyme linked immunosorbent assay (ELISA). Figure 4.3 shows that optimal results of antibody-antigen interaction obtained were using a 5 μg/ml solution of BSA in the presence of 5 M sodium chloride for coating. From the other conditions for optimal antibody-antigen interaction, only 1 μg/ml of BSA coating could induce a measurable interaction with respect to the negative control. The presence of Tween 20 in the BSA solution did not have an effect in the interaction between the antibody and the antigen respect to the negative control and other concentrations of BSA coating did not show any significant difference with respect to the negative control. The limit of detection of antibody for the BSA solution with NaCl was between 1-5 μg/ml of antibody anti-BSA.

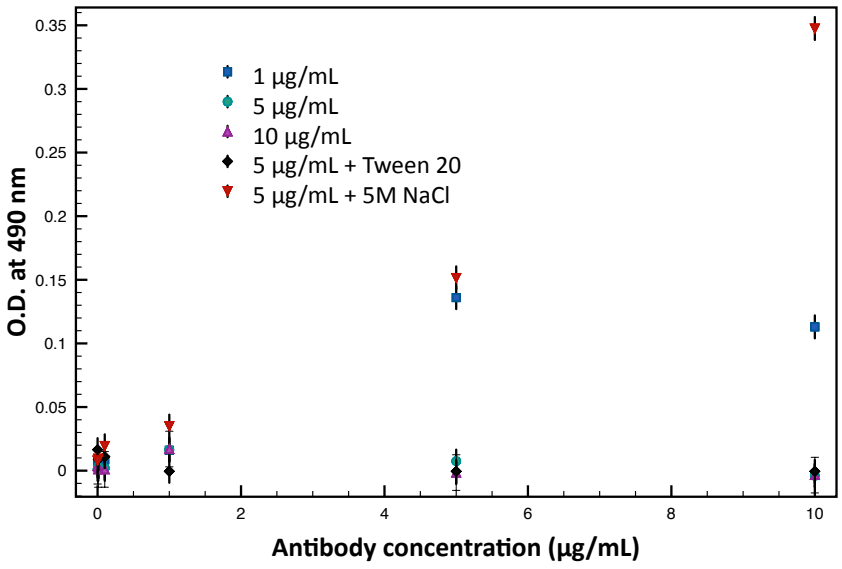

Figure 4.3. Antibody Detection Through ELISA Under Different Conditions.
Microplate results of ELISA with different coating concentrations of BSA (1, 5 and 10 µg/mL) with electrolyte or detergent (Tween 20) addition, testing for detection of a range of antibody anti-BSA concentrations (0-10 µg/mL).

To analyze the detection of antibodies anti-BSA with the conjugated gold nanoparticles, based on the results obtained with the ELISA, 100 µl of 5 M NaCl were added to the conjugated gold nanoparticle solution previous to the addition of the antibody. Static light scattering and visible light extinction of each sample were measured immediately after the addition of the antibody to monitor changes on the surface of the conjugated gold nanoparticles, presumably caused by the antibody-antigen interaction. Figure 4.4 shows how visible light extinction spectrum increases with the increasing addition of antibody (0.01-0.5 µg/ml). As higher amounts of antibody are added, the light extinction decreases again close to the control (1-10 µg/ml). This tendency was also reflected in static light scattering measurements as seen before in other experiments (Figure 2.2).

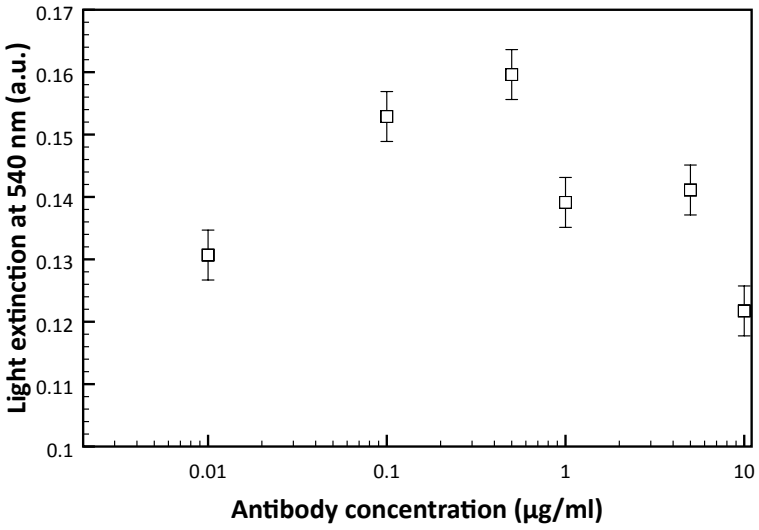

Figure 4.4. Antibody Detection of Conjugated AuNPs at Room Temperature.
Light extinction at RT after 0 min of addition of different concentrations of antibody (0-10 µg/ml).

4.3.3 Dynamic Light Scattering for Insights into Anti-BSA Assays

Once it was established that there is a change in SLS and visible light extinction of conjugated gold nanoparticles in the presence of antibody, dynamic light scattering (DLS) was used for confirmation of the antibody-antigen interaction. DLS of gold nanoparticles from the manufacturer suggests a nominal diameter of 65 nm (Figure 4.5), but the intensity distribution (Khlebstov & Khlebstov, 2011) appears to be relatively broad with a significant tail towards larger sizes. In sharp contrast, BSA attachment appears to significantly narrow the distribution and increase the mean diameter to approximately 80 nm. The intensity distribution change of about 15 nm in diameter appears to be with expected values (Doak, Gupta, Manivannan, Ghosh, & Kahol, 2010; Haiss, Thanh, Aveyard, & Fernig, 2007; Khlebstov & Khlebstov, 2011) and the stabilization and uniformity generated by the process of protein coating and

centrifugation with a surfactant is expected. However, it should be noted that for a second BSA conjugated gold nanoparticles sample, some particles > 4,000 nm were detected at relatively low intensity. This result is corroborated with static light scattering measurements, which indicate that this sample scatters significantly more than the other sample even though conditions to prepare them were identical.

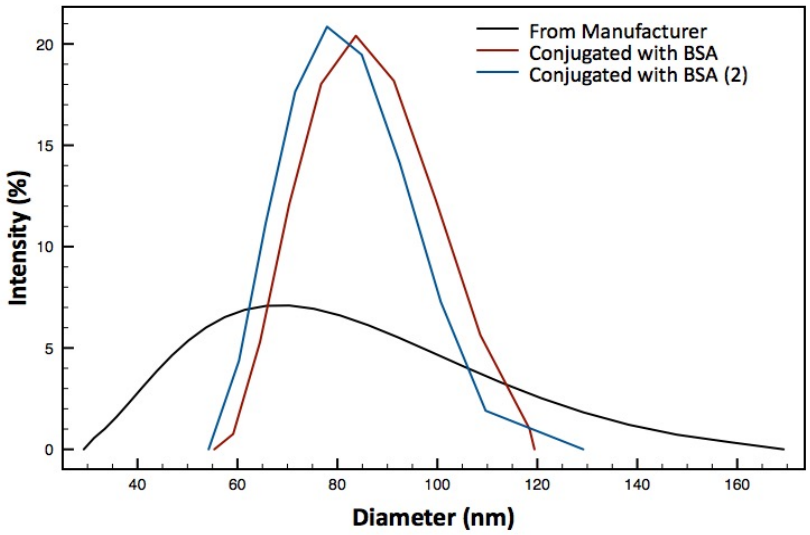

Figure 4.5. Diameter of Conjugated and Unconjugated AuNPs.
Dynamic Light Scattering intensity distribution measurement of 60 nm Gold Nanoparticles as is from the manufacturer and after processing to create a coating of BSA.

DLS intensity distributions were also measured for 60 nm gold nanoparticles with bound BSA and exposed to varying concentration of anti-BSA antibodies from 0-10 micrograms per ml. These analyses can yield reports of relatively large aggregates even with no addition of antibody and were confirmed by the extinction and static light scattering results. It appears that leaving the gold nanoparticles in the presence of the antibody overnight at 4 ˚C can reverse aggregation. Interestingly, when the hydrodynamic radius of different gold nanoparticle sizes are plotted for the highest

intensity regions, in general the distributions shift to higher sizes and the distribution broadens when the particle are equilibrated to higher concentrations of anti-BSA antibody (Figure 4.6). The sole result that does not conform to the trend seen in Figure 4.6 is for a sample of 5 µg/ml of anti-BSA antibody, but that sample contained significant levels of a population of very large (~4,000 nm) diameters.

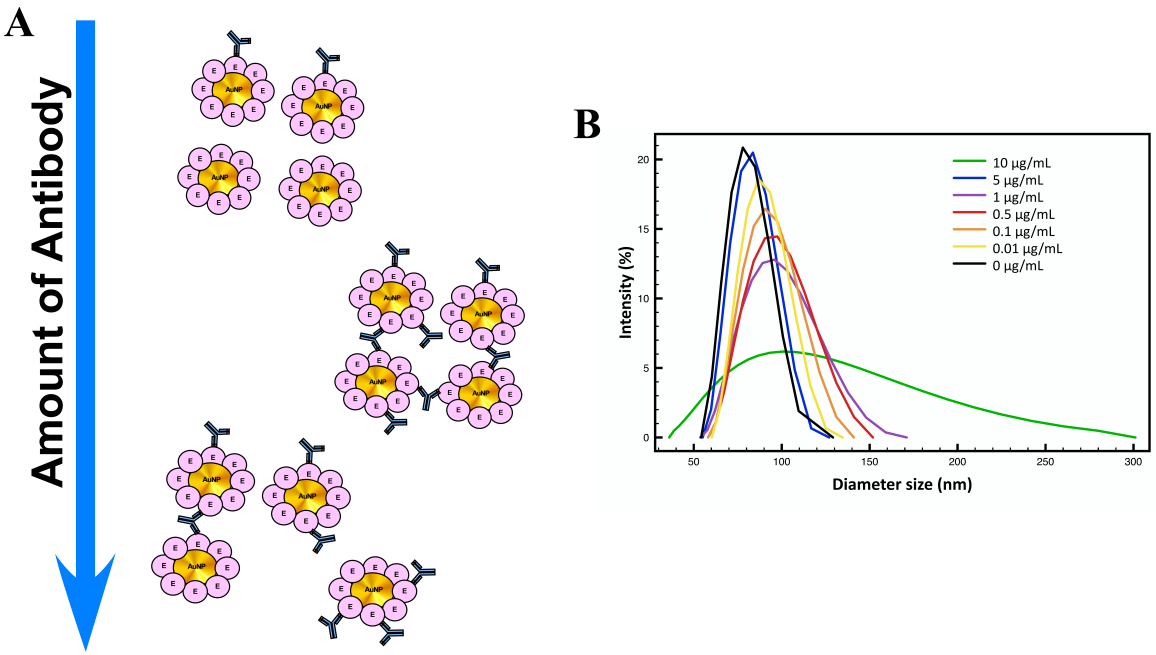

Figure 4.6. Particle Size of Conjugated AuNPs in Presence of Antibody.
A) Cartoon of the hypothesis of the behavior of the BSA system when the amount of antibody added to conjugated AuNPs increases. B) Graph of highest intensity distributions from dynamic light scattering results for anti-BSA assays with antibody concentrations ranging from 0 – 10 µg/ml.

4.3.4 Anti-Protein E Assays In Vitro

To confirm the behavior of the system observed with BSA conjugated gold nanoparticles, protein E conjugated gold nanoparticles were mixed with different concentrations of antibody anti-protein E (0.01-10 µg/ml) and static light scattered was measured. Figure 4.7 shows that more light is scattered in the presence of increasing

amount of antibody except for the curve of 1 μg/ml, which decreased the intensity with respect to 0.5 μg/ml.

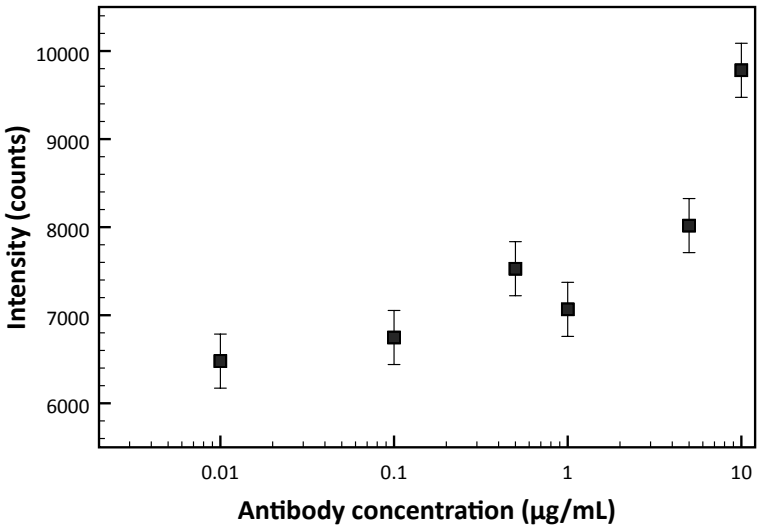

Figure 4.7. Antibody Detection in vitro Using Light Scattering Intensity Counts.
Light scattered of Green light LED at 532 nm by protein E conjugated gold nanoparticles in the presence of different concentrations of antibody anti-protein E (0-10 μg/ml).

The utility of conjugated nanoparticles is most likely in analysis of serum samples from patients, which would have more components such as other antibodies or complement protein, which may affect results differently than the system tested in vitro. To determine the effect of serum components in SLS and visible light extinction, lyophilized human serum was reconstituted and spiked with a known concentration of antibody was added to protein E conjugated gold nanoparticles. Visible Light extinction spectra and static light scattering were measured for samples spiked with different antibody concentrations and a reconstituted serum sample without antibody, as a negative control. Figure 4.8 shows that there is a considerable difference in both light extinction (Figure 4.8A) and light scattered (Figure 4.8B) by the gold nanoparticles in the presence

of antibody at concentrations equal to or higher than 0.5 µg/ml. This observation shows that the gold nanoparticles can effectively detect levels of antibody anti-protein E specifically, despite the presence of other components of human serum.

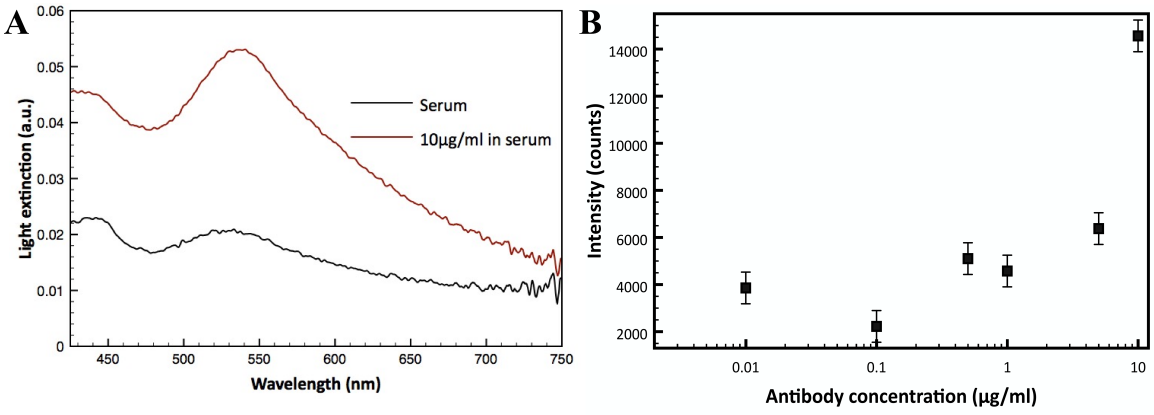

Figure 4.8. Antibody Detection in Reconstituted Human Serum.
A). Light extinction of Protein E conjugated gold nanoparticles in the presence of 10 µg/ml of antibody anti-protein E in human serum, and B). Light scattering of Protein E conjugated gold nanoparticles in the presence 0-10 µg/ml of antibody anti-protein E diluted in human serum. Negative control was human serum.

4.3.5 Detection of Anti-Protein E Antibody in Human Serum Samples

The initial challenge lay in interpreting patient results without an extensive study of the antigen protein structure nor its immunogenic properties when presented on gold nanoparticle surfaces. This makes discerning the performance of the tests with respect to patient Dengue status characterization challenging. The challenge is somewhat reduced by using a dot blot test with the same patient samples and gold conjugate reagents as an orthogonal test. Table 4.1 provides information on the 10 patient serum samples donated by the Arbovirus laboratory of UADY for this study. These samples represent a spectrum of patients including Dengue negative, Dengue serotype 2 positive with a first time

(primary) infection and 2nd time (secondary) infection, patients convalescing from a Dengue serotype 2 infection, and patients with Dengue serotypes 1 and 3 respectively.

Table 4.1. Description On Dengue Status of Human Serum Samples Used in the Feasibility Study.

Patient	Dengue Status	Primary or Secondary Infection	Stage of Disease
1	Negative	N.A.	N.A.
2	Negative	N.A.	N.A.
3	DENV-2	Primary	Initial stage
4	DENV-2	Primary	Initial stage
5	DENV-2	Secondary	Initial stage
6	DENV-2	Secondary	Initial stage
7	DENV-3	Unknown	Initial stage
8	DENV-1	Unknown	Initial stage
9	DENV-2	Unknown	Convalescing > 120 days
10	DENV-2	Unknown	Convalescing > 120 days

Before conjugation of Protein E to gold nanoparticles, the choice of gold nanoparticle size was deemed to be a key variable that needed to be determined. Based on the well understood properties of gold nanoparticles to light scattering via plasmon resonance (Fan, Zheng, & Singh, 2014) near the maximum for spheres of 520-540 nm, a calibration was conducted with a laser light scattering fiber optic spectrometer, the optical caustic sensor, and calculations based on Mie Theory (Fan et al., 2014; nanoComposix, 2016). Figure 4.9 illustrates two key points. First, that the laser light scattering system which is based on 90 degree scattering is sensitive to small changes in particles size at a narrow range of between 30-70 nm diameter particles. Mie Theory calculations illustrate that the total scattering for gold nanoparticles increases more gradually with size, since this calculation takes into account all angles of scattering. The

Optical Caustic sample chamber is seen in Figure 4.9 to fall between the two groups of data, using both a camera and a digital color sensor to collect data. It was also found that the red channel of the smartphone RGB image was most useful based on the LED intensity and shutter speed setting since smartphone sensor saturation "bleeds" signal to the red and blue channels when there is an excess of green in the image. The digital color sensor corroborates that interpretation, as shown in Figure 4.9.

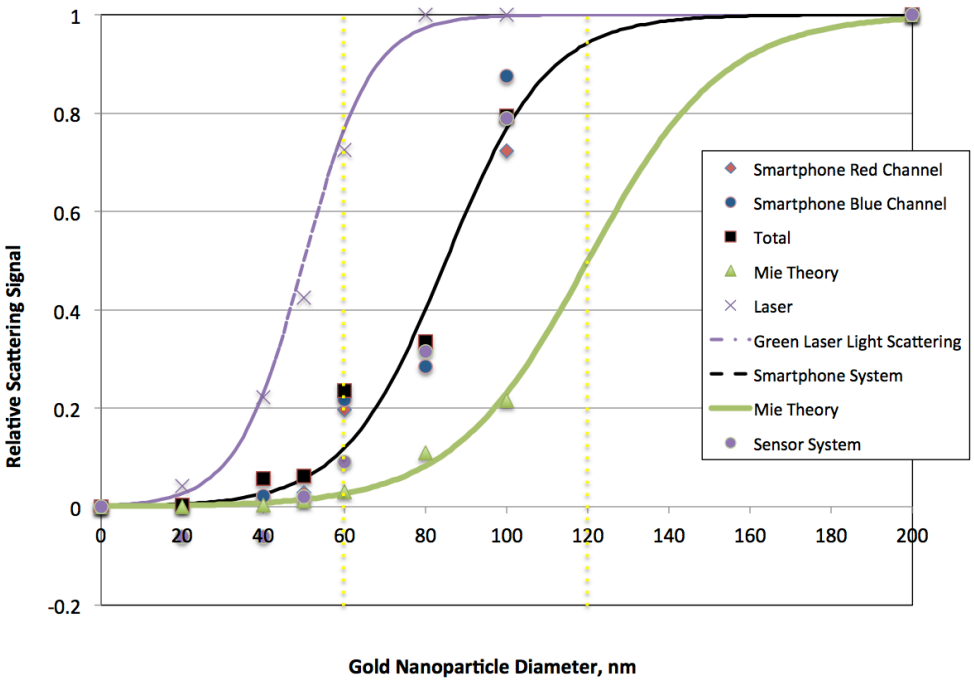

Figure 4.9. Relative Scattering Signal Through Different Methods of Different AuNP Size.
Comparison of gold nanoparticle scattering with green light data for a laser and fiber optic spectrometer, LED/optical caustic smartphone, and LED/optical caustic digital color sensor. Discrete calculations of the total scattering at 532 nm using Mie theory is also shown. Data and calculations are normalized to the maximum value for gold nanoparticles of 200 nm and fitted to a logistic curve. Horizontal dashed lines illustrate the signal difference for 60 and 120 nm diameter gold nanoparticles.

Before commencing patient testing, the 60 nm gold conjugates were inspected and the UV/VIS spectra were recorded for the two batches of particle conjugates (Figure

4.10). Both visual and spectral information verified that the gold conjugates were stable and ready to use at UADY.

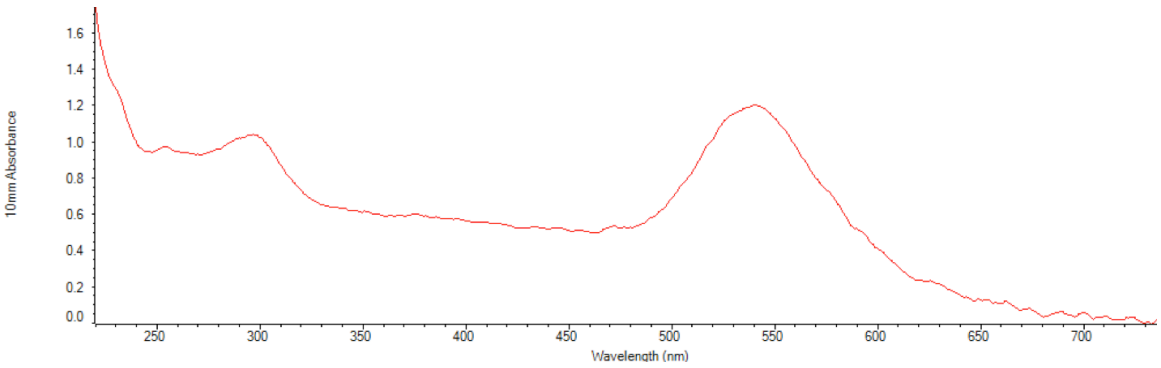

Figure 4.10. Nanodrop Spectrometer UV/VIS Spectrum of Conjugated AuNPs.
The absorbance in the UV is due to the BSA blocking solution. The absorbance maxima at a wavelength of 540 nm is consistent with the expected plasmon resonant peak for conjugated gold nanoparticles of 60 nm diameter.

Table 4.2 summarizes the expected dot blot score based on the protein E gold conjugate reagent (GNP-60-E-3) used, assuming some level of cross-reactivity with other Dengue serotypes and a 50% probability of measuring antibodies reactive to Protein E after 120 days of convalescence. The individual blot samples and the scores of the dot blot are shown in Table 4.2. Overall, the agreement is very good. However, the two dengue negative patients appear to give positive dot blot results.

Table 4.2. Comparison of Dot Blot with Result Reported by the Clinical Laboratory.

Patient	Expected Dengue Result Based on Dengue Serotype and Some Cross-Reactivity (assuming high sensitivity to IgM)	Dot Blot Score (+ or -)	Agreement
1	-	+	NO
2	-	+	NO
3	+	+	YES
4	+	+	YES
5	-	-	YES
6	-	-	YES
7	-	-	YES
8	+	+	YES
9	+	+	YES
10	-	-	YES

The Protein E used while specific for DENV-2, has sensitivity for IgM detection and can have cross-reactivity with other serotypes.

A summary of the three sets of tests with human serum samples and an overall score is given in Table 4.3, while a quantitative comparison of the dot blot is shown in Figure 4.11. The overall score given in Table 4.3 is based on assessing the differences among the three tests using gold nanoparticles made with either 3 or 1 centrifugation step(s) and at different times and temperatures. Based on the results in Table 4.3, it appears that the results with GNP-60-E-1 at 22 C for 15 minutes seem to be most closely related to the characterization based on the dengue patient status information.

Table 4.3. Qualitative Summary of Optical Caustic Scattering Smartphone Sensor Data.

Patient	**GNP-60-E-3 37 C for 30 min**	**GNP-60-E-3 22 C for 15 min Trial 1**	**GNP-60-E-1 22C for 15 min Trial 2**	***Overall Score (+ or -)***
1	weak positive	*positive*	negative	**-**
2	positive	*negative*	positive	+
3	positive	*positive*	positive	+
4	positive	*positive*	weak positive	+
5	positive	*positive*	positive	+
6	positive	*negative*	positive	+
7	negative	*weak positive*	negative	**-**
8	positive	*positive*	negative	**-**
9	positive	*weak positive*	positive	+
10	very weak positive	*positive*	positive	+
PBS Control	negative	*negative*	negative	**NEGATIVE CONTROL**
PBS Control	negative	*negative*	negative	**NEGATIVE CONTROL**

In Table 4.5, there are two overall features to note. First it appears that the smartphone signal saturates at low "signals" from the dot blot experiments. The second feature is that the negative control and patient sample 10 are both low for the dot blot and the optical caustic sensor, but there is disagreement between patient samples 5 and 6 between the two detection methods.

Table 4.5. Comparison of Dot Blot and Optical Caustic Smartphone Sensor.

Patient	Initial Information	Clinically expected result	Dot blot	AuNP-60-E-1 22 C for 15 min
1	Negative	-	+	-
2	Negative	-	+	+
3	DENV-2 (1ary infection)	+	+	+
4	DENV-2 (1ary infection)	+	+	+
5	DENV-2 (1ary infection)	-	-	+
6	DENV-2 (1ary infection)	-	-	+
7	DENV-3	-	-	-
8	DENV-1	+	+	-
9	DENV-2	+	+	+
10	DENV-2	-	-	+
PBS control	N.A.	N.A.	N.A.	-
PBS control	N.A.	N.A.	N.A.	-

Data were recorded at the same sample incubation temperature of 37 ˚C.

4.4 Discussion

One of the more interesting results from our experiments and analyses was in understanding gold nanoparticle changes in the homogeneous immunoassays by comparing visible extinction, static light scattering, and dynamic light scattering data. Also valuable as a guide in selecting conditions and interpreting results were the predicted results obtained with the Online Mie Scattering Calculator (nanoComposix, 2016). Specifically, the calculator was helpful in selecting the appropriate gold nanoparticle size and providing a better understanding of the visible extinction data for the immunoassay measurements since the changes can be subtler near the plasmon resonance peak. In contrast, the research literature (Doak et al., 2010; Driskell et al., 2011; Raj & Sreenivasan, 2010; Thanh & Rosenzweig, 2002) generally provides only one

detection method per article and rarely compares experimental information with theoretical results that are readily accessible to the reader.

At times it can be difficult to comprehend the way that extinction data is interpreted in numerous articles due to a number of calculations done to the raw data. While spectra normalization (Amendola & Meneghetti, 2009) and calculating the ratio of 2 wavelengths for extinction or scattering results (Haiss et al., 2007) can lead to a useful way of calibrating instruments, these methods also obscure how the entire raw spectra can provide important clues on aggregation before, during or after homogeneous immunoassays are conducted. As seen in Figure 4.1, there are changes in extinction al wavelengths below the plasmon peak for particles of different diameters. Immunoassay conditions that lead to a small number of low numbers of particles aggregating will increase the extinction near 400 nm as well as increase the tail of the spectrum at wavelengths greater than the plasmon resonance peak. By normalizing the spectra using absorbance ratios or matching absorbance at 400 nm, the interpretation of the data can also be challenging at low concentrations of gold nanoparticles, since extinction values used in normalizing will be low and subject to more experimental uncertainty. While impractical for calibration and routine use of immunoassays for detection, fitting predicted extinction curves based on possible aggregate populations to the extinction spectra data would nonetheless provide a more mechanistic interpretation of experimental and analytical results.

Another useful illustration of the theoretical calculations is in tracking changes from unmodified gold nanoparticles through aggregate populations in immunoassays. Using the calculator, it can be clearly seen that a layer or “shell” of protein with a

refractive index greater than water will increase overall extinction of light and extinction due to scattering. Since protein layers have been reported to have refractive indices of > 1.33 (Tsai et al., 2011), gold nanoparticle visible light extinction curves before addition of protein should be slightly lower than when protein is bound to the surface. However, at times the extinction and scattering decrease. As noted in Figure 4.5 with dynamic light scattering, gold nanoparticle aggregation can be dispersed by the addition of protein. Also, unless there is an excessive coating of antibody very much higher than the original protein layer, the expected extinction for gold nanoparticle sizes of 60 nm predicted by the calculator should not increase substantially. This is a useful guide to help discern small changes in static light scattering or extinction due to antibody binding versus much larger changes in the spectra or static light scattering at a specific angle when aggregates are formed due to antibody bridging across multiple gold nanoparticles with surface protein.

This behavior was also observed in the BSA conjugated gold nanoparticles experiments. In Figure 4.4, both visible light extinction and light scattering increased the signal progressively, which would indicate aggregation because of antibody bridging. As the antibody concentration increases, it is more probable that two gold nanoparticles are not interacting with the same antibody, but that each nanoparticle has interaction with one or more antibodies separately from other nanoparticles, observed in less aggregation in solution.

Detecting gold nanoparticle changes using 90 degree static light scattering at 532 nm proved to be effective and simple, primarily because 60 nm gold nanoparticle scattering at this angle is relatively easy to detect and because the measurement is

sensitive to small changes in aggregation. Using a conventional quartz cuvette stage and fiber optic detector at 90 degrees from the green laser was sufficient in this system to analyze lower particle concentrations than using light extinction. Of particular value is to detect whether the final preparation of gold nanoparticles are aggregated based on the size versus scattering prediction given in Figure 4.1. We found that the reference values of no antibody present may be difficult to establish experimentally unless guided by the predicted results. Addition of buffer components to minimize protein-protein aggregation or allowing the prepared gold nanoparticles to be stored overnight and removal of any precipitate can help establish a true "zero" since even a small population of aggregates can increase the scattering significantly. Usually, once antibody is present in solution, those aggregates can tend to dissipate thus lowering the measured scattering and creating a problem in data interpretation, which was observed in Figure 4.4 after 30 min at 40 ˚C where the tendency was the same, but the intensity decreased. Testing the conjugated gold nanoparticles before addition of antibody for light scattering, so that an expected value is achieved, would be a useful step to help obtain more reproducible homogeneous assay results.

Dynamic Light Scattering also demonstrated utility in corroborating aggregation and distributions in gold nanoparticles, but there are some challenges in interpreting the information. Khlebstov and Khlebstov (Khlebstov & Khlebstov, 2011) point out that there are anomalies when applying DLS to gold nanoparticles. They suggest using intensity distribution rather than number or volume distributions, and our much more limited experience with 60 nm gold particles is an agreement with that recommendation. As shown in the results section, Figure 4.6 shows a distinct trend in the distribution with

higher antibody concentrations for the anti-BSA assay. The overall trend of a broader distribution with a peak maxima shift to higher diameters for higher concentration of anti-BSA antibody resembles the trend in weight distribution of polymers for polymerizations that follow a Schultz-Flory WCLD. The probability of increasing hydrodynamic radius from DLS measurements with higher antibody concentrations suggests that the particle populations follow an increasing probability for longer chains and higher dispersity. This is similar to the weight distribution as predicted in a Shultz-Flory WCD (Equation 1) for ideal linear step polymerization kinetics (Figure 4.12) (Meira & Oliva, 2011).

$$w(r) = \frac{r}{r_n} e^{-\left(r/r_n\right)} \quad (1)$$

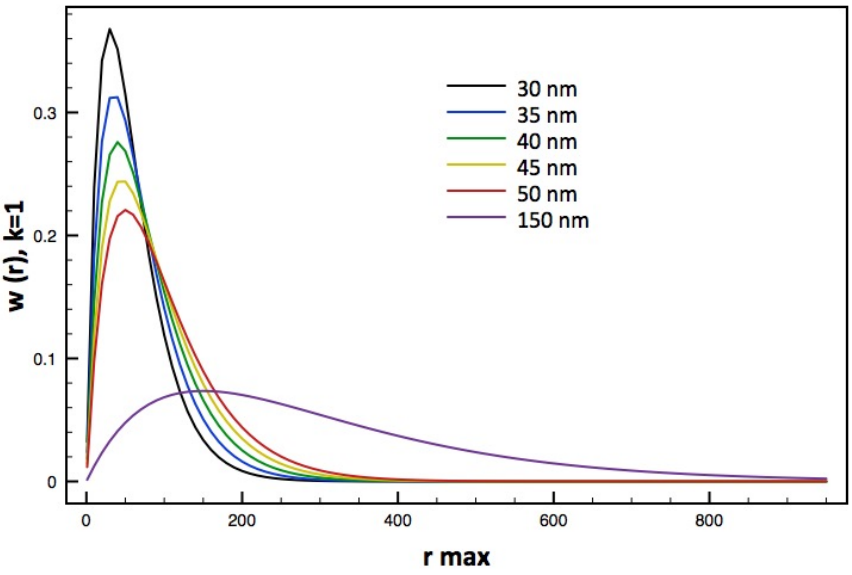

Figure 4.12. Shultz-Flory Distribution of Weight Distribution.
A normalized Shultz-Flory distribution of weight distribution as a function of mean radii (Meira & Oliva, 2011).

However, as noted in the results section, the data in Figure 4.6 for 5 microgram per ml antibody does not follow the trend due to what appears to be large cluster formed rather than a broad distribution. It seems reasonable to assume that both highly distributed and a few highly aggregated populations are possible states given the relatively high concentration of antibody as compared to the number of gold nanoparticles in the assay.

The kinetic effect can also be witnessed in the visible light spectra and static light scattering results obtained for both systems. The intensity count values for the negative control were not always the same. Aggregates are forming at different rates in solution in a random process, even before adding the antibody; therefore defining an absolute zero cannot be done. This is one disadvantage because each time an experiment is performed, a new zero needs to be established.

On the other hand, the presence of electrolytes in solution can improve the antigen-antibody interactions, increasing the signal in static light scattering. In the case of the BSA conjugated nanoparticle system, we hypothesize that electrolytes help BSA get in a conformation that might be more suitable for the antibody recognition. Nevertheless, the addition of electrolytes is not always necessary. Yeo *et al*. (Yeo et al., 2015) in their study with protein E did not use the addition of electrolytes and had successful results, which confirm the results obtained in this study.

When the assay was tested with the human serum samples, the samples were obtained from patients with different serotypes and stages of Dengue (Table 4.1). Patients with early stage and primary dengue infection should present IgM against dengue antigens after a few days of infection and the IgM levels should decrease after 90 days

((WHO), 2009; Cuzzubbo et al., 2001; Da Silva, 2014; Lin et al., 2012; Mustafa et al., 2015; Rosckstroh et al., 2015; Tüiskunen-Bäck & Lundkvist, 2013). Patients with a secondary infection should mostly present IgG antibodies ((WHO), 2009; Da Silva, 2014; Lin et al., 2012; Mustafa et al., 2015; Tüiskunen-Bäck & Lundkvist, 2013). The antigen Protein E used as the reagent conjugated to the gold nanoparticles is a recombinant protein with selectivity towards Dengue Serotype 2 antibodies and is described by the manufacturer as being most sensitive to IgM levels. However, it is known that there can be cross-reactivity to other dengue serotype antibodies as well as from patients who have experienced other arbovirus infections from the group known as flaviviruses such as West Nile, St. Louis Encephalitis, Zika Virus, and Chikungunya (Cuzzubbo et al., 2001). These considerations suggest that there should be some variation in test results, but the variations may be difficult to discern without a more comprehensive series of human serum controls.

The cross-reaction could also be observed with the results of the dot blot and the optical caustic smartphone sensor. In table 4.2, two dengue negative patients appear to give positive dot blot results. It is not clear why this is the case, but perhaps a current or prior flavivirus infection is being detected by the gold conjugate reagent. It is important to note that the sample with PBS added and no human serum was correctly identified as a negative control in the dot blot experiment. It is also important to note that the dot blot test with a monoclonal antibody that reacts with flavivirus group specific antigens (4G2, KPL) was found to be negative (not shown).

The negative result observed with the new sensor suggests that epitopes of the protein envelope needed for the monoclonal antibody to bind to the GNP-60-E-3 were

blocked due to the immobilization of Protein E to the gold nanoparticles (Table 4.3). This is a potentially useful observation for further gold conjugate development, namely if a methodology for Protein E binding to gold based on covalent attachment rather than his-tag is used.

The calibration data determined that using 60 nm gold particles is very practical for the intended application (Figure 4.9). The reason for this is that there is a dramatic (approximately 340%) increase in signal predicted when two 60 nm gold particles aggregate upon antibody-antigen binding, basically the change in relative signal from 60 nm to 120 nm gold particle size.

The Optical Caustic Scattering Smartphone Sensor results show that it saturates with samples that show low signal with the dot blot, which seems reasonable given the high signal change described in Figure 4.9 for aggregates consisting of 60 nm gold particles. The disagreements observed between the dot blot and optical caustic sensor may be due to the higher sensitivity of the optical caustic sensor as compared to the dot blot, which used gold nanoparticles at a higher level of dilution. Dot blots are also considered to be lower in sensitivity due to diffusion and orientation effects when binding to a fixed surface.

Another observation is that patient sample 7 yielded a very weak signal and patient sample 10 is negative based on the dot blot tests, yet the optical caustic sensor data show strong signals. This again may be due to higher sensitivity of the optical caustic system and cross reactivity of the Dengue Serotype 2 recombinant Protein E with other Dengue serotypes. As noted in the results for GNP-60-E-1 at 22 ˚C and 15 minutes seen in Table 4.3, it appears that this cross-reactivity may be diminished by using a

higher dilution of human serum, lower temperature, and allowing some unbound antigen in the gold nanoparticle conjugation suspension.

4.5 References

(WHO), W.-H.-O. (2009). Dengue: guidelines for diagnosis, treatment, prevention and control.

Amendola, V., & Meneghetti, M. (2009). Size Evaluation og Gold Nanoparticles by UV-vis Spectroscopy. *J Phys Chem C, 113*, 4277-4285.

Cuzzubbo, A. J., Endy, T. P., Nisalak, A., Kalayanarook, S., Vaughn, D. W., Ogata, S. A., . . . Devine, P. L. (2001). Use of Recombinant Envelope Proteins for Serological Diagnosis de Dengue Virus Infection in and Immunochromatographic Assay. *Clin Diagn Lab Immunol., 8*(6), 1150-1155.

Da Silva, V. J. M. (2014). A possible fifth Dengue Virus Serotype. *Ned Tijdschr Geneeskd, 158*, A7946.

Doak, J., Gupta, R., Manivannan, K., Ghosh, K., & Kahol, P. (2010). Effect of particle size distributions on absorbance spectra of gold nanoparticles. *Physica E Low Dimens Syst Nanostruct., 42*, 1605-1609.

Driskell, J. D., Jones, C. A., Tompkins, M., & Tripp, R. A. (2011). One-step assay for detecting influenza virus using dynamic light scattering and gold nanoparticles. *Analyst, 136*, 3083-3090.

Engleienne, P. (1998). Use of colloidal gold surface plasmon resonance peak shift to infer affinity constants from the interactions between protein antigens and antibodies specific for single or multiple epitopes. *Analyst, 123*, 1599-1603.

Fan, X., Zheng, W., & Singh, D. (2014). Light scattering and surface plasmons on small spherical
particles. *Light Sci Appl, 3*, e179.

García, A. A., Nuñez, L., Lastra, A., & Mujica, V. (2013). Application of Newton's Zero Order Caustic for Analysis and Measurement: Part III – Light Scattering *Int Res J Pure Appl Chem, 4*(1), 144-158.

Ghosh, S., & Pai, T. (2007). Interparticle coupling effect on the surface plasmon resonance of gold nanoparticles: from theory to applications. *Chem Rev, 107*, 4797-4862.

Haiss, W., Thanh, N. T. K., Aveyard, J., & Fernig, D. G. (2007). Determination of Size and Concentration of Gold Nanoparticles from UV-Vis Spectra. *Anal. Chem, 79*, 4215-4221.

Huang, S.-H. (2006). Gold nanoparticle-based immunochromatographic test for identification of *Staphylococcus aureus* from clinical specimens. *Clinica Chim. Acta, 373*, 139-143.

Huang, X., Jain, P., & El-Sayed, M. (2007). Gold nanoparticles: interesting optical properties and recentapplications in cancer diagnostics and therapy. *Nanomedicine, 2*, 681-693.

Khlebstov, B. N., & Khlebstov, N. G. (2011). On the measurement of gold nanoparticle sizes by the dynamic light scattering method. *Colloid Journal, 73*, 118-127.

Lin, H. E., Tsai, W. Y., Liu, I. J., Li, P. C., Liao, M. Y., Tsai, J. J., . . . Wang, W. K. (2012). Analysis of epitopes on Dengue Virus envelope protein recognized by monoclonal antibodies and polyclonal human sera by a high throughput assay. *PLoS Negl. Trop. Dis., 6*(1), e1447.

Meira, G., & Oliva, H. (2011). Molecular weight distributions in ideal polymerization reactors. An introductory review. *Latin Am. Appl. Res, 41*, 389-401.

Mie, G. (1908). Beiträge zur Optik trüber Medien, speziell kolloidaler Metallösungen. *Ann. Phys., 25*, 377-445.

Mustafa, M. F., Rasotgi, V., Jain, S., & Gupta, V. (2015). Discovery of fifth serotpe of Dengue Virus (DENV-5): A new public health dilemma in dengue control. *Med J Armed Forces India, 71*(1), 67-70.

nanoComposix. (2016). Mie Theory calculator. Retrieved from http://nanocomposix.com/pages/tools

Raj, V., & Sreenivasan, K. (2010). Selective detection and stimation of C-reactive protein in serum using surface-functionalized gold nano-particles. *Anal. Chim. Acta, 662*, 186-192.

Ringe, E., Sharma, B., Henry, A.-I., Marks, L. D., & VanDuyne, R. P. (2013). Single nanoparticle plasmonics. *Phys. Chem. Chem. Phys., 15*, 4110-4129.

Rosckstroh, A., Barzon, L., Pacenti, M., Giorgio, P., Niedrig, M., & Ulbert, S. (2015). Recombinant Envelope-Proteins with Mutations in the Conserved Fusion Loop Allow Specific Serological Diagnosis of Dengue-Infections. *PLoS Negl. Trop. Dis., 9*(11), e0004218.

Sorensen, C. (2013). Q-space analysis of scattering by particles: A review. *J Quant Spectros Radia Transfer, 131*, 3-12.

Thanh, N., & Rosenzweig, Z. (2002). Devevelopment of an aggregation-based immunoassay for anti-protein A using gold nanoparticles. *Anal. Chem., 74*, 1624-1628.

Tsai, D.-H., DelRio, D. W., Keene, A. M., Tyner, K. M., MacCuspie, R. I., Cho, T. J., . . . Hackley, V. A. (2011). Adsoption and Conformation of Serum Abumin Protein on Gold Nanoparticles Investigated using Dimensional Measurements and in situ Spectroscopic Methods. *Langmuir, 27*, 2464-2477.

Tüiskunen-Bäck, A., & Lundkvist, Å. (2013). Dengue Viruses - An Overview. *Infect Ecol Epidemiol., 3*, 19839.

Yeo, E. L. L., Chua, A. J. S., Parthasarathy, K., Yeo, H. Y., Ng, M. L., & Kah, J. Y. C. (2015). Understanding aggregation-based assays: nature of protein corona and number of epitopes on antigen matters. *RSC Adv, 5*, 14982-14993.

Chapter 5

5. SEQUENCE-SPECIFIC DETECTION OF DIFFERENT STRAINS OF LCMV IN A SINGLE SAMPLE USING TENTACLE PROBES

5.1 Introduction

RNA viruses affect most of the population, especially in developing countries, and are the major cause of emerging and re-emerging diseases in humans (Cella et al., 2013; Holmes, 2009; Marston et al., 2014). One of the most important problems with understanding RNA viruses and developing appropriate vaccines/therapies, is their propensity for rapid change due to its high mutation rate because of lack of proofreading property in the encoded RNA polymerase (Domingo et al., 2012; Marston et al., 2014; Moya et al., 2000). High mutation rate rand high replication rate results in quasispecies even in a single host (Domingo et al., 2006; Domingo et al., 2012; Lauring and Andino, 2010; Moya et al., 2000). Presence of quasispecies correlates with enhancement of virulence because of the flexibility of the population of the virus to adapt easily with the dynamics of the host (Lauring and Andino, 2010). This has been observed in poliovirus, where the presence of quasispecies cooperated the entrance of a neovirulent clone in mice (Lauring and Andino, 2010), and in evasion of immunity of Hepatitis C Virus (Domingo et al., 2006).

Current diagnostic methods can detect the virus directly, indirectly, fluorescence-based emerging technologies and immune-based. Indirect detection is achieved by detection of virus particles (antigens) or RNA. Some immune-based methods can be non-specific due to cross-reaction and most of them are expensive and not field-portable (Guzman et al., 2010; Peeling et al., 2010). Fluoresce-based are usually molecular

procedures that are used to detect RNA using reverse transcriptase PCR (RT-PCR), which is sensitive and specific, but is highly prone to false-positive results due to easy contamination ((WHO), 2009; C.D.C., 2010). The most common molecular technique is using a fluorescent dye that binds to dsDNA and using a calibration curve to quantify the amount of DNA. Another fluorescent-based technique is using probes called molecular beacons, which consist in a stem-loop that, when self-hybridized, places the fluorophore on the 5' end in close proximity to the quencher at the 3' end thus quenching the fluorescence. When the molecular beacon encounters its target, it changes to its open conformation and hybridizes with the target leading to the fluorophore to emit a signal. Tentacle Probes are modified molecular beacons because they have a single stranded DNA attached to the stem-loop by a 9-mer chain of polyethylene glycol (PEG). The ~15 nt single stranded DNA is called capture sequence because, as it is implied by its name, it captures the DNA strand and as a consequence it increases the local concentration of the stem-loop around the DNA strand from a range of nM (free probe) to mM (capture probe bound), increasing the probability of the stem-loop to bind to the target (Satterfield et al., 2007a; Satterfield et al., 2007b). This technology was successfully used for the detection of *Yersinia pestis* and *Bacillus anthracis* using the bacterial DNA (Satterfield et al., 2007a), but it has not been tested with any RNA organism or virus.

In this study, we proposed a fast and cost-effective molecular method for detection of RNA viruses. For this purpose, a virus model for RNA viruses, Lymphocytic Choriomeningitis Virus (LCMV) was used. The method intends to differentiate two strains of LCMV: Clone-13, which causes a chronic infection in mice, versus the wilt type Armstrong strain, which causes an acute infection in mice. The difference in type of

infection is due to a single mutation in the S segment of LCMV, C855T, which is a missense mutation observed in an amino acid change in the receptor protein GP1 (F260L). The proposed method uses Tentacle Probes coupled with qPCR and showed that the designed probes to detect Armstrong and Clone-13 strains could differentiate them even with only a single mutation in the RNA that was obtained both in vitro and in vivo. Results also showed that Tentacle Probes could detect specifically each strain with as little as 10 % of presence of one strain in a sample with a mixture of both strains.

5.2 Materials and Methods

5.2.1 Tentacle Probe Design

Both Tentacle Probes were designed based on the generalizations of the principles described by Satterfield *et al.* (Satterfield, West, et al., 2007). Briefly, four hundred possible combinations of detection probes and capture probes were simulated to obtain a suitable probe to detect the strain Clone-13 of LCMV over the Armstrong strain, and vice versa for the detection of Armstrong strain. DINAMelt and UNAFold applications (Markham and Zuker, 2005, 2008) were used to calculate melting temperatures of the detection probe stem, the capture probe-target duplex, and the detection probe-target duplex, independent of each other. The targeted single mutation was located in the loop of the detection probe. The detection and capture probes were designed with predicted melting temperatures around the predicted assay temperature of 60 °C. The melting temperature for the stem-loop structure was chosen 7–10 °C above the assay conditions (70 °C). The most appropriate probe from the simulated probes with the previous characteristics was purchased from Biosearch Technologies as a custom oligonucleotide

to use for the detection of each strain (Biosearch Technologies, Petaluma, CA, https://www.biosearchtech.com). The calculations obtained for each probe are summarized in Table 5.1.

Table 5.1. Probe Sequences for each Strain and their Thermodynamic Parameters Calculated.
Equilibrium constants and ratio of probe predicted to fluoresce for each probe.

Probe sequence	**$K_{stemloop}$**	**$K_{detectionT}$ (μM^{-1})**	**$K_{captureT}$ (μM^{-1})**	**Fraction of fluorophore predicted to be fluorescing with Target**	**Fraction of fluorophore predicted to be fluorescing with Non-Target**
Clone13: FAM-cgtaagTTCCTCTCACGaacttcg-BHQ-PEG9-acattcacctggactttgtcagactc	62.35	82.53	$1.43x10^{8}$	0.5447	0.0053
Armstrong: FAM-cgtagtGATTCTTCACtacg-BHQ-PEG9-agcgggcacattcacctgg	26.44	33.93	$6.9x10^{9}$	0.3188	0.0276

5.2.2 RNA Isolation and cDNA Obtention

RNA isolation from BHK21 cell virus collection in vitro was performed following the guanidinine thiocyanate-phenol-chloroform (GNTC) procedure described before (Chomczynski & Sacchi, 2006) with some modifications. Briefly, virus supernatant was mixed with GNTC in a 1:2 ratio, followed by the addition of 0.1 volumes of 2 M sodium acetate pH=4, 1 volume of Acid phenol pH=4.3 and 0.3 volumes of chloroform-isoamyl-alcohol 24:1 (Sigma Aldrich Inc., St. Louis, MO, http://www.sigmaaldrich.com/united-states.html). Samples were centrifuged at 20000×*g*

for 30 min at 4 ˚C, then the aqueous phase was transferred into a new tube and 1.1 volumes of isopropanol were added and left at -20 ˚C overnight. Next, samples were centrifuged at 20000×*g* for 30 min at 4 ˚C, supernatant was discarded and 1 volume of 70 % ethanol was added. Another centrifugation step at the same conditions was performed, after which the supernatant was removed completely, the tube was air-dried and the pellet was resuspended in nuclease-free water. cDNA was obtained in a two-step procedure with Omniscript RT kit (QIAGEN, Valencia, CA, https://www.qiagen.com/us/) and posteriorly amplifying the fragment with PCR using Phusion® High-Fidelity DNA polymerase (New England Biolabs, Ipswich, MA, https://www.neb.com). The primers were designed to obtain a 538 nt amplicon of the S segment of LCMV that includes the C855T mutation found in Clone-13. These are the following: Forward: 5'AGCCAGTGTAGAACCTTCAGAG3' and Reverse: 5'AGTGGTTCCTCATCAGTAGTTG3'. The cycling conditions for the PCR were the following: 30 sec at 94 ˚C, 30 cycles of 20 sec at 94 ˚C, 30 sec at 50 ˚C and 2 min at 72 ˚C, and a final extension of 5 min at 72 ˚C.

RNA from plaques from a previous plaque assay of unknown samples was obtained mixing SM buffer with the extracted plaques and letting them sit overnight at 4 ˚C. Then, RNA was isolated using the RNAqueous® Total RNA Isolation Kit (Thermo Fisher Scientific, Waltham, MA, https://www.thermofisher.com/us/en/home.html). All RNA concentrations were measured using Nanodrop 1000. cDNA was obtained through RT-PCR performed with SuperScriptIII One step RT-PCR system with Platinum® Taq DNA polymerase (Thermo Fisher Scientific, Waltham, MA, https://www.thermofisher.com/us/en/home.html). Primers used were the same used for

the PCR described. The cycling conditions were the following: 30 min at 50 ˚C, 2 min at 94 ˚C, 35 cycles of 15 sec at 94 ˚C, 30 sec at 55 ˚C and 2 min at 68 ˚C, and a final extension of 5 min at 68 ˚C.

5.2.3 Melting Curve and qPCR

The melting curve from the probe was obtained to determine the temperature at which the target and non-target were best differentiated. To a 20 µL reaction with 10 µl of the designed tentacle probe (final concentration: 50 nM) and 10 µL either 1 nM of target or non-target DNA, fluorescence at 10 ˚C until 90˚C every 0.6 ˚C/sec was measured. For the qPCR, the primers were designed to obtain a 150 nt amplicon of the S segment of LCMV that contained the C855T mutation found in Clone-13 strain compared to Armstrong strain, and are the following: Forward: 5'CAGGTCCTTTTGGGATGTCCAG3', Reverse: 5'CTCTGCAGCAAGAATCATCCATTTG3'. For these experiments a 20 µl reaction included we used 1.5 U/rxn of Platinum® Taq DNA polymerase, 0.1 µM of the tentacle probe, 0.5 µM of each primer, 5 mM (Clone-13) or 1.5 mM (Armstrong) $MgCl_2$, 1X Buffer, 0.2 mM dNTPs and 0.25 nM of DNA (sample, target or non-target). The cycling conditions for the qPCR were the following: 2min at 95 ˚C, 40 cycles of 1 sec at 90 ˚C and 3 min at 50 ˚C. The mechanism is illustrated in Fig. 1. These conditions were standardized for each probe as shown in reuslts. qPCR was performed in a ViiA 7 Real-Time PCR System from Life technologies (Thermo Fisher Scientific, Waltham, MA, https://www.thermofisher.com/us/en/home.html). Each sample was tested at least in

triplicate. Raw fluorescence counts per cycle were further analyzed for comparison between samples.

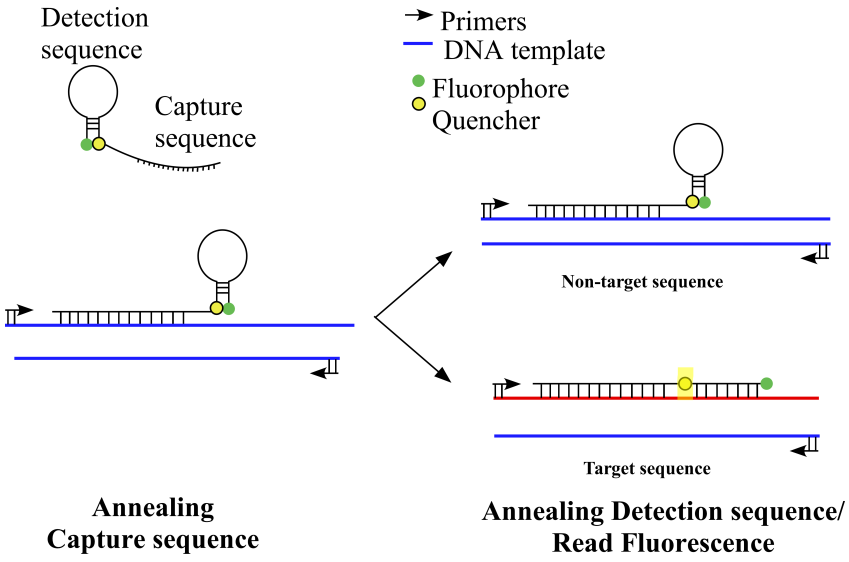

Figure 5.1. Tentacle Probe Mechanism of Detection of the Target Sequence. Adapted from (Satterfield, West, et al., 2007).

5.3 Results

The differentiation of strains or genotypes of viruses can determine and, in many cases, predict the virulence of an infection. In the case of Dengue, for example, it is important to determine the serotype as a method of surveillance in the population to try to prevent hemorrhagic fevers (Guzman et al., 2010; McCausland and Crotty, 2008; Peeling et al., 2010). In the case of LCMV, a different strain or genotype can determine the type of infection: chronic (Clone-13) or acute (Armstrong). For this purpose a tentacle probe was designed to detect Clone-13 over Armstrong and vice versa. The target mutation is in the sequence of the surface protein GP1 (C855T) of the virus that makes an amino acid change (F260L) and it is the main determinant for a chronic or acute infection. The

thermodynamic parameters obtained using DINAMelt and UNAFold applications (Markham and Zuker, 2005, 2008) were used to calculate the equilibrium constants for each one of the hybridization steps of the capture and detection probe described by Satterfield *et al* (Satterfield et al., 2007b), to predict the fraction of probe fluorescing with the target or non-target. These predictions helped determine the most suitable combination of detection and capture sequence among more than ~400 possible sequences that were simulated.

For the probe designed to detect Clone-13 strain, the calculations predicted that the ratio of probe fluorescing with the target would be 54.47 % versus 0.53 % with the non-target (Table 5.1). For the probe designed to detect the Armstrong strain the percentages were 31.88 % and 2.76 % with the target vs the non-target, respectively. The prediction is not accurate because as observed in the melting curve for both probes (Figure 5.2), the detection of the non-target was considerably higher than 0.05 % and 2.76 %. With the thermodynamic calculations it could also be determined the increase in the equilibrium constant when it takes into account the hybridization of the capture sequence (Table 5.1), rather than when it is not present in the probe such as in molecular beacons.

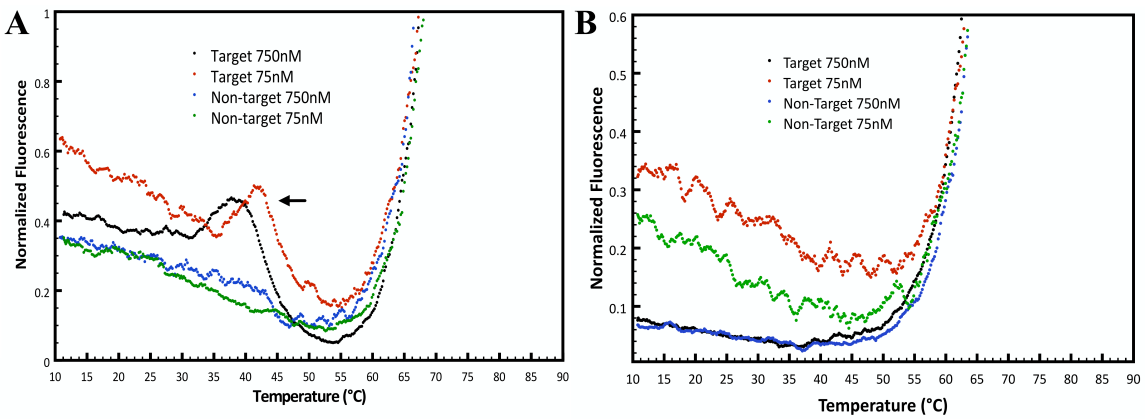

Figure 5.2. Melting Curve to Confirm the Annealing Temperature to be Used.
Determination of the optimal annealing temperature with a melting curve of the A) Clone-13 detection probe and B) Armstrong detection probe, to differentiate between target and non-target with a melting curve ran at 75 and 750 nM of the initial target or non-target DNA.

5.3.1 Melting Curve and Optimization of Conditions for qPCR

To confirm the overall melting temperature calculated by DINAMelt and UNAFold of each one of the probes, a melting curve was performed at different DNA concentrations for the target and the non-target in each case. Figure 5.2A shows that the best range at which the Clone-13 probe differentiates the target (Clone-13) and non-target (Armstrong) DNA is around 40 ˚C, but annealing temperatures in PCR are known to be best in the 45-60 ˚C range. For this purpose, qPCRs were performed at 4 different annealing temperatures along this range: 45, 50, 55 and 60 ˚C. Figure 5.3A shows raw fluorescence counts of the target (solid lines) and non-target (dashed lines) at each annealing temperature with the Clone-13 probe. After each cycle it is observed how raw fluorescence is increasing Although at each temperature there is a visible difference between target and non-target, the best differentiation at maximum fluorescence was

observed using an annealing temperature of 50 ˚C with ~1.3 fold of maximum fluorescence.

For the Armstrong probe, Figure 5.2B shows the melting curve for this probe and it suggests that the best range at which it can differentiate best target (Armstrong) and non-target (Clone-13) DNA is between 40-50 ˚C, but practical limits on cooling make those impractical and amplification is less reliable at lower temperatures. Four different qPCRs were performed with different annealing temperatures along this range: 42, 45, 48 and 50 ˚C, and were evaluated for the best differentiation between target and non-target. Figure 5.3B shows normalized fluorescence counts to the maximum non-target fluorescence at each temperature tested and Figure 5.3C shows raw fluorescence counts for the same temperatures. Both graph suggest that the best annealing temperature for this probe is 50 ˚C, showing ~1.85 fold of maximum fluorescence for the target versus non-target. It is important to mention that for this probe it is not observed the exponential phase in the fluorescence curves, as it is expected in a qPCR curve, in both raw and normalized fluorescence counts (Figure 5.3B and 5.3C).

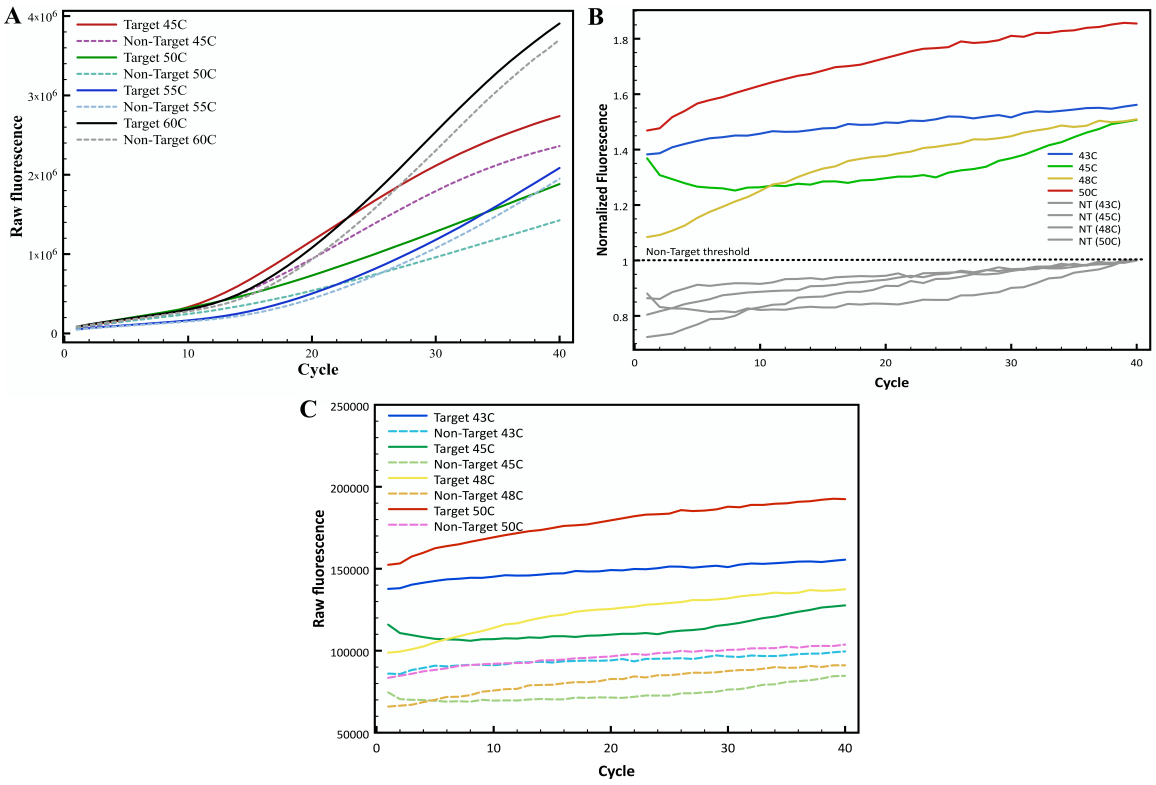

Figure 5.3. Optimization of Annealing Temperature for Clone-13 Probe and Armstrong Probe.
A) Raw fluorescence measured at different annealing temperatures (45, 50, 55 and 60 ˚C) of Clone-13 (solid lines) and Armstrong DNA (dashed lines) with the Clone-13 probe. B) Normalized Fluorescence to the maximum non-target fluorescence at different annealing temperatures (43, 45, 48 and 50 ˚C) of Armstrong (color lines) and Clone13 DNA (gray lines) with the Armstrong probe, and C) Raw fluorescence counts at the same annealing temperatures of Armstrong (solid lines) and Clone-13 DNA (dashed lines) with the Armstrong probe.

For the annealing temperature, all the thermodynamic calculations were based in an assay temperature of 60 °C for each probe, although as observed with the melting curve for each probe (Figure 5.2), the melting temperature for each was lower than expected, and by 60 °C the probe was completely dissociated for both the target and the non-target. The best annealing temperature for each probe was chosen because it gave the maximum differentiation between target and non-target at the same DNA concentration.

After determining which was the optimal annealing temperature to differentiate target and non-target DNA, two other parameters were optimized: the optimal initial sample DNA concentration for each reaction and the $MgCl_2$ concentration needed in the reaction. The concentration of $MgCl_2$ is crucial for the activity of the enzyme and even the salt effect on DNA. Three or four concentrations (0.5, 1.5, 3 and 5 mM) were tested for best results, including the concentration suggested to use by the manufacturer of the enzyme employed. Results showed that for the Clone-13 probe the most suitable concentration to use was 5 mM with ~1.4 fold maximum fluorescence of the target vs non-target, and for Armstrong probe, the most suitable concentration to use was 1.5 mM with ~1.5 fold maximum fluorescence of the target vs non-target (not shown).

Finally, to determine the minimal concentration at which the fluorescence is best for target detection, three initial DNA concentrations were evaluated: 0.1, 1 and 10 nM. Figure 5.4A shows the normalized fluorescence counts obtained with different starting concentrations of sample DNA for the Clone-13 probe and Figure 5.4B shows the same but with the Armstrong probe. Both graphs show that differentiation between target and non-target is best when using a sample concentration of 1 nM as a starting DNA concentration. Although 10 nM of DNA also showed good results, the best fluorescence differentiation between target and non-target is using 1 nM of sample DNA.

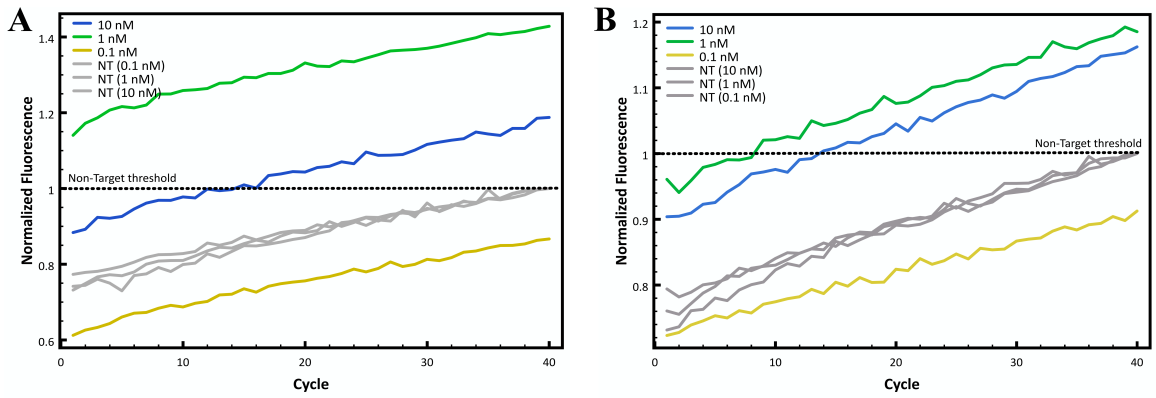

Figure 5.4. Optimization of Minimum Starting Concentration of DNA in Sample
A) Fluorescence counts of Clone13 (color lines) and Armstrong DNA (gray lines) with different initial DNA concentrations. B) Fluorescence counts of Armstrong (color lines) and Clone13 DNA (gray lines) with different initial DNA concentrations.

5.3.2 Determination of Specificity and Sensitivity for Each Probe

Once the conditions for the probes were optimized, a blind experiment was performed to determine the specificity of each probe. The experiment consisted in measuring the fluorescence by qPCR of 10 samples, 5 target and 5 non-target, that were organized randomly by another scientist, who knew the order of these samples. With the fluorescence results obtained, the samples were assigned as target or non-target compared to a positive and negative control, and afterwards the assignment was compared to the real identity of the samples. A sample was assigned as target if the maximum normalized fluorescence was higher than a threshold: the mean of the non-target maximum normalized fluorescence plus two standard deviations ($\overline{X_{NT}} + 2\sigma_{NT}$). This was defined as the statistically significant threshold or limit of detection between target and non-target. The experiment was performed in triplicate for each probe. For the Clone-13 probe, 9 of 10 samples were assigned accurately: 4 true positives, 1 false negative, 5 true negatives, and 0 false positives (results not shown). For the Armstrong probe, 7 of 10 samples were

assigned accurately: 3 true positives, 2 false negatives, 4 true negatives, and 1 false positive (results not shown).

5.3.3 Quasi-species Detection

After the conditions of the qPCR for the probes were optimized and it was shown that the probes could detect specifically each strain in samples with mixtures, serum samples from mice infected with an unknown strain of LCMV, suspected to be Clone-13, were tested to detect Clone-13 or Armstrong strain. Plaque assay was performed with these samples and RNA was isolated from plaques from each sample in triplicate. qPCR with the Clone-13 probe was performed to test for the presence of this strain in the samples. Figure 5.5 shows the normalized fluorescence of the three samples tested compared to a positive control (target) and a negative control (non-target). It is observed that the maximum fluorescence for the three samples was above the proposed threshold in previous experiments ($\overline{X_{NT}} + 2\sigma_{NT}$). Furthermore, a t-student test was performed comparing the mean of each sample to the mean of the target or the non-target, resulting in a p value of 0.15 or a 15 % probability of having false positives. To compare the results with other detection method, the DNA obtained from the samples was sequenced and confirmed the results obtained with the tentacle probe for Clone-13 detection.

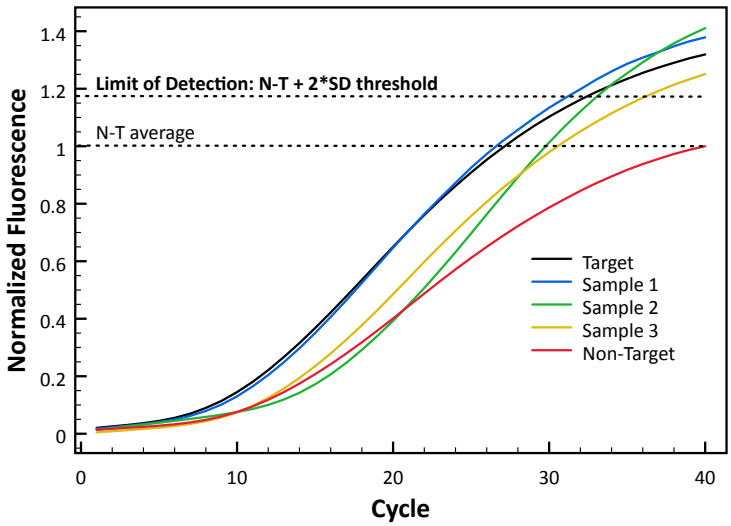

Figure 5.5. Quasi-Species Test of three Serum Samples Obtained from Mice.
Serum from infected mice with an unknown LCMV strain was tested to detect Clone-13 with the correspondent probe. The dashed line represents the non-target threshold proposed ($\overline{X_{NT}} + 2\sigma_{NT}$).

5.3.4 Detection of a Strain in a Mixture of Viruses

Detection of specific viruses even between the same family is essential, especially in clinical samples where samples sometimes present more than one viral infection at a time or more than one viral strain. To further test the lower limit of detection of one strain in a mixture of the other, mixtures of target and non-target in different proportions were tested to detect Clone-13 strain using its specific probe. Figure 5.6 shows the normalized maximum fluorescence of the mixtures of Clone13 and Armstrong samples ranging from 0.1-100 % of Clone-13 DNA. The dashed line represent the limit of detection proposed for the blind experiment ($\overline{X_{NT}} + 2\sigma_{NT}$). It is observed that the probe can detect to a lower limit of detection of approximately 10 % of the Clone-13 when it is present in a mixture with Armstrong DNA.

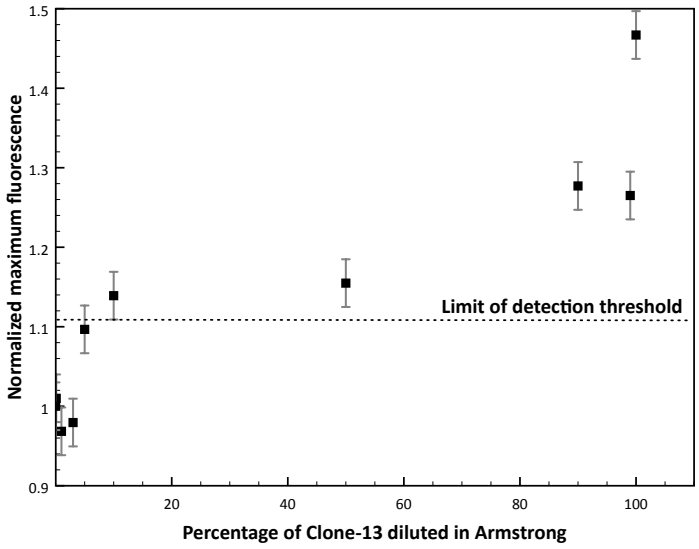

Figure 5.6. Determination of the Limit of Detection of the Clone-13 Probe.
The probe designed to detect Clone-13 is diluted in Armstrong by combining different proportions of Clone-13 (target) and Armstrong (non-target) DNA.

5.4 Discussion

Fast and cost-effective detection methods for viruses are currently needed for opportune diagnosis and treatment of viral disease. In this study we tested the specificity of Tentacle Probes to detect one strain of LCMV that only differs from the other strain in three point mutations, specifically one missense mutation in the region studied (S segment). The mutation that was studied causes a change in one amino acid of the receptor protein GP1, which also changes the type of infection induced (chronic vs. acute) and is the main reason why we chose this mutation above the other two mutations present. The design of the probe for the detection of each strain was following the calculations proposed by Satterfield *et al.* In here, the calculated thermodynamic parameters (i.e. enthalpy, entropy) with DINAMelt application were used to calculate the equilibrium constants and therefore estimate the probe fluorescing when is bound to the

target and non-target (Table 5.1). The predicted amount of probe fluorescing for both probes did not agree as precisely with what was observed. For the Clone-13 probe, the predicted difference in fluorescence between the target and the non-target was 50 % higher, while the fluorescence obtained experimentally was ~40 % higher, on average. A similar behavior was observed with the probe designed to detect Armstrong strain. This can be attributed to the fact that the predicted calculations did not take into account any kinetic factors, but only thermodynamic. Kinetic factors, like size of the probe, not only can be as important as the thermodynamic ones, but also can define entirely how much time a step in the qPCR might need in order to achieve the conformation desired in the case of the stem-loop (open or closed) (Gao et al., 2006; Satterfield et al., 2007b).

Validation of the method was described in detail by optimizing the qPCR conditions for each probe, including annealing temperature, $MgCl_2$ concentration and starting sample DNA concentration (Figure 5.3 and 5.4). The annealing temperature was expected to be higher than the melting temperature of the individual regions (capture and detection) because the principles of cooperativity indicate that the affinities of each part of the probe should be slightly weaker than the affinity required to achieve binding of the whole probe. However, as mentioned before, calculations did not take into account important kinetic factors such as the size of the whole probe and each part in separate (Gao et al., 2006) that might have affected the variance in the experimental annealing temperature. It is important to mention that the curves observed with the Armstrong probe at all temperatures did not show the exponential region usually observed with qPCR curves and as it was observed with the Clone-13 probe. This is an indication that the Armstrong probe is not as fit as the Clone-13 probe and is in agreement with the

thermodynamic predictions of fluorescence with the target and the non-target, where the differentiation with the Armstrong probe is not as pronounced as the differentiation predicted with the Clone-13 probe (Table 5.1).

$MgCl_2$ concentration is another important factor because it has a high contribution in ionic strength of the reaction and therefore influence directly into the thermodynamics. The calculations were performed to use 5 mM of $MgCl_2$ and 1.5 mM for the Clone-13 and Armstrong probe, respectively. The concentration used for the calculation of the Clone-13 probe was the one recommended by Satterfield *et al.* and the concentration used for the calculations of the Armstrong probe was the one recommended by the manufacturer to use for an optimal reaction using Platinum Taq polymerase. There was an agreement of the expected optimal concentration of $MgCl_2$ with the one observed for the Clone-13 probe and Armstrong probe. This shows that the ionic strength used in the calculations accurately predicted the optimal salt concentration in the reaction.

It could be observed that the calculations showed a better differentiation between target and non-target for the Clone-13 probe than for the Armstrong probe (Table 5.1). The difference between the two concentrations of $MgCl_2$ for the calculations might be one of the factors for the lower efficiency of the Armstrong probe compared to the Clone-13 probe. This difference in efficiency of detecting one strain or the other can also be attributed to the thermodynamic advantage of the Clone-13 probe due to the presence of the cytosine in the mutation site, instead of the thymine like Armstrong probe. Cytosine will hybridize with a guanine forming three hydrogen bonds, meaning the base-pairing will be more stable than the hybridization of the mismatch, meaning the anomalous cytosine-adenine pairing, favoring the hybrid between the probe and the target (C-G). For

the Armstrong probe, the thymine from the probe will hybridize with the adenine forming only two hydrogen bonds with the target instead of the hybrid with the non-target (mismatch), meaning the anomalous thymine-guanine pairing, which would form three hydrogen bonds. Although the probability of the hybridization of with the Armstrong probe with the mismatch is low due to the necessary conversion from the keto-thymine to the enol-thymine conformation, the hybridization of thymine and adenine (Armstrong probe-target) is less favored thermodynamically than the hybridization guanine-cytosine (Clone-13 probe-target), in terms of Gibbs free energy.

Experimentally it was shown that each probe designed could differentiate effectively one strain from the other. The blind tests performed with each probe to determine the specificity and sensitivity gave a sense of how accurate the probe could detect the target strain. The Clone-13 probe showed a better specificity giving results with only 10 % of false-negatives. On the other hand, the Armstrong probe showed results with 20 % of false-negatives and 10 % of false positives. It was expected that the Armstrong probe would have a higher probability of obtaining an inaccurate result, due to the smaller difference of expected fluorescence with the target vs. non-target in the initial calculations. Nevertheless, these percentages could be lower and further experiments with a bigger sample size (>10 samples) could be used to determine the percentage of false-positives and false-negatives more accurately.

It is important to highlight that Tentacle Probes can be used as a method to monitor the evolution of a virus, specifically its quasispecies and can be more cost-effective than other methods like hairpin probes (~$16/sample) or deep sequencing (~$35/sample).

In conclusion, this method reduced false-positives compared to common real time PCRs used for other RNA viruses such as Dengue (C.D.C., 2010) with a difference of only one point mutation between strains. The reduction of false-positives with this method is an advantage when using it with clinical samples overall in tropical regions, where many viruses with similar symptoms affect the same population (i.e. Dengue and Zika virus) (Guzman et al., 2010; Tsai and Halstead, 2001). Furthermore, detection of viral strains in serum using this method was established when we could accurately detect Clone-13 virus in the serum samples from infected mice (Figure 5.5).

Also, the probes could effectively differentiate each strain in virus mixing experiments with the two strains. Clone-13 probe can detect down to 10 % of Clone-13 diluted in Armstrong (Figure 5.6). The detection of one strain in a mix of other strains of viruses has a high impact in a detection method because it simulates the conditions of many clinical samples. This experiment in particular intended to illustrate two important viral phenomena: the presence of quasispecies in the population and even in the same host of viral strains and co-infection of two viruses in one host. Infections with RNA viruses can often result in the formation of quasispecies of virus strains that can rapidly adapt and can develop resistance to anti-viral drugs or vaccines (Domingo et al., 2012). Quasispecies of viral strains differ between them in a few mutations, even in only one mutation (Domingo et al., 2012; Holmes, 2009; Katzelnick et al., 2015; Lauring and Andino, 2010). Accurate detection of one of these quasispecies over another one can be crucial to determine possible treatment of the infection, the pathogenicity and the evolution of a determined virus in a population. Another scenario where detection of one viral strain in a mixed sample is essential is in viral co-infections. Co-infection of two

unrelated viruses that affect the same population is very common in the "real world" (McAfee et al., 2015). The presence of two or more viruses in a host can modulate the immune response and/or alter the disease (Kenney et al., 2015; McAfee et al., 2015). Therefore, the use of Tentacle Probes and qPCR for the detection of RNA viruses can be widely applied in many situations where high specificity and reduction of false-positives is needed.

5.5 References

(WHO), W.-H.-O. (2009). Dengue: guidelines for diagnosis, treatment, prevention and control.

C.D.C., C.f.D.C.a.P. (2010). Dengue: Epidemiology, Clinical and Laboratory Guidance.

Cella, L.N., Blackstock, D., Yates, M.A., Mulchandani, A., and Chen, W. (2013). Detection of RNA viruses: Current technologies and future perspectives. Crit Rev Eukaryot Gene Expr *23*, 125-137.

Chomczynski, P., and Sacchi, N. (2006). The single-step method of RNA isolation by acid guanidinum thiocyanate-phenol-chloroform extraction: twenty-something years on. Nature Protocols *1*, 581-585.

Domingo, E., Martín, V., Perales, C., Grande-Pérez, A., García-Arriaza, J., and Arias, A. (2006). Viruses as Quasispecies: Biological Implications. Curr Top Microbiol Immunol *299*, 51-82.

Domingo, E., Sheldon, J., and Perales, C. (2012). Viral Quasispecies Evolution. Microbiol Mol Biol Rev *76*, 159-216.

Gao, Y., Wolf, L.K., and Georgiadis, R.M. (2006). Secondary structure effects on DNA hybridization kinetics: a solution versus surface comparison. Nucleic Acids Res *34*, 3370-3377.

Guzman, M.G., Halstead, S.B., Artsob, H., Buchy, P., Farrar, J., Gubler, D.J., Hunsperger, E., Kroeger, A., Margolis, H.S., Martinez, E.*, et al.* (2010). Dengue: A continuing global threat Nat Rev Microbiol *8*, S7-16.

Holmes, E.C. (2009). RNA virus genomics: a world of possibilities. J Clin Invest *119*, 2488-2495.

Katzelnick, L.C., Fonville, J.M., Gromowski, G.D., Bustos Arriaga, J., Green, A., James, S.L., Lau, L., Montoya, M., Wang, C., VanBlargan, L.A.*, et al.* (2015). Dengue viruses cluster antigenically but not as discrete serotypes. Science *349*, 1338-1343.

Kenney, L.L., Cornberg, M., Chen, A.T., Emonet, S., de la Torre, J.C., and Selin, L.K. (2015). Increased Immune Response Variability during Simultaneous Viral Coinfection Leads to Unpredictability in CD8 T Cell Immunity and Pathogenesis. J Virol *89*, 10786-10801.

Lauring, A.S., and Andino, R. (2010). Quasispecies Theory and the Behavior of RNA viruses. PLoS Pathog *6*, e1001005.

Markham, N.R., and Zuker, M. (2005). DINAMelt web server for nucleic acid melting prediction. Nucleic Acids Res *33*, W577-W581.

Markham, N.R., and Zuker, M. (2008). UNAFold: software for nucleic acid folding and hybridization. In Bioinformatics, Volume II. Structure, Function and Applications, J.M. Keith, ed. (Totowa, N.J.: Humana Press), pp. 3-31.

Marston, H.D., Folkers, G.K., Morens, D.M., and Fauci, A.S. (2014). Emerging Viral Diseases: Confronting Threats with New Technologies. Sci. Transl. Med. *6*, 253ps210.

McAfee, M.S., Huynh, T.P., Johnson, J.L., Jacobs, B.L., and Blattman, J.N. (2015). Interaction between unrelated viruses during in vivo co-infection to limit pathology and immunity. Virology *484*, 153-162.

McCausland, M.M., and Crotty, S. (2008). Quantitative PCR technique for detecting lymphocytic choriomeningitis virus in vivo. Journal of virological methods *147*, 167-176.

Moya, A., Elena, S.F., Bracho, A., Miralles, R., and Barrio, E. (2000). The evolution of RNA viruses: A population genetics view. PNAS *97*, 6967-6973.

Peeling, R.W., Artsob, H., Pelegrino, J.L., Buchy, P., Cardosa, M.J., Devi, S., Enria, D.A., Farrar, J., Gubler, D.J., Guzman, M.G.*, et al.* (2010). Evaluation of diagnostic tests: dengue. Nature Rev Microb *8*, S30-S37.

Satterfield, B.C., Kulesh, D.A., Norwood, D.A., Wasieloski, L.P., Jr., Caplan, M.R., and West, J.A. (2007a). Tentacle Probes: differentiation of difficult single-nucleotide polymorphisms and deletions by presence or absence of a signal in real-time PCR. Clin Chem *53*, 2042-2050.

Satterfield, B.C., West, J.A., and Caplan, M.R. (2007b). Tentacle probes: eliminating false positives without sacrificing sensitivity. Nucleic Acids Res *35*, e76.

Tsai, T.F., and Halstead, S.B. (2001). Tropical Viral Infections. Infect Dis Clin Prac *10*, 107-115.

Chapter 6

6. CONCLUSIONS, RECOMMENDATIONS AND FUTURE WORK

Viral detection methods need to evolve every day to detect in a timely manner emergent or re-emergent viruses. The constant evolution of viruses is an implicit challenge for diagnosis and treatment, especially for RNA viruses because of the high rate of mutation. The methods described in this dissertation were proposed to solve some of the challenges present in current methods: speed, cost-effectiveness and specificity. Monitoring the optical changes of conjugated gold nanoparticles as biosensors is a widely studied area, but the proposed method measures changes on the surface of gold nanoparticles through static light scattering and an caustic optical device, which detects successfully the presence of antibodies in vitro and in serum from infected patients. Agreement between this new method and current methods such as dot blot, confirms the accuracy and functionality of the method and the device. Nevertheless, as observed with the method proposed to detect virus particles, the preparation of the gold nanoparticles is crucial to avoid instability and to improve coverage of the gold nanoparticle, increasing the chances of detection of the target. To improve the efficacy of conjugated gold nanoparticles, an optimization of the preparation of gold nanoparticles was performed, leading to the design of a detailed protocol for the preparation of conjugated gold nanoparticles that showed successful results. Application of the protocol for preparation of homogeneous assay with non-covalent conjugation can benefit broadly the field specifically in the preparation of biosensors.

On the other hand, detection with Tentacle Probes coupled with qPCR gave enough specificity to be able to detect one viral strain in a mixture of virus strains. The

technique has been previously used with other organisms and the potential application in other areas of virology, like detection of quasi-species of a virus or co-infection of related viruses, can give a better understanding about viral infections and/or effective treatment in a timely manner. Although the design of the Tentacle Probes is based on thermodynamic parameters, the technique still needs some improvements at the time of predicting more accurately the expected fluorescence and taking into account kinetic factors to predict the behavior of the probe better. For future studies with RNA viruses it should be studied if the step synthetizing cDNA can be avoided and thus minimize the time of the method. In conclusion, two fast and cost-effective methods were developed for the detection of antibodies and virus strains and hopefully this study can give a better understanding to the field and contribute to the improvement of diagnostic methods for viruses.

REFERENCES

(WHO), W.-H.-O. (2009). Dengue: guidelines for diagnosis, treatment, prevention and control.

Acuna, G., Grohmann, D., & Tinnefeld, P. (2014). Enhancing single-molecule fluorescence with nanophotonics *FEBS Lett, 588*(19), 3547-3552.

Ahmed, R., Salmo, A., Butler, L. D., Chiller, J. M., & Oldstone, M. B. A. (1984). Selection of Genetic Variants of Lymphocytic Choriomeningitis Virus in Spleens of Persistently Infected Mice: Role in Suppression of Cytotoxic T Lymphocyte Response and Viral Response. *Journal of Experimental Medicine, 60*, 521-540.

Amendola, V., & Meneghetti, M. (2009). Size Evaluation og Gold Nanoparticles by UV-vis Spectroscopy. *J Phys Chem C, 113*, 4277-4285.

Aslan, K., Holley, P., Davies, L., Lakowicz, J., & Geddes, C. (2005). Angular-Ratiometric Plasmon-Resonance Based Light Scattering for Bioaffinity Sensing. *JACS, 127*, 12115-12121.

Aslan, K., Lakowicz, J. R., & Geddes, C. D. (2004). Nanogold-plasmon-resonance-based glucose sensing. *Anal Biochem, 330*(1), 145-155. doi:10.1016/j.ab.2004.03.032

Bogdan, N., Rodriguez, E. M., Sanz-Rodriguez, F., de la Cruz, M. C., Juarranz, A., Jaque, D., . . . Capobianco, J. A. (2012). Bio-functionalization of ligand-free upconverting lanthanide doped nanoparticles for bio-imaging and cell targeting. *Nanoscale, 4*(12), 3647-3650. doi:10.1039/c2nr30982c

Brewer, S., Glomm, W., Johnson, M., Knag, M., & Franzen, S. (2005). Probing BSA Binding to Citrate-Coated Gold Nanoparticles and Surfaces. *Langmuir, 21*, 9303-9307.

C.D.C., C. f. D. C. a. P. (2010, 2013). Dengue: Epidemiology, Clinical and Laboratory Guidance. Retrieved from http://www.cdc.gov/Dengue/epidemiology/index.html

Carter, J. R., Balaraman, V., Kucharski, C. A., Fraser, T. S., & Fraser Jr, M. J. (2013). A novel dengue virus detection Method that couples DNAzyme and gold nanoparticle approaches. *Virology Jounal, 10*.

Cella, L. N., Blackstock, D., Yates, M. A., Mulchandani, A., & Chen, W. (2013). Detection of RNA viruses: Current technologies and future perspectives. *Crit Rev Eukaryot Gene Expr, 23*(2), 125-137.

Chen, C., Wang, W., Ge, J., & Zhao, X. S. (2009). Kinetics and thermodynamics of DNA hybridization on gold nanoparticles. *Nucleic Acids Res, 37*(11), 3756-3765.

Chomczynski, P., & Sacchi, N. (2006). The single-step method of RNA isolation by acid guanidinum thiocyanate-phenol-chloroform extraction: twenty-something years on. *Nature Protocols, 1*(2), 581-585.

Compton, O. C., & Osterloh, F. E. (2007). Evolution of size and shape in the colloidal crystallization of gold nanoparticles. *Journal of American Chemical Society, 129*, 7793-7798.

Cuzzubbo, A. J., Endy, T. P., Nisalak, A., Kalayanarook, S., Vaughn, D. W., Ogata, S. A., . . . Devine, P. L. (2001). Use of Recombinant Envelope Proteins for Serological Diagnosis de Dengue Virus Infection in and Immunochromatographic Assay. *Clin Diagn Lab Immunol., 8*(6), 1150-1155.

Da Silva, V. J. M. (2014). A possible fifth Dengue Virus Serotype. *Ned Tijdschr Geneeskd, 158*, A7946.

Daniel, M.-C., & Astruc, D. (2004). Gold Nanoparticles: Assembly, Supramolecular Chemistry, Quantum-Size-Related Properties and Applications toward Biology, Catalysis and Nanotechnology. *Chemistry Reviews, 104*, 293-346.

Doak, J., Gupta, R. K., Manivannan, K., Ghosh, K., & Kahol, P. K. (2010). Effect of particle size distributions on absorbance spectra of gold nanoparticles. *Physica E: Low-dimensional Systems and Nanostructures, 42*(5), 1605-1609. doi:10.1016/j.physe.2010.01.004

Domingo, E., Sheldon, J., & Perales, C. (2012). Viral Quasispecies Evolution. *Microbiol Mol Biol Rev, 76*(2), 159-216.

Driskell, J. D., Jones, C. A., Tompkins, S. M., & Tripp, R. A. (2011). One-step assay for detecting influenza virus using dynamic light scattering and gold nanoparticles. *Analyst, 136*(15), 3083-3090. doi:10.1039/c1an15303j

Du, B., Li, Z., & Cheng, Y. (2008). Homogeneous immunoassay based on aggregation of antibody-functionalized gold nanoparticles coupled with light scattering detection. *Talanta, 75*, 959-964.

Engleienne, P. (1998). Use of colloidal gold surface plasmon resonance peak shift to infer affinity constants from the interactions between protein antigens and antibodies specific for single or multiple epitopes. *Analyst, 123*, 1599-1603.

Fan, X., Zheng, W., & Singh, D. (2014). Light scattering and surface plasmons on small spherical
particles. *Light Sci Appl, 3*, e179.

Fukushi, S., Tani, H., Yoshikawa, T., Saijo, M., & Morikawa, S. (2012). Serological assays based on recombinant viral proteins for the diagnosis of arenavirus hemorrhagic fevers. *Viruses, 4*(10), 2097-2114. doi:10.3390/v4102097

Gao, Y., Wolf, L. K., & Georgiadis, R. M. (2006). Secondary structure effects on DNA hybridization kinetics: a solution versus surface comparison. *Nucleic Acids Res, 34*(11), 3370-3377.

García, A. A., Nuñez, L., Lastra, A., & Mujica, V. (2013). Application of Newton's Zero Order Caustic for Analysis and Measurement: Part III – Light Scattering *Int Res J Pure Appl Chem, 4*(1), 144-158.

Ghosh, S., & Pai, T. (2007). Interparticle coupling effect on the surface plasmon resonance of gold nanoparticles: from theory to applications. *Chem Rev, 107*, 4797-4862.

Gilger, C., Grigiori, F., De Beaufort, C., Michel, G., Freilinger, J., & Hentges, F. (2001). Differential binding of IgG and IgA antibodies to antigenic determinants of bovine serum albumin. *Clin. Exp Immunol, 123*, 387-394.

Guzman, M. G., Halstead, S. B., Artsob, H., Buchy, P., Farrar, J., Gubler, D. J., . . . Peeling, R. W. (2010). Dengue: A continuing global threat *Nat Rev Microbiol, 8*(12 Suppl), S7-16.

Haiss, W., Thanh, N. T. K., Aveyard, J., & Fernig, D. G. (2007). Determination of Size and Concentration of Gold Nanoparticles from UV-Vis Spectra. *Anal. Chem, 79*, 4215-4221.

Hoen, A. G., Keller, M., Verma, A. D., Buckeridge, D. L., & Brownstein, J. S. (2012). Electronic Event–based Surveillance for Monitoring Dengue, Latin America. *Emerging Infectious Diseases, 18*(7), 1147-1150. doi:10.3201/eid1808.120055

Holmes, E. C. (2009). RNA virus genomics: a world of possibilities. *J Clin Invest, 119*(9), 2488-2495.

Huang, S.-H. (2006). Gold nanoparticle-based immunochromatographic test for identification of *Staphylococcus aureus* from clinical specimens. *Clinica Chim. Acta, 373*, 139-143.

Huang, X., Jain, P., & El-Sayed, M. (2007). Gold nanoparticles: interesting optical properties and recentapplications in cancer diagnostics and therapy. *Nanomedicine, 2*, 681-693.

Ijeh, M. (2011). *Covalent gold nanoparticle-antibody conjugates for sensitivity improvement in LFIA*. (Doctor in Philosophy), Hamburg University, Hamburg, Germany.

Jelinek, T. (2009). Trends in the Epidemiology of Dengue Fever an their Relevance for Importation to Europe. *Eurosurveillance, 14*(25), 1-3.

Katzelnick, L. C., Fonville, J. M., Gromowski, G. D., Bustos Arriaga, J., Green, A., James, S. L., . . . Smith, D. J. (2015). Dengue viruses cluster antigenically but not as discrete serotypes. *Science, 349*(6254), 1338-1343.

Kenney, L. L., Cornberg, M., Chen, A. T., Emonet, S., de la Torre, J. C., & Selin, L. K. (2015). Increased Immune Response Variability during Simultaneous Viral Coinfection Leads to Unpredictability in CD8 T Cell Immunity and Pathogenesis. *J Virol, 89*(21), 10786-10801.

Khlebstov, B. N., & Khlebstov, N. G. (2011). On the measurement of gold nanoparticle sizes by the dynamic light scattering method. *Colloid Journal, 73*, 118-127.

Kim, T., Lee, C.-H., Joo, S.-W., & Lee, K. (2008). Kinetics of gold nanoparticle aggregation: Experiments and modeling. *J Colloid interf Sci., 318*(2), 238-243.

Koenderink, A. F., Alù, A., & Polman, A. (2015). Nanophotonics: Shrinking light-based technology. *Science, 348*(6234), 516-521.

Korns Johnson, D., & Homann, D. (2012). Accelerated and improved quantification of lymphocytic choriomeningitis virus (LCMV) titers by flow cytometry. *PLoS One, 7*(5), e37337. doi:10.1371/journal.pone.0037337

Kumar, S., Aaron, J., & Sokolov, K. (2008). Directional conjugation of antibodies to nanoparticles for synthesis of multiplexed optical contrast agents with both delivery and targeting moieties. *Nat Protoc, 3*(2), 314-320. doi:10.1038/nprot.2008.1

La Belle, J. T., Faichild, A., Demirok, U. K., & Verma, A. (2013). Method for fabrication and verification of conjugated nanoparticle-antibody tuning elements for multiplexed electrochemical biosensors. *Methods, 61*, 39-51.

Lauring, A. S., & Andino, R. (2010). Quasispecies Theory and the Behavior of RNA viruses. *PLoS Pathog, 6*(7), e1001005.

Lin, H. E., Tsai, W. Y., Liu, I. J., Li, P. C., Liao, M. Y., Tsai, J. J., . . . Wang, W. K. (2012). Analysis of epitopes on Dengue Virus envelope protein recognized by monoclonal antibodies and polyclonal human sera by a high throughput assay. *PLoS Negl. Trop. Dis., 6*(1), e1447.

Linares, E. M., Kubota, L. T., Michaelis, J., & Thalhammer, S. (2012). Enhancement of the detection limit for lateral flow immunoassays: Evaluation and comparison of bioconjugates. *J. Immunol Methods, 375*, 264-270.

Marston, H.D., Folkers, G.K., Morens, D.M., and Fauci, A.S. (2014). Emerging Viral Diseases: Confronting Threats with New Technologies. Sci. Transl. Med. *6*, 253ps210.

McAfee, M. S., Huynh, T. P., Johnson, J. L., Jacobs, B. L., & Blattman, J. N. (2015). Interaction between unrelated viruses during in vivo co-infection to limit pathology and immunity. *Virology, 484*, 153-162.

McCausland, M. M., & Crotty, S. (2008). Quantitative PCR technique for detecting lymphocytic choriomeningitis virus in vivo. *J Virol Methods, 147*(1), 167-176. doi:10.1016/j.jviromet.2007.08.025

Meira, G., & Oliva, H. (2011). Molecular weight distributions in ideal polymerization reactors. An introductory review. *Latin Am. Appl. Res, 41*, 389-401.

Mie, G. (1908). Beiträge zur Optik trüber Medien, speziell kolloidaler Metallösungen. *Ann. Phys., 25*, 377-445.

Mohammad, A. M., Abdelrahman, A. I., El-Deab, M. S., Okajima, T., & Ohsaka, T. (2008). On the aggregation phenomena of Au nanopartiles: effect of substrate roughnes on the particle size. *Colloids Surf., A, 318*, 78-83.

Moya, A., Elena, S. F., Bracho, A., Miralles, R., & Barrio, E. (2000). The evolution of RNA viruses: A population genetics view. *PNAS, 97*(13), 6967-6973.

Mustafa, M. F., Rasotgi, V., Jain, S., & Gupta, V. (2015). Discovery of fifth serotpe of Dengue Virus (DENV-5): A new public health dilemma in dengue control. *Med J Armed Forces India, 71*(1), 67-70.

nanoComposix. (2016). Mie Theory calculator. Retrieved from http://nanocomposix.com/pages/tools

Neuman, B. W., Adair, B. D., Burns, J. W., Milligan, R. A., Buchmeier, M. J., & Yeager, M. (2005). Complementarity in the supramolecular design of arenaviruses and retroviruses revealed by electron cryomicroscopy and image analysis. *J Virol, 79*(6), 3822-3830. doi:10.1128/JVI.79.6.3822-3830.2005

Peeling, R. W., Artsob, H., Pelegrino, J. L., Buchy, P., Cardosa, M. J., Devi, S., . . . Yoksan, S. (2010). Evaluation of diagnostic tests: dengue. *Nature Rev Microb, 8*(12), S30-S37.

Perelman, L. T. (2006). Optical diagnostic technology based on light scattering spectroscopy for early cancer detection. *Expert Rev Med Devices, 3*(6), 787-803.

Pham, V. D., Hoang, H., Phan, T. H., Conrad, U., & Chu, H. H. (2012). Production of antibody labeled gold nanoparticles for influenza virus H5N1 diagnosis kit development. *Adv. Nat. Sci.: Nanosci. Nanotechnol., 3*, 45017-45024.

Raj, V., & Sreenivasan, K. (2010). Selective detection and stimation of C-reactive protein in serum using surface-functionalized gold nano-particles. *Anal. Chim. Acta, 662*, 186-192.

Raoof, M., Corr, S. J., Kaluarachchi, W. D., Massey, K. L., Briggs, K., Zhu, C., . . . Curley, S. A. (2012). Stability of antibody-conjugated gold nanoparticles in the endolysosomal nanoenvironment: implications for noninvasive radiofrequency-based cancer therapy. *Nanomedicine, 8*(7), 1096-1105. doi:10.1016/j.nano.2012.02.001

Ringe, E., Sharma, B., Henry, A.-I., Marks, L. D., & VanDuyne, R. P. (2013). Single nanoparticle plasmonics. *Phys. Chem. Chem. Phys., 15*, 4110-4129.

Rosckstroh, A., Barzon, L., Pacenti, M., Giorgio, P., Niedrig, M., & Ulbert, S. (2015). Recombinant Envelope-Proteins with Mutations in the Conserved Fusion Loop Allow Specific Serological Diagnosis of Dengue-Infections. *PLoS Negl. Trop. Dis., 9*(11), e0004218.

Satterfield, B. C., Bartosiewicz, M., West, J. A., & Caplan, M. R. (2010). Surpassing Specificity limits of Nucleic Acid probes via Cooperativity. *J Mol Diagn, 12*(3), 359-367.

Satterfield, B. C., Kulesh, D. A., Norwood, D. A., Wasieloski, L. P., Jr., Caplan, M. R., & West, J. A. (2007). Tentacle Probes: differentiation of difficult single-nucleotide polymorphisms and deletions by presence or absence of a signal in real-time PCR. *Clin Chem, 53*(12), 2042-2050. doi:10.1373/clinchem.2007.091488

Satterfield, B. C., West, J. A., & Caplan, M. R. (2007). Tentacle probes: eliminating false positives without sacrificing sensitivity. *Nucleic Acids Res, 35*(10), e76.

Sigma-Aldrich, C. (2016). Phenol Red, ACS reagent. Retrieved from http://www.sigmaaldrich.com/catalog/product/sial/114529?lang=en&region=US

Singh, V., Nagappan Nair, S. P., & Aradhyam, G. K. (2013). Chemistry of conjugation to gold nanoparticles affects G-protein activity differently. *J Nanobiotechnology, 11*, 7.

Sorensen, C. (2013). Q-space analysis of scattering by particles: A review. *J Quant Spectros Radia Transfer, 131*, 3-12.

Strauss, J. H., & Strauss, E. G. (2007). *Viruses and Human Disease* (2nd Edition ed.): Academic Press

Thanh, N., & Rosenzweig, Z. (2002). Devevelopment of an aggregation-based immunoassay for anti-protein A using gold nanoparticles. *Anal. Chem., 74*, 1624-1628.

Thermo Fisher Scientific, I. (2016). Medium Essential Medium (MEM). Retrieved from https://www.thermofisher.com/us/en/home/life-science/cell-culture/mammalian-cell-culture/classical-media/mem.html

Thobhani, S., Attree, S., Boyd, R., Kumarswami, N., Noble, J., Szymanski, M., & Porter, R. A. (2010). Bioconjugation and characterisation of gold colloid-labelled proteins. *J Immunol Methods, 356*(1-2), 60-69. doi:10.1016/j.jim.2010.02.007

Tsai, D.-H., DelRio, D. W., Keene, A. M., Tyner, K. M., MacCuspie, R. I., Cho, T. J., . . . Hackley, V. A. (2011). Adsoption and Conformation of Serum Abumin Protein on Gold Nanoparticles Investigated using Dimensional Measurements and in situ Spectroscopic Methods. *Langmuir, 27*, 2464-2477.

Tsai, T. F., & Halstead, S. B. (2001). Tropical Viral Infections. *Infect Dis Clin Prac, 10*(2), 107-115.

Tüiskunen-Bäck, A., & Lundkvist, Å. (2013). Dengue Viruses - An Overview. *Infect Ecol Epidemiol., 3*, 19839.

van Dijk, M. A. (2007). *Nonlinear-optical studies of single gold nanoparticles.* (Doctor in Philosophy), University of Leiden.

Wong, W. R., Krupin, O., Sekaran, S. D., Mahamd Adikan, F. R., & Berini, P. (2014). Serological diagnosis of dengue infection in blood plasma using long-range surface plasmon waveguides. *Anal Chem, 86*(3), 1735-1743. doi:10.1021/ac403539k

Yang, Y., Matsubara, S., Nogami, M., & Shi, J. (2007). Controlling the aggregation behavior of gold nanoparticles. *Mat Sci Eng B, 140*, 172-176.

Yeo, E. L. L., Chua, A. J. S., Parthasarathy, K., Yeo, H. Y., Ng, M. L., & Kah, J. Y. C. (2015). Understanding aggregation-based assays: nature of protein corona and number of epitopes on antigen matters. *RSC Adv, 5*, 14982-14993.

Zhang, J. X. J., & Hoshino, K. (2014). *Molecular Sensors and Nanodevices: Principles, Designs and Applications in Biomedical Engineering*: William Andrew Applied Science Publishers.

Zhou, X., Ramachandran, S., Mann, M., & Popkin, D. L. (2012). Role of Lymphocytic Choriomeningitis Virus (LCMV) in understanding Viral Immunology: Past Present and Future Y. *Viruses, 11*, 2650. doi:- 10.3390/v4112640 M1 - Journal Article

APPENDIX A

A. PROTOCOL FOR PREPARATION OF CONJUGATED GOLD NANOPARTICLES

PROTOCOL FOR PREPARATION OF CONJUGATED GOLD NANOPARTICLES

Conjugation:

An aliquot of 1 ml containing 2.6 x 10^{10} particles/ml of 60 nm gold colloids (Ted Pella Inc, Redding, CA, http://www.tedpella.com) are combined with 10 microliters of freshly prepared pH = 5 acetate buffer prior to the addition of 100 microliters of the protein concentration necessary for ~90 %, in the case of BSA at least 2 mg/ml. A frozen cold pack should be placed on the tube and the mixture is gently rocked using an orbital table for 30 minutes.

Centrifugation:

After 30 minutes of incubation, 2.5 µl of a 10 % solution of Tween 20 (Sigma-Aldrich Corp., St. Louis, MO http://www.sigmaaldrich.com) is added to the mixture, and the mixture is rocked again for 5 minutes. Three centrifugation steps are conducted in order to reduce the concentration of the unbound protein to gold nanoparticles. The centrifugation conditions used are adapted from Cytodiagnostics Inc. (www.cytodiagnostics.com) recommended conditions for each particle size used. To minimize aggregation of gold nanoparticles and ensure re-suspension after centrifugation all centrifugation steps should be at 4 ˚C.

For 60 nm gold colloids, the first centrifugation was for 30 minutes at 1125×*g*. Immediately after centrifugation, as much of the supernatant as possible was carefully removed from the pellet. Once this was accomplished, 1 ml of pH = 5 acetate buffer was added to re-suspend the pellet. 2.5 µl of 10% Tween 20 was then added to the suspension and the mixture was gently rocked for 5 minutes. Afterwards, the suspension was centrifuged again for 15 minutes at 1125×*g*. The same procedure was used following the

second centrifugation as the first. For the 3rd centrifugation, time was shortened to 10 minutes. After the third and final centrifugation, the pellet was resuspended in 1 ml PBS buffer with azide in preparation for the gold nanoparticle immunoassays.

When the amount of protein is not enough to cover ~90 % of the surface of the gold nanoparticle, a blocking agent can be added to bind the empty spaces on the surface not covered by the protein. For the last resuspension, 500 µl of a solution of blocking agent are added and then rocked during 5 min on ice. After rocking, 500 µl of PBS are added to the gold nanoparticles. The volume of blocking agent or concentration may vary depending on each system.

Incubation:

Incubation of the sample with the gold nanoparticle solution shows a similar trend at both room temperature and 37 ˚C, although it is highly recommended to incubate at 37 ˚C for 30 min.